

# Interactions of Rapidly Moving Bodies in Terrestrial Atmosphere\*

K. P. CHOPRA

*Polytechnic Institute of Brooklyn, Brooklyn, New York, and Aerodynamics Laboratory, Freeport, New York*

## CONTENTS

I. Introduction	153
II. Aerodynamic Drag	154
III. Electrohydrodynamic Effects of Artificial Earth Satellites. I	
A. Electrohydrodynamics. Introduction	156
B. Collisions in an Ionized Gas	157
C. Charge on a Body	158
D. Satellite Potential	160
IV. Electrohydrodynamic Effects of Artificial Earth Satellites. II. Coulomb Drag	
A. Introduction	161
B. Jastrow-Pearse Theory	161
C. Beard's Modification	162
D. Kraus-Watson Theory	163
E. Chopra-Singer Theory	164
F. Comparison of Drag Estimates	165
V. Induction Drag	
A. Introduction	165
B. Translational Induction Drag of a Sphere	166
C. Rotational Induction Drag of a Sphere	167
D. Comparison with Viscous Drag. Decay Time	167
E. Sphere in a Viscous Fluid	168
F. Sphere in a Strong Magnetic Field	168
G. Large Magnetic Reynolds Number	170
H. Tumble of a Body in a Magnetic Field	170
I. Conclusions and Discussion	171
VI. Wave Drag	
A. Introduction	173
B. Waves in an Ionized Gas	173
(a) Electromagnetic Waves	173
(b) Magnetohydrodynamic Waves	174
(c) Electrostatic Waves	174
(d) Space-Charge Waves	175
(e) Collective Motion	176
C. Chopra-Singer Hypothesis	176
D. Greifinger's Theory	176
E. Conclusions	177
VII. Upper Atmosphere	
A. Introduction	177
B. Satellite Potential	179
C. Ion-Concentration	179
D. Electron-Concentration	179
E. Electron-Temperature	179
F. Satellite Potential as a Diagnostic Tool	180
G. Satellite Wake	180
H. Satellite Spin	180
I. Atmospheric Density, Pressure, and Temperature	182
VIII. Experimental Studies (Suggested)	
Simulated Studies in the Laboratory	183
Experiment I	183
Experiment II. Low-Density Wind Tunnel	184
Acknowledgments	188
Bibliography	188

## I. INTRODUCTION

RECENT estimates of density of the upper atmosphere of the earth, based on the orbital data of Sputnik I and Explorer I, disagree with those obtained previously from ionization gauge measurements. Sterne, Schilling and Folkart (1)<sup>1</sup> find that atmospheric densities at altitudes of 229 and 368 km are 9 and 14 times the ARDC estimates of Mizner and Ripley (2). Harris and Jastrow (3) of NRL estimated the density at an altitude of 400 km at 40 times the corresponding ARDC value. By extrapolating the recent rocket measurements (4) to an altitude of 185 km, they constructed a model atmosphere extending to a height of 500 km. Fuller accounts of the investigations of the two groups have recently been published (5, 6). Kallmann (7), Siry (8), and Paetzold (9) have constructed atmospheric models extending to higher altitudes. In deriving atmospheric properties, Kallmann used the perfect gas laws and the hydrostatic equation. Warwick (10) has estimated density from the decay of the spin of Sputnik I. King-Hele (11) has given a review of the estimates of the atmospheric density.

These estimates are in complete disagreement except that they indicate higher values of the atmospheric density than was predicted by the rocket data. These estimates disregard the fact that the physical properties, especially the electrical properties, of the upper atmosphere differ considerably from those of the lower atmosphere. Several electrohydrodynamic and magnetohydrodynamic phenomena occur which are likely to contribute to the drag of the artificial earth satellite. The long-range forces between the charged particles, and the effect of the magnetic field on the microscopic and macroscopic motion of charged particles are mainly responsible for these phenomena.

Any relative motion between a conducting material and a magnetic field causes electric currents in the material. These currents interact with the magnetic field to produce a force called induction drag (12). Induction drag of an artificial earth satellite would be caused by the electric currents induced inside the body of the satellite or in the terrestrial atmosphere. This drag mechanism has been investigated by several authors (13-20).

The influence of the magnetic field on the motion of an artificial earth satellite may also be understood in another way. An electrically conducting body moving

\* Supported in part by the U. S. Air Force Office of Scientific Research, Air Research and Development Command.

<sup>1</sup> References in parentheses are listed in numerical order in the Bibliography.

in a magnetic field gets polarized and acts as an electric dipole which constitutes a scattering center for the approaching charged particles (19). This approach makes the induction drag resemble the electrodynamic or Coulomb drag. Here a body moving in an ionized gas would acquire an electric charge through collisions with charged particles. If in addition there is a strong source of ultraviolet radiation, then its charge may become positive because of the preponderant effects of photoemission. Secondary emission, if any, would likewise affect the nature and magnitude of the charge. The magnetic field tends to restrain the flux of charged particles in a direction normal to the magnetic lines of force. Rotation of a conducting body in a magnetic field also causes a charge distribution to appear on the surface of the body (21-23). In any case, the trajectories of electrons and ions of the medium are affected by the charge of the body, and transfer their momentum to the body. This drag mechanism has been considered by several authors (24-29). Estimates of the various charging processes and Coulomb drag have been reviewed and reported recently (30-32).

Finally, motion of a highly charged body in the presence of an external magnetic field may excite plasma waves, with the body consequently losing its kinetic energy to the waves. This mechanism has been called the wave drag and has been discussed by Chopra and Singer (27), and Greifinger (33).

In Secs. II-VI, the basic phenomena concerning the interactions of a body moving in a conducting fluid with a pervading magnetic field are discussed. The last section deals with the summing up of the theoretical features relevant to the motion of the artificial earth satellites and the estimates of the atmospheric properties.

In the problems discussed here, the deceleration of the body is considered of prime importance, and no attempt is made to investigate its heating, melting, or vaporization. In the physical theory of meteor flight (34-36), on the other hand, the melting and vaporization of the body play the main role, and in most cases, the deceleration is relatively unimportant.

## II. AERODYNAMIC DRAG

At altitudes corresponding to the perigee of the artificial earth satellites or above, atmospheric conditions are such that molecular mean free paths are several times larger than the satellites. Accordingly, atmospheric particles strike the satellite unaffected by the interactions with those being reemitted. These conditions correspond to what is called the free-molecule-flow regime of aerodynamics. Hence the flow characteristics are studied by the techniques of the kinetic theory.

In order to explain this less-understood particle-surface interaction, two parameters were introduced by Maxwell (37) and von Smoluchowski (38). Maxwell postulated that a fraction  $\sigma$  of the oncoming particles become temporarily absorbed by the surface only to be

reemitted diffusely with a kinetic temperature corresponding to the wall temperature. The remainder of the particles,  $1-\sigma$ , undergo specular reflection. Therefore, the parameter  $\sigma$  represents the exchange of tangential momentum between the wall and the incident particles. On the other hand, von Smoluchowski suggested that the empirical results of heat transfer through a rarefied gas can be best explained by assuming that the reemitted molecules have a velocity corresponding to a temperature  $T_{re}$  which lies somewhere between the wall temperature  $T_w$  and the kinetic temperature  $T_0$  of the oncoming particles and is given by the relation

$$T_{re} = T_0 + \alpha(T_w - T_0), \quad (1)$$

where  $\alpha$  is called the accommodation coefficient, and represents the exchange of tangential energy between the wall and the incident particles. Schaaf and Chambré (39) introduced a third parameter  $\sigma'$  to represent the exchange of normal momentum between the gas and the solid. In the limiting cases of complete specular reflection and complete diffuse reemission, these parameters have the values

$$\sigma = \sigma' = \alpha = 0 \quad (\text{complete specular reflection}),$$

$$\sigma = \sigma' = \alpha = 1 \quad (\text{complete diffuse reemission}).$$

The drag of a spherical body of radius  $a$  and moving at a speed  $v$  is then given by

$$F = (\pi/2)\rho a^2 v^2 (2 - \sigma' + \sigma) \quad (2)$$

on the assumption that  $\sigma$  and  $\sigma'$  are constants over the entire surface. It follows from Eq. (2) that the sphere experiences exactly the same drag force in the two limiting cases. This leads to a very misleading result that the actual gross force probably does not lie in between these two limiting situations. For instance, the drag coefficient

$$C_D = F / (\pi/2)\rho a^2 v^2 = 2 - \sigma' + \sigma \quad (3)$$

may assume any value between 1 and 3, depending on the specific interaction model. Moreover, there appears to be no justification for the assumption that  $\sigma$  and  $\sigma'$  are constants or assume appropriate average values over the entire surface.

In view of these difficulties, Schaaf (40) suggested another model for the particle-surface interaction which incorporates the dependence of the interaction parameter on the local angle of attack of the surface element, and the effect of dissociation of the molecular constituent of the atmosphere during collision with the surface. This model has the following features.

The atmosphere at perigee altitudes consists of atomic oxygen and molecular nitrogen in the ratio 1:4. Both the constituents exchange momentum and energy with the surface each time a collision occurs, except that for a fraction  $f$  of the nitrogen molecules undergoing dissociation, we must subtract the dissociation energy of 9.7 eV from the combined energy of the two

product nitrogen atoms. The surface interaction can then be described in terms of three parameters, viz., the energy accommodation coefficients  $\alpha_O$  and  $\alpha_{N_2}$  for atomic oxygen and molecular nitrogen, respectively, and the fraction  $f$  of nitrogen molecules which dissociate. In terms of these parameters, the pressure exerted on the sphere is given by

$$p = \rho v^2 \sin \vartheta \left[ \sin \vartheta + \frac{\rho_0}{\rho} \left( \frac{\pi(1-\alpha_O)}{8} \right)^{\frac{1}{2}} + \frac{(1-f)\rho_{N_2}}{\rho} \left( \frac{\pi(1-\alpha_{N_2})}{8} \right)^{\frac{1}{2}} \right], \quad (4)$$

where  $\rho$  is the atmospheric density. The dependence of pressure  $p$  on the parameters  $\alpha_O$ ,  $\alpha_{N_2}$ , and  $f$ , and on the angle of attack  $\vartheta$  is evident in Eq. (4). On assuming that  $\alpha_O$ ,  $\alpha_{N_2}$ , and  $f$  are constant over the entire surface, the integration over the surface yields for the drag force

$$F = \frac{\pi}{2} \rho a^2 v^2 \left[ 2 + \frac{\sqrt{2}\pi}{3} \left\{ \frac{\rho_O}{\rho} (1-\alpha_O)^{\frac{1}{2}} + (1-f) \frac{\rho_{N_2}}{\rho} (1-\alpha_{N_2})^{\frac{1}{2}} \right\} \right]. \quad (5)$$

On using the empirical estimates of Hurlbut and Stein (41) for aluminium surface, viz.,

$$\alpha_O \sim 0.45, \quad \alpha_{N_2} \sim 0.50,$$

one obtains for the drag coefficient

$$C_D = F/(\pi/2)\rho a^2 v^2 = 2.1 \quad (\text{for complete dissociation}), \\ = 2.6 \quad (\text{for no dissociation}).$$

Schamberg (42) has formulated a hyperthermal free-molecule-flow model of the particle-satellite surface interaction based on the molecular beam data, in which the estimates of the drag coefficient are made by using the infinite speed ratio (ratio of the satellite speed and the mean thermal speed of the molecules). This involves an error of about 6% but completely eliminates the elaborate calculations involving the speed ratio. Further, the effect of the random motion of the molecules is suppressed by considering that all molecules have the same speed (equal to the satellite speed) relative to the surface. After interaction with the wall, the molecules are reemitted or reflected in a conical beam having a half-angular width  $\Phi_0$ . The angle of reflection or reemission  $\vartheta_r$  (represented by the inclination of the axis of the cone to the surface) is related to the angle of incidence  $\vartheta_i$  by the equation

$$\cos \vartheta_r = (\cos \vartheta_i)^\nu, \quad (6)$$

where

$$\nu = 1 \quad (\text{specular reflection}) \\ = \infty \quad (\text{diffuse reemission}).$$

The hyperthermal drag coefficient is then represented

by

$$C_D = F/\frac{1}{2}\rho v^2 A = 2[1 + (1-\alpha)^{\frac{1}{2}} \varphi(\Phi_0) f(\nu, \text{shape})], \quad (7)$$

where  $\alpha$  is the accommodation coefficient estimated on the assumption of elastic collisions, and  $f(\nu)$ , for a few specific body-shapes, is given by

$$f(\nu) = \sin \vartheta_i (1 - \cos^{2\nu} \vartheta_i)^{\frac{1}{2}} - \cos^{\nu+1} \vartheta_i \quad (8a)$$

for (i) a flat plate with angle of attack  $\vartheta_i$ , or (ii) a circular cone with zero angle of attack but semiapex angle equal to  $\vartheta_i$ ; and

$$f(\nu) = 2 \left\{ \int_0^1 x [(1-x^2)(1-x^{2\nu})]^{\frac{1}{2}} dx - \frac{1}{\nu+3} \right\} \quad (8b)$$

for a spherical body. The integral in Eq. (8b) acquires values  $\frac{1}{4}$  and  $\frac{1}{3}$  for complete specular reflection and complete diffuse reemission, respectively. Further, the factor

$$\varphi(\Phi_0) = \frac{1 - (2\Phi_0/\pi)^2 \frac{1}{2} \sin(2\Phi_0) - (2\Phi_0/\pi)}{1 - 4(2\Phi_0/\pi)^2 \sin\Phi_0 - (2\Phi_0/\pi)} \quad (9)$$

represents the ratio of the axial momentum carried away from the surface to the momentum that would be carried away if all the molecules in the beam were aligned with its axis. It assumes values of 1 and  $\frac{2}{3}$  in the cases of complete specular reflection and complete diffuse reemission.

For a satellite tumbling in a random fashion about its three principal axes, the time-averaged drag coefficient is given by

$$\bar{C}_D = (A_s/4\bar{A}) C_{D \text{ sphere}}, \quad (10)$$

where  $\bar{A}$  is the average of the three principal projected areas of the tumbling body,  $A_s$  is the surface area, and  $C_{D \text{ sphere}}$  is the drag coefficient of a sphere obtained by substituting the value of  $f(\nu)$  appropriate to the sphere [i.e., (8b)] in Eq. (7). The values of  $(A_s/4\bar{A})$  for specific convex bodies have been calculated (42) and assume values between 1 (for a sphere) and  $\frac{2}{3}$  (for a flat plate). Therefore, the sphere has the lowest average drag coefficient  $\bar{C}_D$  of all the randomly tumbling shapes, and the maximum value exceeds that of a sphere by at most 50%.

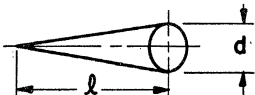
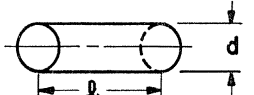





If the axis of tumble is fixed with respect to the flight direction, one can obtain a precise estimate of the time-averaged drag. For example, the time-averaged drag coefficient of a flat plate tumbling at constant angular velocity is given by

$$\bar{C}_D = (4/\pi) \sin \mu [1 + \varphi(\Phi_0) (1-\alpha)^{\frac{1}{2}} f(\nu, \mu)], \quad (11)$$

where  $f(\nu, \mu)$  is a complicated function of  $\nu$  and the yaw angle  $\mu$ . Similarly, a circular cylinder, of diameter  $d$  and length  $l$  tumbling about a yawed transverse axis which makes an angle  $\mu$  with the flight direction, experiences an average drag given by

$$\bar{C}_D(\mu) = \bar{C}_{D1} + [(4l/\pi d)/(\sin \mu + \cos \mu)] (\bar{C}_{D2} + \bar{C}_{D3}), \quad (12)$$

TABLE I. Effect of attitude and tumbling on drag of representative satellites.<sup>a</sup> Assumed surface interaction: diffuse reemission ( $\nu \rightarrow \infty$ ), accommodation coefficient = 0.50.

Satellite	195882 Sputnik III				1958ε Explorer IV					
Shape	Cone				Cylinder					
Dimensions	 $d = 5.67 \text{ ft}$ $l = 11.75 \text{ ft}$ $\frac{d}{l} = 0.48$				 $d = 0.52 \text{ ft}$ $l = 6.67 \text{ ft}$ $\frac{d}{l} = 0.078$					
Flight Attitude	X		Drag Coeff. $C_D$	Relative Reference Area, $A'$	Relative Drag, $C_D A'$	X		Drag Coeff. $C_D$	Relative Reference Area, $A'$	Relative Drag, $C_D A'$
"Forward"			2.22	1.00	2.22			2.94	1.00	2.94
"Backward"			2.94	1.00	2.94	← Same as "Forward" →				
"Sideways"			2.75 <sup>c</sup>	1.32	3.63			2.75	16.3	44.9
Random Tumbling <sup>b</sup>	$\left(\frac{A \text{ surf.}}{4 \bar{A}}\right) = 1.09$		2.86	1.21	3.46	$\left(\frac{A \text{ surf.}}{4 \bar{A}}\right) = 1.19$		3.13	11.2	35.0

<sup>a</sup> Reproduced from Schamberg (42).

<sup>b</sup> For random tumbling  $C_D = \bar{C}_D$ , as defined by Eq. (12) and  $A' = \bar{A}/[(\pi/4)d^2]$ .

<sup>c</sup> Approximated by drag coefficient of cylinder with axis normal to stream.

<sup>d</sup> Normalized on the base area  $(\pi/4)d^2 = 25.2 \text{ ft}^2$ .

<sup>e</sup> Normalized on the base area  $(\pi/4)d^2 = 0.212 \text{ ft}^2$ .

where

$$\begin{aligned} \bar{C}_{D1} &= (4/\pi) \sin\mu [1 + \varphi(\Phi_0)(1-\alpha)^{1/2} f(\nu, \mu)], \\ \bar{C}_{D2} &= (4/\pi) \sin\mu [1 + \varphi(\Phi_0)(1-\alpha)^{1/2} f_{ey1}(\nu) f(\nu, \mu)], \\ \bar{C}_{D3} &= 2 \cos\mu [1 + \varphi(\Phi_0)(1-\alpha)^{1/2} f_{ey1}(\nu) f(\nu, 90^\circ - \mu)]. \end{aligned} \quad (13)$$

Also, a right circular cone of length  $l$  and base diameter  $d$  tumbling about a yawed transverse axis has an average drag coefficient equal to half the corresponding value for a right circular cylinder of length  $l$  and diameter  $d$ . Table I of Schamberg (42) is reproduced here. This shows that tumbling may cause the drag force on a right circular cone (Sputnik III) to vary by almost 60%, while that on a right cylinder (Explorer IV) may vary by a factor of 15.

This hyperthermal free-molecule-flow model indicates that the drag coefficient is sensitive to the nature of the interaction accommodation coefficient, and tumbling. Though quite detailed, it does not include the effect of molecular dissociation at impact.

If the molecular mean free path is of the order of the size of the body, then the characteristics of the incident flux are modified by the interaction of emitted molecules with the free stream within the gas ahead of the body. This transitional regime between the free-molecule-flow and continuum flow has been studied by Baker and Charwat (43). They assume that all the incident molecules are reemitted diffusely after impact at a nonablating body moving at a hyperthermal speed. At high Mach numbers and strong radiative cooling, the drag coefficient of a sphere is then given by

$$C_D = C_{DFM} [1 - (0.15 R_e / C_{DFM}) (T_0 / T_w)^{1/2}] \quad (14)$$

where  $C_{DFM}$  is the free-molecule-flow value of the drag coefficient, and  $R_e$  is the Reynolds number.

While the hypersonic rarefied gas flow problems have been treated by methods of kinetic theory, Adams and Probstein (44) argue that the continuum-flow-approach is applicable at least up to the region where the flow begins to behave like a free-molecule-flow. This implies, according to them, that the accommodation coefficient for energy transfer in the transition region is not an important consideration.

### III. ELECTROHYDRODYNAMIC EFFECTS OF ARTIFICIAL EARTH SATELLITES. I

#### A. Electrohydrodynamics. Introduction

Lehnert (24) in 1956 was the first to discuss the various electrohydrodynamic effects connected with the motion of an artificial earth satellite. His predictions may be summarized as follows.

The mean-free-path of charged and neutral particles is much greater than the dimensions of the satellite (45). Coulomb scattering dominates the collision processes at high altitudes (46), although the inelastic collisions are more effective in reducing the electron energy. The cross section for photoionization of air is considerable down to wavelengths of about 300 Å (47), and a large number of electrons are released with kinetic energies of the order of ionization potentials of oxygen and nitrogen. Therefore, the mean energy of electrons is likely to exceed the value corresponding to the thermal equilibrium (48) and must be below the ionization potential. In a situation of thermal equilibrium, the

satellite acquires a negative charge corresponding to a potential of the order of  $-1$  v mainly through the electron accretion along the magnetic lines of force; the ion accretion of the front half of the sphere hardly affects this potential. The electric field caused by polarization in the magnetic field is negligible compared to the electric field of the satellite charge. Each charged particle suffers a Coulomb scattering in the field of the satellite. This causes momentum transfer to ions in a direction perpendicular to the path of the satellite and to electrons in a direction along the magnetic field lines (49, 50). On the day side, the energy losses  $W_e$  and  $W_i$ , caused per unit time by electron and ion scattering are given by

$$W_e/W_m \approx 40X, \quad W_i/W_m \approx 0.18X, \quad (15)$$

where  $W_m$  is the energy loss caused per unit time by the mechanical drag, and  $X$  is the degree of ionization. This holds in regions of low density. In the ionosphere, however, the satellite charge is large enough to blast off the electrons, and the remaining positive ions create an electric field to screen off the satellite potential. Accordingly, the momentum transfer takes place within the Debye distance (51). The separation of charge caused by the motion gives rise to an increase in electrostatic energy and in plasma oscillations. Further, the interaction with the terrestrial magnetic field may set up magneto-ionic (52) waves.

Although we may not agree with all of these predictions, Lehnert's pioneering note forms the foundation of the basic electrohydrodynamic processes associated with the motion of artificial earth satellites.

### B. Collisions in an Ionized Gas

Let us first study the nature of collisions in an ionized gas in the presence of a magnetic field. The average frequency  $\nu_{12}$ , for particles of mass  $m_1$ , of collisions with particles of mass  $m_2$  is given by (53)

$$\nu_{12} = 2n_2\sigma_{12}^2 [2\pi kT(1/m_1 + 1/m_2)]^{1/2}, \quad (16)$$

where  $k$  is the Boltzmann constant, and  $\sigma_{12} = \frac{1}{2}(\sigma_1 + \sigma_2)$  is the joint diameter or the effective distance between centers at collision between the particles. For a collision between two neutral particles or between a neutral and a charged particle, the effective diameter is a moderate multiple (between 1 and 5) of  $10^{-8}$  cm. The mean free path  $\lambda_{12}$  is then given by

$$\lambda_{12} = (\bar{v}_1/\nu_{12}) = [\pi n_2 \sigma_{12}^2 (1 + m_1/m_2)]^{-1}, \quad (17)$$

where  $\bar{v}_1 = (8kT/\pi m_1)^{1/2}$  is the mean speed of the particles of mass  $m_1$ . For collisions between particles of the same kind,

$$\nu_{11} = 4n_1\sigma_{11}^2(\pi kT/m_1)^{1/2}, \quad \lambda_{11} = 1/\sqrt{2}\pi n_1\sigma_{11}^2, \quad (18)$$

whereas if one of the kinds of particles is electron, then the average collision frequency for an electron with neutral particles is

$$\nu_{e1} = \frac{1}{4}\pi n_1\sigma_1^2\bar{v}_e \quad \text{or} \quad \lambda_{e1} = 4/\pi n_1\sigma_1^2. \quad (19)$$

It follows from Eqs. (18) and (19) that

$$\lambda_{e1} = 4\sqrt{2}\lambda_{11}. \quad (20)$$

Coulomb interaction is responsible for collisions between charged particles. Since the number of particles at equal distance from any point is directly proportional to the square of the distance, this Coulomb interaction exhibits a long range. Consequently, the effective diameter for collisions between charged particles is larger in magnitude than that between neutral particles. For a collision between an electron and an ion, the effective diameter (cm) is of the order of  $10^{-5}Z_i(300/T)$ , where  $Z_i$  is the number of unit charges on the ion. For a collision between two ions, it is about  $10^{-5}Z_iZ_i'(300/T)$ , where  $Z_i$  and  $Z_i'$  are the number of unit charges on the two ions. Owing to the large magnitude of these effective diameters, the collision frequencies are not seriously affected by the presence of moderate number of neutral particles. For example, in a slightly ionized gas at  $1000^\circ\text{K}$  and consisting of singly charged ions, electrons and neutral particles, the Coulomb collision frequency is of the same order as the neutral collision frequency when

$$n_e \sim n_i \sim 10^{-5}n. \quad (21)$$

Again, assuming that the effective diameter for any pair of charged particles is the same, and neglecting the electron mass in comparison to the ion mass, the electron-electron, ion-ion, and electron-ion collision frequencies for a singly ionized neutral gas are in the ratio

$$\nu_{ee} : \nu_{ii} : \nu_{ei} :: \sqrt{2} : (2m_e/m_i)^{1/2} : 1. \quad (22)$$

A more elaborate expression, that of Mazumdar (54), for the electron-ion collision frequency, which exhibits a dependence on the electron density and temperature, is

$$\nu_{ei} = \frac{4\pi}{3} \frac{n_e e^4}{(2\pi m_e)^{1/2} (kT)^{3/2}} [\log_n(T\lambda_i)^2 - 24.58], \quad (23)$$

while that obtained by Cowling (55) is of the form

$$\nu_{ei} = \frac{\pi n_e e^4}{m_e v_e^3} \left[ \alpha + 2\beta \log_n \left( \frac{n_e^{-1/2} m_e v_e^2}{e^2} \right) \right]^{-1}, \quad (24)$$

with  $\alpha$  and  $\beta$  each of the order of unity. In his numerical estimates, Nicolet (46) adopts the form

$$\nu_{ei} = [34 + 8.36 \log_{10}(T^{3/2}/n_e^{1/2})] n_e T^{-3/2}. \quad (25)$$

For this discussion, we use a less rigorous but more convenient form of expression,

$$\nu_{ei} \sim 4.8 \times 10^3 (n_e/T^{3/2}). \quad (26)$$

As an illustration, let us consider the terrestrial atmosphere at an altitude of 300 km, which is characterized by the following physical parameters:

$$\begin{aligned} n_e \sim n_i \sim 2 \times 10^6/\text{cc}, \quad n \sim 2 \times 10^9/\text{cc}, \quad T \sim 1500^\circ\text{K}, \\ v_e \sim 2.6 \times 10^7 \text{ cm/sec}, \quad \text{and} \quad v \sim v_i \sim 10^5 \text{ cm/sec}. \end{aligned}$$

Then it follows from Eqs. (25) and (26) that

$$\nu_e \sim \nu_i \sim 4 \times 10^3/\text{sec}, \text{ and } \nu_n \sim 1/\text{sec}$$

or

$$\lambda_e \sim 6.5 \times 10^3 \text{ cm}, \quad \lambda_i \sim 25 \text{ cm}, \text{ and } \lambda \sim 10^5 \text{ cm}. \quad (27)$$

Hence the ion mean free path is smaller than the electron mean free path by a factor of  $(m_e/m_i)^{1/2}$ , and is of the order of tens of centimeters at altitudes of interest. The large Coulomb cross sections are balanced by the large neutral particle density only at lower altitudes. The ion mean free path exceeds 300 km only in the far outer regions where the ion density is such that

$$n_i < 5 \times 10^{-4} T^2. \quad (28)$$

Also for the neutral mean free path to attain microscopic magnitudes, say of the order of  $10^{-6}$  cm, the particle density must be of the order of  $10^{20}/\text{cc}$ .

These conclusions are in contrast with those of Grad (56) who remarks:

We speak of free paths rather than collision times since the former are about the same size for electrons and ions. . . . At the temperature existing in the atmosphere, the Coulomb cross section is much greater than the neutral cross section. This is counterbalanced by the fact that the neutral density is usually much greater than the charged particle density. The Coulomb mean free path is always large (at least 300 km), but the neutral mean free path can range from microscopic values at low altitudes to values large compared to the Coulomb mean free path.

The term "collision" could be applied to cover broader aspects of interactions between charged particles than just the close and distant collisions discussed previously. Some of these aspects have been discussed by Bohr (49) and more recently by Burgers (57).

\* \* \*

If a magnetic field of strength  $\mathbf{H}$  pervades the ionized atmosphere, then a particle carrying a charge  $Ze$  and moving at a velocity  $\mathbf{v}$  experiences an interaction force  $Ze\mathbf{v}_1\mathbf{H}/c$  in a direction normal to both the magnetic field and  $\mathbf{v}_1$ , where  $\mathbf{v}_1$  is the component of  $\mathbf{v}$  in a direction normal to  $\mathbf{H}$ , and  $c$  is the velocity of light. Under the influence of this force the particle gyrates around the magnetic field with a frequency

$$\nu_e = ZeH/2\pi mc \text{ cps}. \quad (29)$$

where  $m$  is the mass of the gyrating particle. The radius  $r_e$  is given by

$$r_e = mv_1c/ZeH. \quad (30)$$

The particle is said to spiral freely if it completes one revolution before it suffers a collision. Hence, the condition for free spiral is that the mean free path must exceed  $2\pi$  times the radius of gyration, or the collision frequency be less than the cyclotron frequency

$$\nu_{\text{coll}} < \nu_{\text{cycl}} \quad \text{or} \quad \lambda > 2\pi r_e \quad (31)$$

or

$$n_2 < (ZeH/4\pi c\sigma_{12}^2)[2\pi mkT(1+m_1/m_2)]^{-1/2}.$$

Since the Coulomb collision frequency between different kinds of charged particles is of the same order if electrons are involved in the collisions (22), we may consider that the electron density represents the charged particle density and the electron-electron collision frequency is the representative Coulomb collision frequency. Then the condition for free spiral is determined by the inequality

$$n_e < (H/A)T^{3/2}, \quad (32)$$

where  $A$  is the ratio of the particle mass to the proton mass.

When the particles are free to spiral, they may be said to be tied to the magnetic lines of force or frozen in the magnetic field. For singly charged particles with a kinetic temperature of  $1500^\circ\text{K}$  in the terrestrial magnetic field, we have

$$\begin{aligned} r_{ce} &\sim 5 \text{ cm}, & r_{ci} &\sim 500 \text{ cm}, \\ \nu_{ce} &\sim 9 \times 10^5 \text{ sec}^{-1}, & \nu_{ci} &\sim 36 \text{ sec}^{-1}. \end{aligned} \quad (33)$$

Comparison of Eqs. (27) and (33) and the use of (31) leads to the conclusion that the electrons spiral freely in the earth's magnetic field while the ions do not. In other words, the terrestrial magnetic field restricts the transverse motion of electrons whereas ions move unaffected by the terrestrial magnetic field.

### C. Charge on a Body

A body in an ionized gas acquires charge through collisions with ions and electrons. For comparable electron and ion temperatures, the electrons move faster than the ions. Therefore, the flux of electrons hitting the body is larger than the corresponding ion flux resulting in the body acquiring a negative charge at a rate

$$\frac{dQ^-}{dt} = -n_e \left( \frac{8kT_e}{\pi m_i} \right)^{1/2} \left[ 1 - \left( \frac{m_i T_e}{m_e T_i} \right)^{1/2} e^{-e|V|/kT_e} \right] \quad (34)$$

on the assumption that there are equal number of ions and electrons. For a negatively charged body at a potential  $V$ , the effective cross section for ion accretion is increased by a factor of  $[1+eV/(\frac{1}{2}m_i v_i^2)]$ , while that for electron accretion is decreased by a factor of the order of  $[1-eV/(\frac{1}{2}m_e v_e^2)]$  (for  $eV < \frac{1}{2}m_i v_i^2$  and  $\frac{1}{2}m_e v_e^2$ ). The equilibrium potential  $V_{\text{eq}}$  is characterized by the equal electron and ion-accretion rates, and is given by

$$V_{\text{eq}} = (kT_e/2) \log_n(m_i T_e/m_e T_i) \text{ volts } (kT_e \text{ in eV}). \quad (35)$$

Assuming equal ion and electron temperatures, i.e.,  $kT_e \sim kT_i \sim 0.15$  eV, and  $m_i/m_e \sim 14 \times 1840$ , we have  $V_{\text{eq}} \sim 0.8$  v. In deriving this expression, the mean thermal speeds of ions and electrons are considered as the representative speeds of the charged particles. The

TABLE II. Surface interactions.

Primary particle	Secondary particle	Primary particle energy (ev)	Coefficient of interaction
Electron	Electron (emission)	>10 to 20	1 for Cu at 200 ev
Positive ion	Electron (reflection)	...	20%
	Electron	>100	10 <sup>-2</sup> to 10 <sup>-1</sup> for 1000-ev ions
	Positive ion	...	10 <sup>-2</sup> for Cs <sup>+</sup> of 1000 ev from tungsten
	Neutralized ion	...	10 <sup>-4</sup> for 100- to 600-ev Ar <sup>+</sup> and H <sup>+</sup> ions from Cu
	Negative ion	>110	10 <sup>-4</sup> for 200-ev H <sup>+</sup> ion from Ni
	Sputtered neutral particle	>100	10 <sup>-4</sup> for Hg <sup>+</sup> of 10 ev; 0.2 to 0.6 for N <sub>2</sub> of 100 ev

more exact calculation should take the energy spectrum of particles into account; however, as expected, use of mean thermal speeds does not introduce any serious error.

\* \* \*

Under the impact of high-energy incident particles a body may emit electrons or ions (58) and hence may acquire an electric charge. These phenomena are important only for very high energies of the primaries.

Primary electrons, of a few electron-volt energy, do not cause appreciable secondary electron emission. About 20% of electrons may be reflected back with full energy. True secondary emission of electrons begins to appear at primary energies of 10 to 20 ev. (See Table II.)

The impacts of positive ions on a surface may result in emission of secondary electrons or negative ions or a neutral atom. The primary ion energies of 100 ev or less are quite ineffective for these processes. A positive ion may cause emission of a negative ion of a different nature. The threshold energy of incident ions for this process is also of the order of 100 ev. The reflection of positive ions is not important. The emission of neutral atoms is possible through interactions of the ions and the surface. The effect is observable at energies of the order of 100 ev or above. Wehner (59) observed a yield of 10<sup>-4</sup> atoms/ion for Hg<sup>+</sup> ions of 10-ev energy. However, for 125-ev N<sub>2</sub> molecules, the yield ranges between 0.2 to 0.6 atoms/ion. Sputtered neutral atoms do not influence the charge on the body.

Hence, we may conclude that surface interactions do not play a significant role in charging a body through particle impacts at ordinary gas temperatures.

\* \* \*

When ultraviolet light or x rays are present, photons liberate electrons from the surface of the body leaving a positive charge on it. Here the electron accretion

competes with the ion accretation and the photoejection of electrons. An equilibrium potential of the body is established that is determined by equalization of positive and negative charging rates. The actual sign and magnitude of the charge and potential of the body depends on the relative importance of the charging processes. If  $V_{eq}$  is the equilibrium potential, only photons of energy exceeding  $eV_{eq} + \phi$ , where  $\phi$  is the work function, are effective in causing the electron emission.

Since the electron flux  $n_e v_e$  is greater than the corresponding ion flux  $n_i v_i$  for comparable electron and ion temperatures, a body is negatively charged if the electron flux  $n_e v_e$  exceeds the number  $n_{ph}$  of photoelectrons emitted per second. If we consider  $T \sim 1500^\circ K$ ,  $n_e \sim n_i \sim 10^6/cc$ , we have for the two cases

$$(1) \quad n_{ph} < n_i v_i, \\ V_{eq} = (kT_e/2) \log_n [(m_i/m_e)(T_e/T_i)] \text{ volts} \\ \approx 0.8 \text{ v (negative)} \quad (kT_e \text{ in ev})$$

$$(2) \quad n_{ph} \sim 10^{12} > n_i v_i, \\ V_{eq} = kT_e \log_n (n_e v_e / n_{ph}) \sim 0.3 \text{ v (negative).}$$

For negatively charged bodies, only the long-wavelength part of the spectrum gives almost all of the photoelectrons.

Alternatively, the body acquires a positive charge if

$$n_{ph} > n_e v_e,$$

and if we further assume that the photoelectron flux is inversely proportional to the fourth power of the potential, then the equilibrium potential  $V_{eq}$  is given by

$$V_{eq} = (n_{ph}/n_e v_e)^{1/4}. \quad (37)$$

For  $kT_e \sim 0.15$  ev,  $n_e \sim 5 \times 10^5/cc$ , and  $n_{ph} \sim 10^{19}/cm^2/sec$ ,

$$V_{eq} \approx +31.6 \text{ v.}$$

Only the high-energy electrons produced by the short-wavelength photons can escape from positively charged bodies.

\* \* \*

A spherical body of radius  $a$  cm rotating with angular speed in a magnetic field  $H$  produces (21-23) electromotive forces which are balanced within the body by an electrostatic field resulting from a uniform charge distribution throughout the sphere. This charge distribution within the sphere is compensated by an equal and opposite surface charge so distributed that the external electric field is that of an axial quadrupole whereas the internal field turns out to be directed towards the axis of rotation with intensity proportional to the distance from the axis. The corresponding potential for  $r \geq a$  is

$$V = \frac{1}{2} V_p (a/r)^3 (3 \cos^2 \vartheta - 1) \text{ esu} \quad (38)$$

with surface charge density equal to  $-\mu \epsilon_0 \omega a H_p \cos^2 \vartheta$ ,

TABLE III. Potential due to rotation in a magnetic field.

Body	$a$ (cm)	$B_p$ (gauss)	$\omega$ (rad/sec)	$V_p$ (v)
Sun	$7 \times 10^{10}$	1	$3 \times 10^{-6}$	$4.9 \times 10^7$
Laboratory model (Swann)	3.17	...	506	$1.72 \times 10^{-2}$ <sup>a</sup>
Earth satellite	25	0.3	0.75	$4.7 \times 10^{-7}$

<sup>a</sup> Against observed value  $1.8 \times 10^{-2}$  v.

where

$$V_p = \omega(\mu H_p) a^2 / 3c \quad (39)$$

is the potential of the pole with respect to infinity, and  $\mu H_p$  is the magnetic induction at the pole. Swann (21) performed experiments to verify this phenomenon and found experiment and theory in reasonable agreement. Table III lists three typical examples of spherical bodies, showing that this phenomenon is not of any significance for bodies of sizes of our interest. It may, however, play an important role for bodies of cosmical sizes.

The negative charge on a spherical body in an ionized gas or a plasma is shielded by a concentric spherical shell, containing positive ions, of thickness characterized by the Debye shielding length

$$\lambda_D = (kT_e / 4\pi n_e e^2)^{1/2} = 6.9(T_e / n_e)^{1/2}.$$

Typical values of  $\lambda_D$  are given in Table IV.

If the body is in motion, the spherical shell becomes an ellipsoid and finally a paraboloid. There is a concentration of positive ions in front, and ion trails behind it. The charge on the moving body is not shielded by a space charge because, for body speed exceeding the thermal speed of ions, the body moves out of the space-charge region before the space charge has a chance to establish itself. For this to happen, the time  $t_s$  taken by the body to move a distance  $\lambda_D$  must be less than the relaxation time of the charged particles. If the mean ion collision time is considered to be the representative relaxation time of the charged particles, then this interval is greater than  $t_s$  by a factor of 50 for a body speed of  $8 \times 10^5$  cm/sec in an atmospheric charged particle density of  $10^6$  particles/cc at a kinetic temperature of  $1500^\circ\text{K}$ . Hence, for all practical purposes, a body moving at a speed exceeding the thermal speed of ions proceeds unshielded and behaves like an ion but of a macroscopic linear dimension and carrying an enormous charge.

TABLE IV. Debye shielding distance  $\lambda_D$ (cm).

$kT_e$ (ev)	$T_e$ (°K)	$n_e$ per cc			
		$10^3$	$10^4$	$10^5$	$10^6$
0.1	1160	7.0	2.2	0.7	0.2
0.5	5800	10.7	5.0	1.1	0.6
1.0	11 600	22.2	7.0	2.2	0.7
1.5	17 400	27.2	8.7	2.7	0.9

## D. Satellite Potential

The considerations of the preceding section may now be applied to a spherical satellite of 25-cm radius, moving at  $8 \times 10^5$  cm/sec. The corresponding ion and electron thermal speeds at an altitude of 500 km are of the order of  $10^5$  and  $2 \times 10^7$  cm/sec, respectively. Hence, for the most part of the atmosphere, the representative speeds are such that  $v_i < v_s < v_e$  unless  $T > 2 \times 10^5$  °K. At the corresponding kinetic energies, the interactions between the incident charged particles and the satellite surface are ineffective.

Since the ion thermal speed is less than the satellite speed, the ion flux is determined by the number of ions swept by the satellite along its path. On the other hand, the mean thermal speed of electrons exceeds the satellite speed and would hit it from all sides. But their motion, unlike that of ions, is subject to a stronger influence of the terrestrial magnetic field. Only electrons of appropriate speeds moving along the magnetic lines of force are able to reach the satellite surface.

TABLE V. Potential of artificial earth satellite ( $v_s \sim 8 \times 10^5$  cm/sec;  $n_{ph} \sim 10^{17}$ /cm<sup>2</sup>/A/sec from Al).

	(1) <sup>a</sup>	(2) <sup>a</sup>	(3)
Altitude (km)	242	795	$2 \times 10^4$
Gas temperature (°K)	1100	4000	$10^5$
Electron density (per cc)	$10^6$	$4 \times 10^5$	$10^2$
Ion density (per cc)	$5.2 \times 10^5$	$1.8 \times 10^5$	$10^2$
Mean thermal speed of electrons (cm/sec)	$2.2 \times 10^7$	$4 \times 10^7$	$7 \times 10^8$
Ions (cm/sec)	$1.3 \times 10^5$	$2.5 \times 10^5$	$5 \times 10^6$
Electron flux	$4.5 \times 10^{13}$	$3.2 \times 10^{13}$	$2.8 \times 10^{11}$
Ion flux	$4.2 \times 10^{11}$	$1.4 \times 10^{11}$	$2 \times 10^9$
Equilibrium potential $V_{eq}$ calc (volts)	-0.27	-0.9	-21, +100 <sup>b</sup>
$V_{eq}$ obs	-2.0	-6.4	...
Effective electron temperature, $T_e$ (°K)	7500	$1.5 \times 10^4$	...

<sup>a</sup> Russian Sputnik.

<sup>b</sup> Positive potential is obtained on the assumption of photoelectron flux  $V_{eq}^{-4}$  and  $n_{ph} \sim 10^{19}$ /cm<sup>2</sup>/sec.

As a representative number of photoelectrons, we adopt the value of  $10^5$  to  $10^7$ /cm<sup>2</sup>/A for an Al surface exposed to solar radiation. Hence, at least in the lower parts of the atmosphere, the outward flux of photoelectrons is negligible compared to the oncoming flux of electrons and ions. Accordingly, the satellite is negatively charged. Chang and Smith (32) have emphasized this point in an interesting way. However, the author persists in believing that at least in the outer parts of the terrestrial atmosphere and in the interplanetary space, the photoelectric effect is important. The first two columns of Table V describe the pertinent conditions at altitudes of 242 and 795 km, respectively, from Sputnik data. The third column refers to somewhat speculative conditions at an altitude of  $2 \times 10^4$  km. The positive potential of 100 v is obtained on the assumption that in the equilibrium state, the photoelectron flux equals  $n_{ph} V_{eq}^{-4}$  with  $n_{ph} \sim 10^{19}$ /cm<sup>2</sup>/sec. As is evident, the observed equilibrium potentials at altitudes



of 242 and 795 km are higher than the calculated values and are predominantly negative. This could be possible only by assuming higher temperatures of the electron gas. The corresponding temperatures are  $7500^\circ$  and  $15\,000^\circ\text{K}$ , respectively. This question is considered further in Sec. VII.

#### IV. ELECTROHYDRODYNAMIC EFFECTS OF ARTIFICIAL EARTH SATELLITES. II. COULOMB DRAG

##### A. Introduction

The studies of the preceding section show that:

(1) Distant collisions between charged particles are quite significant compared to the close collisions between all kinds of particles.

(2) The body moving in an ionized atmosphere acquires an electric charge mainly through collisions with charged particles. The surface interactions for pertinent incident energies are insignificant, except in that about 20% of electrons are reflected back. The pervading magnetic field, if any, tends to restrict the transverse flux of electrons, while the ions move practically unaffected because of the smaller mean-free path. The polarization charge due to rotation in a magnetic field is negligible. The significance of the photoelectric effect is uncertain because of lack of knowledge of solar radiation. Presumably, the photoejection of electrons becomes important in the far outer regions.

(3) Comparison of theoretical estimates, even neglecting the photoelectric effect and electron reflection, yields a value for the negative potential which is smaller than the corresponding values observed with the Russian Sputnik.

(4) The charge on the body is shielded as long as the speed of the body is less than the mean thermal speed of the charged particles forming the space charge. On the contrary, if the speed of the body exceeds the mean thermal speed of the charged particles, the body moves unshielded.

In this section, the drag experienced by the body owing to the interaction with charged particles is studied. The trajectories of electrons and ions are affected by the charge of the body and transfer of momentum to the body results. Estimates of the "charge" or the "Coulomb" drag have been made by Jastrow and Pearse (26), Chopra and Singer (27), and Kraus and Watson (28).

##### B. Jastrow-Pearse Theory

Jastrow and Pearse (26) assume that the electron energy distribution is Maxwellian corresponding to the electron temperature  $T_e$ . On neglecting the photoelectric effect, and the influence of the terrestrial magnetic field on the motion of charged particles, they obtain a value of  $-7$  ev for the equilibrium potential on the artificial satellite assuming  $kT_e \sim 1.5$  ev. This corresponds to  $T_e \sim 17\,400^\circ\text{K}$ . The ion flux is determined by the

number of ions swept per second by the satellite body along its trajectory. This implies that the mean thermal speed of ions is less than the speed of the satellite, i.e.,  $v_i < 8 \times 10^6$  cm/sec. Accordingly, their calculation involves an inherent assumption that the electrons and ions are not in thermodynamic equilibrium.

Further, the negatively charged satellite is assumed to polarize the atmosphere in its neighborhood. The distribution of electric charge is given by Poisson's equation,

$$\nabla^2 V = 1 - 4\pi n_e [1 - e^{-eV/kT_e}]. \quad (41)$$

This equation yields a shielding distance equal to the Debye length  $\lambda_D$ .

In contrast to this approximation, they follow the argument that, while the ion distribution maintains its normal value in the neighborhood of the sphere, the electron density must drop to zero within a distance  $l+a$  from the satellite such that the positive charge in the shell between  $a$  and  $a+l$  cancels the negative charge of the sphere. The potential  $V$  is then determined from the spherically symmetrical solution of Poisson's equation subject to the boundary conditions

$$V(a) = V_{eq}, \quad \text{and} \quad V(a+l) = 0. \quad (42)$$

On assuming  $l \ll a$ , the solution yields for the shielding distance

$$l = (2eV_{eq}/kT_e)^{1/2} \lambda_D. \quad (43)$$

In the situation discussed by Jastrow and Pearse,

$$\lambda_D \sim 2 \text{ cm}, \quad kT_e \sim 1.5 \text{ ev.}, \quad V_{eq} \sim -7 \text{ v},$$

and hence  $l \sim 12.5$  cm compared to the radius of 25 cm for the satellite. With this estimate, the effective cross section of the satellite for ion encounters is 2.25 times its value for collisions with neutral atoms. Hence the drag experienced by a spherical satellite due to the Coulomb interaction is given by

$${}^c F_{JP} = \pi m_i n_i [1 + (V_{eq}/2\pi n_e a^2 e)^{1/2}]^2 a^2 v_s^2 \quad (44)$$

with a drag coefficient

$${}^c C_{D,JP} = 2(n_i/n) [1 + (V_{eq}/2\pi n_e a^2 e)^{1/2}]^2. \quad (45)$$

For potentials of the order of a few volts, electron density of the order of  $10^6/\text{cc}$  and the satellite radius of the order of 25 cm,  $(V_{eq}/2\pi n_e a^2 e)^{1/2}$  is of the order of unity. Hence for moderate satellite potentials the Coulomb drag is significant only for high degree of ionization. Under the application of this force alone, the sphere should decelerate with a decay time

$${}^c \tau_{JP} = M v_s / {}^c F_{JP}, \quad (46)$$

where  $M$  is the mass of the satellite.

This kind of calculation is based on the hypothesis that only those charged particles, which are situated within a distance  $a+l$  from the center of the sphere, are effective in causing the drag. The satellite charge is ineffective for ions outside the shell. The cross section

presented to ions by the satellite antennas makes an appreciable contribution to the charge drag.

However, this solution is subject to several serious objections:

(1) Strictly speaking, the spherical symmetric solution is valid only for bodies at rest. It may be applied, to a first degree of approximation, to slowly moving bodies. Spherical symmetry does not apply to bodies moving at speeds greater than the thermal speed of the ions.

(2) The shielding length  $l$  has been determined subject to the restriction that  $l \ll a$ , and hence does not apply to the case considered by Jastrow and Pearse where  $l \sim a$ .

(3) The satellite moves at a faster speed than the ions and hence moves out of the shell before the shell has a chance to form. For a given satellite speed, this objection becomes invalid at high thermal ion speeds exceeding the satellite speed.

### C. Beard's Modification

Beard (29) introduced a pervading magnetic field in the Jastrow-Pearse problem and adopted  $kT_e \approx 0.1$  ev instead of the 1.5 ev they assumed. His analysis neither brings about any substantial improvements over Jastrow-Pearse theory nor does it throw any more light in the problem. Rather it is subject to more serious objections. We first quote from his paper:

In this analysis, the effect of the magnetic field is twofold. Firstly, the magnetic field restrains the incident flux of electrons. Secondly, a conducting satellite moving across a magnetic field  $H$  develops a potential<sup>2</sup> of the order of  $10^{-8} v_s H$  v/cm, where  $H$  is in gauss, and  $v_s$  is the satellite speed in cm/sec. The electrons moving along the electric field  $E$  get accelerated while those moving against it get decelerated. Assuming the electric field  $E$  to be constant, the difference in energy  $\Delta \mathcal{E}$  lost to the particles directed with the electric field and that gained from particles oppositely directed is then estimated to be<sup>3</sup>

$$\Delta \mathcal{E} \sim e(\mathcal{E}_s)^2 / m_e v_s^2 \sim \frac{1}{2} m_e v_s^2, \quad (47)$$

where  $s$  is the total distance moved normal to the surface of the satellite. This is the average energy of electrons with reference to the satellite. This has been interpreted in terms of the electrons acquiring a drift velocity  $v_D$ , equal to the satellite speed  $v_s$ , due to the induced electric field. Thus the electrons impact with slightly increased velocity  $v = (v_e^2 + v_s^2)^{1/2}$ , compared to the surrounding fluid. This means that the electrons acquire the satellite speed before impact rather than at impact. If the electrons do

not impact they leave the satellite with their original velocities. The result is that the charged particles impact on the satellite skin with energies independent of the presence of a magnetic field, i.e., the charges do not experience the emf caused by the magnetic field.

If the satellite is charged positively, however, a drift current will develop around the vehicle in such a direction as to cancel the earth's magnetic field in the vicinity of the vehicle. Some Ohmic heating could result. If the satellite were negatively charged, only positive charges would be in the vicinity of the satellite, and due to their high collision rate, negligible drift current would result. An excess of positive ions will surround the satellite for a distance given correctly by Jastrow and Pearse.

Photoelectrons have so much greater energy than the electrons treated here that their inductive reaction on the satellite is very much smaller than the effects treated above. They will not raise the satellite potential appreciably. Photoelectrons and secondaries leaving the satellite lose the satellite velocity with respect to the medium as they leave the magnetically induced electric field of the satellite. This gives the satellite a slight push.

As should be obvious, his conclusions are self-contradictory. In the first place, the electric field  $\mathbf{E} \sim 10^{-8} v_s \times \mathbf{H}$  is induced inside the satellite and is not felt outside because the electric currents caused by this field either (i) are closed within the satellite or (ii) cause piling up of opposite charges in front and behind them, thus setting up an electrostatic field which tends to neutralize the induced electric field. In other words, the satellite is electrostatically shielded. Moreover, this field is very small compared to the field due to the charge on the satellite. The induced electric field  $\mathbf{E}$  outside the satellite would be set up only if the original magnetic field in the atmosphere were altered by the mere presence of the satellite. We return to this point in the next section.

The derivation of Eq. (47) involves the distance  $s$  which is not clearly specified. For the same reason, it is difficult to appreciate how

$$\Delta \mathcal{E} \sim \frac{1}{2} m_e v_s^2$$

can be obtained. Also, the drift velocity, in his theory, is of the order of  $10^{-2}$  times the mean electron speed. Hence, the corresponding increase in impact energy is of the order of  $10^{-4}$  times the induction-free energy of electrons. The collision rate for ions is not greater than that of the electrons; it is the mean-free path which brings about the difference in behavior of ions and electrons. The shielding of the earth's magnetic field by the drift current is not clearly brought out. This last problem is analogous to the creation of a ring current in the theories of geomagnetic storm effects (60). Similarly, the magnetic field has no effect on the

<sup>2</sup> The word "potential" used in the main paper is a misnomer for electric field.

<sup>3</sup> The notation is changed slightly to correspond to that in this paper.

secondary particles produced in surface-particle or surface-radiation interactions.

Thus this analysis goes no further than Jastrow and Pearse, and is subject to all the objections in the preceding section besides those stated here.

#### D. Kraus-Watson Theory

Kraus and Watson (28) have considered physical processes associated with the rapid motion of a satellite in the ionosphere. These processes bear a close resemblance to what is obtained in supersonic aerodynamics. In particular they consider (i) a Mach cone extending beyond the body, (ii) an increase in the ionization in the Mach cone, and (iii) the drag experienced by the body.

A body carrying an electric charge and moving at a speed greater than the ion thermal speed in the terrestrial atmosphere may induce a collective motion of ions which results in the formation of a wake behind it. In order to study the structure of the wake, distinction is made between the two limiting cases of small and large relaxation times for the electron gas. These conditions refer to the local thermodynamic equilibrium and non-equilibrium, respectively. The first limit approximates to the supersonic flow in a dense gas, and is treated by the linearized hydrodynamic equation. In the second limit, the recourse must be had to the Boltzmann transport equation. The results are similar in the two cases.

The half-cone angle  $\vartheta$  of the wake behind a negatively charged body moving at a speed  $v_s$  greater than the mean thermal speed of ions is, for small Debye length, given by

$$\tan \vartheta = [(v_s/A)^2 - 1]^{-\frac{1}{2}} \quad (48)$$

with

$$A^2 = a_i^2 + \lambda_D^2 \omega_{pi}^2 = a_i^2 (1 + T_e/T_i), \quad (49)$$

where  $\omega_{pi} = (4\pi n_i e^2 / m_i)^{\frac{1}{2}}$  is the ion plasma frequency, and  $a_i$  is the ion sound speed. This angle is only a few degrees if temperature equilibrium is assumed, while for higher electron temperatures the wake angle increases.

On using the Boltzmann transport equation, the flow potential  $G$  about the body is found to be

$$G = \frac{2eQ\lambda_D}{m_i A^2} \frac{[(z - v_s t)^2 - \{(v_s/A)^2 - 1\} |X_1|^2]^{\frac{1}{2}}}{[(z - v_s t)^2 (1 + \Gamma^2/A_0^2) - \{(v_s/A)^2 - 1\} |X_1|^2]} \quad (50)$$

with

$$A_0 = (a_e/2)X,$$

and

$$\Gamma = (a_e/2)(\pi/2)^{\frac{1}{2}} (a_e/a_i)^2 X \epsilon^{-(a_e/a_i)X}, \quad (51)$$

where

$$X = 1 + \{1 + 3(a_i/a_e)^2\}^{\frac{1}{2}}, \quad (51')$$

and  $a_e$  is the electron sound speed provided  $\Gamma/A_0$  is small. For negligible values of  $\Gamma/A_0$ , Eq. (50) reduces to

$$G = (2eQ\lambda_D^2/m_i A^2) [(z - v_s t)^2 - \{(v_s/A)^2 - 1\} |X_1|^2]^{-\frac{1}{2}} \quad (52)$$

which is exactly the result obtained from the linearized hydrodynamic equations.

The increase in electron density in the wake is given by

$$\frac{n_e'}{n_e} = \frac{eaV_{eq}}{\lambda_D(T_e + T_i)\{(v_s/A)^2 - 1\}^{\frac{1}{2}}}, \quad (53)$$

where  $T_e$  and  $T_i$  are expressed in electron volts, and  $Q = aV_{eq}$ .

Finally, following Bohm and Pines (61), they estimate the electrohydrodynamic drag as the product of the electric field at the position of the body and the charge, which is then written as

$${}^e F_{KW} = [2\pi n_e (aV_{eq}e)^2 / (\frac{1}{2}m_i v_s^2)] L, \quad (54)$$

where

$$L = \log_n \{(\lambda_D/a)^2 - 1\} - \{(\lambda_D/a)^2 / [1 + (\lambda_D/a)^2]\}. \quad (55)$$

In his estimate of the drag, Kraus assumes  $L \sim 1$ . The corresponding drag coefficient  ${}^e C_{D,KW}$  and the decay time  ${}^e \tau_{KW}$  are

$${}^e C_{D,KW} = 2(n_e/n) [eV_{eq} / (\frac{1}{2}m_i v_s^2)]^2, \quad (L \sim 1) \quad (56)$$

and

$${}^e \tau_{KW} = Mv_s / {}^e F_{KW},$$

respectively. The ratio of the Coulomb and neutral drags is

$${}^e F_{KW} / {}^n F \sim 6 \times 10^{-3} V_{eq}^2 (n_e/n), \quad (57)$$

whence it follows that for satellite potentials of the order of a few volts, Coulomb drag is significant only for a high degree of ionization.

This theory is not free from serious objections:

(1) One great limitation is that the size of the body must be small compared to the Debye distance, which is of the order of a few centimeters at altitude of our interest. Therefore, the moving body must be very small. The best suited application is found in micrometeorites, interplanetary or interstellar dust particles. It is certain that this theory is not applicable to the artificial earth satellites.

(2) The expression for the satellite drag has been derived following the treatment of Bohm and Pines. The phenomenon discussed by Kraus and Watson does not have any resemblance to that discussed by Bohm and Pines. Hence, a justification should be given for assuming that the drag is equal to the product of the satellite charge and the value of the electric field at the point of location of the satellite. On the contrary, the phenomenon in question results from the increased electron density in the wake. This fact should form the basis for calculation of the drag.

(3) Similarly, we may take exception to the authors' claim that their physical mechanism bears close analogy to the Čerenkov radiation (62) of a charged particle

traveling in a dielectric. The resemblance occurs only in the form of two integrals occurring in the two theories, and not in the basic physical mechanisms.

(4) A comment of minor significance may be made on the mechanisms by which a satellite may acquire an electric charge. Their conclusion that the "photoelectric effect is ineffective because the Sputnik's potential has been observed to be negative" may not always be correct because a negative potential may as well be obtained through a balance of photoelectric effect and electron accretion when ion accretion is small compared to the photoelectron flux.

(5) Kraus cited the radar observations of a trail behind the Sputnik as confirmation of his theory. While not discounting the significance of electrohydrodynamic processes as such, the trail could have been formed by other mechanisms also. It is well known that a body moving at supersonic speed leaves an ionized trail behind it. Another factor responsible for this trail is the behavior of the electrostatic shield of the charge on a rapidly moving body. Since the satellite speed is greater than the ion thermal speed, the positive ion shell surrounding the negatively charged satellite, instead of being spherical, has a paraboloidal form, thus leaving an excess of positive ions trailing behind it.

### E. Chopra-Singer Theory

Whereas Jastrow-Pearse theory is valid for the case where the electric field of the satellite is confined only to the sheath and does not penetrate the outer region, the Kraus-Watson calculation of the drag follows the analogy of the self-force of a charged particle. Both of these theories have a limited scope for application to the artificial earth satellites. Their results are significant for bodies of linear dimensions small compared to the Debye shielding distance moving in almost completely ionized atmospheres.

Chopra and Singer (27) conjecture that the electric field of the charged satellite is not confined to the sheath alone. As we have seen earlier in Sec. III, the electrostatic sheath surrounding a charged satellite loses its usual meaning. Rather, the electric field penetrates the whole atmosphere, its intensity falling as the inverse square of distance. But the number of particles at equal distance from the center of the satellite increases as the square of distance. Therefore, the region of influence extends to a larger linear dimension.

In the region where the electric field of the charged satellite is significant, the motion of the charged particles is modified by the Coulomb interaction with the satellite field. Since the masses of the charged particles are negligible compared to the mass of the satellite, the electrons and ions describe hyperbolic orbits about the charged satellite. In these encounters, the charged particles gain momentum in a direction perpendicular to the path of the satellite (50). As a consequence the satellite speed is reduced. The problem is then analogous

to the one discussed by Bohr (49). Following Chandrasekhar (63) and Spitzer (64), the decrease in the speed of the satellite is given by

$$\Delta v_s = - \frac{8\pi n_1 (aV_{eq})^2 (Z_1 e)^2}{M v_1^2} \times \left( \frac{1}{M} + \frac{1}{m_1} \right) \mathcal{G} \left( \frac{v_s}{v_1} \right) \log_n \left( \frac{\lambda_D}{\rho_0} \right), \quad (58)$$

where  $n_1$ ,  $Z_1 e$ , and  $v_1$  are, respectively, the particle density, charge, and root-mean-square speed of the particle of mass  $m_1$ ,  $\rho_0$  is the impact parameter, and  $\mathcal{G}(v_s/v_1)$  is related to the error function  $\varphi(v_s/v_1)$  according to

$$\mathcal{G}(x) = [\varphi(x) - x\varphi'(x)]/2x^2, \quad x = v_s/v_1 \quad (59)$$

and

$$\varphi(x) = \frac{2}{\pi^{1/2}} \int_0^x \exp(-x^2) dx.$$

Then the Coulomb drag  ${}^c F_{cs}$ , responsible for the deceleration of the satellite, is given by

$${}^c F_{cs} = 16\pi \left( \frac{1}{m_1} + \frac{1}{M} \right) \frac{n_1 (aV_{eq})^2 (Z_1 e)^2}{v_1^2} \times \mathcal{G} \left( \frac{v_s}{v_1} \right) \log_n \left( \frac{\lambda_D}{\rho_0} \right). \quad (60)$$

For singly charged particles, since  $m_1 \ll M$ , the last equation reduces to

$${}^c F_{cs} = \frac{16\pi n_1 (aV_{eq})^2 e^2}{m_1 v_1^2} \mathcal{G} \left( \frac{v_s}{v_1} \right) \log_n \left( \frac{\lambda_D}{\rho_0} \right). \quad (61)$$

The corresponding drag coefficient  ${}^c C_{D,cs}$  is given by

$${}^c C_{D,cs} = \frac{32}{3} \left( \frac{n_1}{n} \right) \frac{e^2 V_{eq}^2}{m_1 v_s^2 k T_1} \mathcal{G} \left( \frac{v_s}{v_1} \right) \log_n \left( \frac{\lambda_D}{\rho_0} \right) \quad (62)$$

When subject to this force alone, the kinetic energy of the satellite is reduced to  $(1/\epsilon)$  times its original value in a time  ${}^c \tau_{cs}$  given by

$${}^c \tau_{cs} \sim \frac{M v_s}{{}^c F_{cs}} \sim \frac{m_1 M v_s v_1^2}{16\pi n_1 (aV_{eq})^2 e^2 \mathcal{G}(v_s/v_1) \log_n(\lambda_D/\rho_0)}. \quad (63)$$

We distinguish between two cases according as the satellite speed is greater or less than the root-mean-square speed of the charged particles.

*Case (i):*  $v_s > v_1$ . When the speed of the charged body exceeds the root-mean-square speed of the charged particles, the function  $\mathcal{G}(v_s/v_1)$  is of the form of

$$\mathcal{G}(v_s/v_1) \sim (v_1^2/2v_s^2). \quad (64)$$

Here the drag force is inversely proportional to the

TABLE VI. Comparison of Coulomb drag estimates.

Altitude (km)	Drag force $F$ (dynes)				Drag coefficient $C_D$				Decay time ( $\times 10^{11}$ sec)			
	250	500	800	$2 \times 10^4$	250	500	800	$2 \times 10^4$	250	500	800	$2 \times 10^4$
Drag theory												
Neutral	$1.92 \times 10^2$	2.9	0.08	$2.6 \times 10^{-5}$	2	2	2	2	$4 \times 10^{-4}$	$2.7 \times 10^{-2}$	1	$3 \times 10^3$
Jastrow-Pearse	0.02	0.04	$7 \times 10^{-3}$	$5 \times 10^{-5}$	$1.7 \times 10^{-4}$	0.02	0.18	6	4	2	10	$1.6 \times 10^3$ <sup>a</sup>
Kraus-Watson	$6 \times 10^{-3}$	0.04	0.05	$2 \times 10^{-4}$	$6 \times 10^{-5}$	$2.6 \times 10^{-4}$	1.3	1.8	1.6	40	60	400 <sup>b</sup>
Chopra-Singer				0.1				55				20 <sup>b</sup>
Ions	0.07	0.53	0.24	0.02	$7 \times 10^{-6}$	0.32	6.1	$7.7 \times 10^3$	1.1	0.15	0.33	4 <sup>a</sup>
Electrons	0.26	0.75	0.34	$5 \times 10^{-4}$	$2.6 \times 10^{-5}$	0.50	1.38	$1.9 \times 10^3$	0.3	0.1	0.23	0.16 <sup>b</sup>
				0.01				45				160 <sup>a</sup>
								$1.1 \times 10^3$				6.8 <sup>b</sup>

<sup>a</sup> -21 volts.

<sup>b</sup> 100 volts.

square of the satellite speed, so the decay time is proportional to the cube of the satellite speed. Hence, Eqs. (61), (63), and (62), respectively, reduce to

$$\begin{aligned} {}^e F_{cs} &= [8\pi n_1 a^2 (eV_{eq})^2 / m_1 v_s^2] \log_n(\lambda_D / p_0), \\ {}^e C_{D,cs} &= 4(n_1/n) (eV_{eq} / \frac{1}{2} m_1 v_s^2)^2 \log_n(\lambda_D / p_0), \\ {}^e \tau_{cs} &= m_1 M v_s^3 / 16\pi n_1 (aV_{eq})^2 e^2 \log_n(\lambda_D / p_0). \end{aligned} \quad (65)$$

This case is of particular interest in the Coulomb interactions of ions with the electric field of the satellite.

Case (ii):  $v_s < v_1$ . The function  $\mathcal{G}(v_s/v_1)$  is here proportional to the speed of the satellite, and therefore the corresponding drag force is given by

$${}^e F_{cs} = 10(m_1/T_1^3)^{1/2} n_1 (aV_{eq})^2 \log_n(\lambda_D/p_0) v_s \quad (66)$$

with the drag coefficient<sup>4</sup>

$${}^e C_{D,cs} = [20/(\pi^2 m_1 T_1^3)^{1/2}] (n_1/n) (V_{eq}^2/v_s) \times \log_n(\lambda_D/p_0). \quad (67)$$

In Eqs. (66) and (67)  $V_{eq}$  is expressed in volts. The corresponding decay time  ${}^e \tau_{cs}$  approaches a constant limit

$${}^e \tau_{cs} = M T_1^{3/2} / 10 m_1^{1/2} n_1 (aV_{eq})^2 \log_n(\lambda_D/p_0). \quad (68)$$

In the satellite problem, this case is of particular interest in the Coulomb interactions of electrons with the electric field of the artificial earth satellite. Here, Eqs. (66), (67), and (68), respectively, become<sup>5</sup>

$$\begin{aligned} {}^e F_{cs} &= 3 \times 10^{-13} T_e^{-3/2} n_e (aV_{eq})^2 \log_n(\lambda_D/p_0) v_s, \\ {}^e C_{D,cs} &= (1/12 T_e^{3/2}) (n_e/n) V_{eq}^2 \log_n(\lambda_D/p_0), \\ {}^e \tau_{cs} &= 3 \times 10^{12} [M T_e^{3/2} / n_1 (aV_{eq})^2 \log_n(\lambda_D/p_0) v_s]. \end{aligned} \quad (69)$$

For the same kinetic temperature, the electron contribution to drag is smaller than the ion contribution by a factor of  $(m_e/m_i)^{1/2}$ .

## F. Comparison of Drag Estimates

We consider four typical altitudes: 250, 500, 800, and  $2 \times 10^4$  km. The first two are typical perigee altitudes while the latter two are typical apogee altitudes.

<sup>4</sup> It is assumed that the gas particles have an average mass  $m_1$ .

<sup>5</sup> It is assumed that the average mass of the gas particles is equal to proton mass and the speed of the satellite equals  $8 \times 10^6$  cm/sec.

The values of the various physical parameters are from Table IX. The drag force, drag coefficient, and decay time are calculated in each case, and listed in Table VI. The first column lists the corresponding values relevant to the neutral drag of a sphere where surface and Coulomb interactions have been neglected. In Chopra-Singer theory, estimates of ionic and electronic contributions are made separately. The appropriate formulas from the three theories have been used at each altitude. For example, at the altitude of  $2 \times 10^4$  km in Chopra-Singer theory, the formulas (66) to (69) have been used, while, at the other three altitudes, formulas (65) and (69) have been adopted. At a height of  $2 \times 10^4$  km the gas is supposed to consist of protons and electrons, and two estimates for each of the electron and ion contributions to the drag correspond to hypothetical values of the satellite potential, viz., -21 v and +100 v, respectively.

## V. INDUCTION DRAG

### A. Introduction

If a material of finite electrical conductivity  $\sigma$  cgs units moves with velocity  $\mathbf{v}$  across a magnetic field  $\mathbf{H}$ , electric current density

$$\mathbf{j} = \sigma [\mathbf{E} + (1/c)(\mathbf{v} \times \mathbf{H})] \quad (70)$$

is induced in the material. Here  $\mathbf{E}$  is produced by the currents if either (i) they are such as to cause appreciable change in the original magnetic field, or (ii) they cause piling up of charges in front of and behind them. In the absence of either of these circumstances, i.e., when the induced electric currents neither modify the original magnetic field nor cause electrostatic charge separation, the induced current density is given by

$$\mathbf{j} = (\sigma/c) [\mathbf{v} \times \mathbf{H}]. \quad (71)$$

These electric currents interact with the original magnetic field to produce a mechanical force

$$\mathbf{F} = (1/c) [\mathbf{j} \times \mathbf{H}] \quad (72)$$

which opposes the motion of the conducting material. This mechanical force is called "induction drag" (12, 13).

When induced electric currents are large enough that they alter the magnetic field appreciably, then the electric field  $\mathbf{E}$  is given by

$$\text{curl } \mathbf{E} = -(1/c)(\partial \mathbf{H} / \partial t). \quad (73)$$

When combined with Maxwell equations,

$$\text{curl } \mathbf{H} = (4\pi/c) \mathbf{j} \quad (74)$$

and

$$\text{div } \mathbf{H} = 0, \quad (75)$$

Eqs. (70) and (73) yield

$$\partial \mathbf{H} / \partial t = \text{curl}(\mathbf{v} \times \mathbf{H}) + (c^2/4\pi\sigma) \nabla^2 \mathbf{H}. \quad (76)$$

On defining  $l$  as a characteristic length, the two terms on the right-hand side of Eq. (76) are of the order of  $vH/l$  and  $c^2H/4\pi\sigma l^2$ , respectively. These two terms are of the same order if

$$4\pi(\sigma/c^2)lv \sim 1. \quad (77)$$

The expression  $4\pi(\sigma/c^2)lv$  is called the magnetic Reynolds number.

When the magnetic Reynolds number is very small compared to unity, i.e., if  $l \ll [4\pi(\sigma/c^2)v]^{-1}$ , the first term on the right-hand side of Eq. (76) is small compared to the second, and we have

$$\partial \mathbf{H} / \partial t = (c^2/4\pi\sigma) \nabla^2 \mathbf{H}. \quad (78)$$

In such a case the changes in  $\mathbf{H}$  brought about by the induced electric currents are wiped out before they attain appreciable magnitude by a process akin to diffusion. Then the mechanical effects of the induced currents are governed by Eq. (72).

On the other hand, when the magnetic Reynolds number exceeds unity, i.e., if  $l \gg [4\pi(\sigma/c^2)v]^{-1}$ , the first term dominates the second, and Eq. (76) becomes

$$\text{curl } \mathbf{E} = -(1/c)(\partial \mathbf{H} / \partial t) = -(1/c) \text{curl}(\mathbf{v} \times \mathbf{H}) \quad (79)$$

or

$$\mathbf{E} + (1/c)(\mathbf{v} \times \mathbf{H}) = 0,$$

and the medium behaves as if it possesses infinite electrical conductivity and carries a frozen-in magnetic field, and the induced electric currents  $\mathbf{j}$  completely vanish or reduce to inappreciable magnitudes. When the magnetic field is not very strong, a large volume of moving gas will drag the magnetic lines of force along with it. On the other hand, a moving strong local magnetic field may push a suitable volume of gas along with it. The phenomenon is called electromagnetic shielding and may be partial or complete depending on the relative magnitudes of the two terms on the right-hand side of Eq. (76).

Another phenomenon which causes the reduction of the mechanical effects of induced electric currents exists where the electric currents polarize the conductor. Here the currents are such that

$$\text{div } \mathbf{j} \neq 0, \quad (80)$$

and the polarization electric field  $\mathbf{E}$  is of purely electrostatic origin and derivable from a potential  $\varphi$ . It is directed so as to balance the electric field  $(1/c)\mathbf{v} \times \mathbf{H}$  induced by the motion across the magnetic field. This balance may be exact or partial, and the phenomenon is called electrostatic shielding.

The induction drag is more significant when the shielding effects are negligible. This would happen in the case of a magnetohydrodynamic flow characterized by a low Reynolds number and an induced electric current with a vanishing divergence.

Several authors (12-20) have discussed the problems pertaining to the induction drag of bodies.

## B. Translational Induction Drag of a Sphere

Chopra (13) investigated the induction drag experienced by (i) a magnetized sphere of radius  $a$  and uniform magnetic intensity  $\mathbf{H}_0$  moving with velocity  $\mathbf{v}$  in a direction parallel to  $\mathbf{H}_0$  in an inviscid fluid of electrical conductivity  $\sigma$ , and (ii) an electrically conducting sphere of radius  $a$  moving with velocity  $\mathbf{v}$  in an inviscid fluid of electrical conductivity  $\sigma$  with a pervading magnetic field  $\mathbf{H}_0$  such that the velocity  $\mathbf{v}$  is directed along the magnetic field.

In (i), the magnetic field of the magnetized sphere in the surrounding space is that due to a dipole of moment

$$\mathbf{v} = \frac{1}{2} \mathbf{H}_0 a^3 \quad (81)$$

placed at the center of the sphere with its axis parallel to  $\mathbf{H}_0$ . In (ii), however, if the spherical material is of infinite electrical conductivity, there are no magnetic lines of force inside the sphere, but for points external to it, the magnetic field  $\mathbf{H}_0$  is modified to the extent of a dipole of moment given by Eq. (81) placed at the center of the sphere with the dipole axis antiparallel to  $\mathbf{H}_0$ . On the other hand, if the sphere has a finite electrical conductivity, the magnetic field  ${}^i\mathbf{H}$  inside the sphere is given by

$${}^i\mathbf{H} = [3/(\mu+2)]\mathbf{H}_0, \quad (82)$$

where  $\mu$  is the magnetic permeability of the sphere, while for points external to the sphere, the magnetic field is the resultant of  $\mathbf{H}_0$  and the field due to a dipole of moment

$$\mathbf{v} = [(\mu-1)/(\mu+2)]\mathbf{H}_0 a^3 \quad (83)$$

placed at the center of the sphere.

Electric currents are induced in the surrounding fluid due to the motion of an appropriate dipole. The currents are also induced in a sphere of finite electrical conductivity [case (ii)] only if the velocity of the sphere has a component in a direction normal to  $\mathbf{H}_0$ . In the problems discussed by Chopra, the currents are induced only in a surrounding atmosphere because  $\mathbf{v} \parallel \mathbf{H}_0$ . He estimates the induction drag by equating the rate of loss of kinetic energy of the sphere to the rate at which the Joule dissipation of energy of the induced electric currents takes place. The same results may also

be obtained by calculating the force exerted on the equivalent magnetic dipole by the induced electric currents.

On assuming that shielding effects are absent, he finds for the induction drag

$${}^i\mathbf{F} = (8\pi/5)[(\mu-1)/(\mu+2)]^2 H_0^2 (\sigma/c^2) a^3 \mathbf{v}, \quad (84)$$

and for a sphere of perfect electrical conductivity

$${}^i\mathbf{F} = (2\pi/5)(\sigma/c^2) H_0^2 a^3 \mathbf{v}. \quad (85)$$

Since the expressions (84) and (85) are derived on the assumption of no shielding, their validity depends essentially on the magnetic Reynolds number.

Jeffimenko (19) has considered a similar problem of greater practical interest. He calculates the induction drag of a conducting spherical shell, of inner and outer radii  $b$  and  $a$  moving in a circular orbit in the geomagnetic equatorial plane. The induced electric currents are given by Eq. (70) where the electric field  $\mathbf{E}$  is derived from a scalar potential  $\varphi$  such that

$$\mathbf{E} = -\text{grad } \varphi. \quad (86)$$

The potential  $\varphi$  is finite at the center of the sphere, vanishes at infinity and satisfies the Laplace equation

$$\nabla^2 \varphi = 0. \quad (87)$$

The electric currents are continuous at the boundaries  $r=a$  or  $b$ . On assuming that the induced currents do not affect the magnetic field, he obtains for the induction drag

$${}^i\mathbf{F} = \frac{8\pi}{3} \left( \frac{\sigma\sigma'}{c^2} \right) \frac{a^3 B^2}{(2\sigma + \sigma') + 3\sigma b^3/(a^3 - b^3)} \mathbf{v}, \quad (88)$$

where  $\mathbf{B}$  is the magnetic induction and  $\sigma'$  is the electrical conductivity of the sphere. For a solid sphere ( $b \rightarrow 0$ ) this becomes

$${}^i\mathbf{F} = \frac{8\pi}{3} \left( \frac{\sigma\sigma'}{c^2} \right) \frac{a^3 B^2}{(2\sigma + \sigma')} \mathbf{v}. \quad (89)$$

On making a further assumption that  $\sigma' \gg \sigma$ , these expressions reduce to

$${}^i\mathbf{F} = (8\pi/3)(\sigma/c^2) a^3 B^2 \mathbf{v} \quad (90)$$

which<sup>6</sup> is independent of the conductivity of the sphere and thickness of the shell provided that  $\delta \gg \sigma/\sigma'$ . Here  $b/a \sim (1-\delta)$  and  $\delta$  is a small number ( $<1$ ). The induction drag is apparently due to currents induced only in the surrounding medium. In this respect alone, this case would correspond to the infinite conductivity of the sphere. For an extremely thin shell with  $\delta \ll \sigma/\sigma'$ , the induction drag is given by

$${}^i\mathbf{F} = (8\pi/3)(\delta\sigma'/c^2) a^3 B^2 \mathbf{v}. \quad (91)$$

The induction drag in this case is extremely small. The assumption  $\sigma' \gg \sigma$  is appropriate for the motion of

<sup>6</sup> The digit 3 in the denominator of Eq. (20) of the original reference (19) should be omitted.

satellite bodies in the terrestrial atmosphere or interplanetary or interstellar space.

### C. Rotational Induction Drag of a Sphere

In the preceding section we considered the spin-free motion of a spherical body in a conducting atmosphere with a suitably oriented magnetic field of constant strength along the path. In this section we discuss the simple rotation of a spherical body in a conducting medium in the presence of a magnetic field.

Chopra (13) estimated the rotational induction drag of (i) a magnetized sphere of radius  $a$  and uniform magnetic intensity  $\mathbf{H}_0$  rotating with angular velocity  $\boldsymbol{\omega}$  about an axis coinciding with a diameter parallel to  $\mathbf{H}_0$  in an inviscid fluid of electrical conductivity  $\sigma'$ , and (ii) a sphere of radius  $a$  and of electrical conductivity  $\sigma$  rotating with angular speed  $\boldsymbol{\omega}$  in a nonviscous fluid of electrical conductivity  $\sigma'$  with a pervading magnetic field  $\mathbf{H}_0$  such that the axis of rotation coincides with the diameter parallel to  $\mathbf{H}_0$ .

Both these cases amount essentially to the rotation of a magnetic dipole of appropriate moment in a conducting medium. The electric currents are induced in the surrounding medium as well as inside the sphere, and the rotational induction drag is calculated by equating the rate of loss of kinetic energy to the rate of Joule dissipation of the induced electric currents. On assuming that shielding effects are absent, he finds for the rotational induction moment

$$\mathbf{D} = 2\pi(\sigma/c^2) H_0^2 a^5 \boldsymbol{\omega}, \quad (92)$$

provided that  $\sigma = \infty$  in case (ii). If, however,  $\sigma'$  is finite, the currents are induced inside the sphere also, and we have

$$\mathbf{D} = 8\pi H_0^2 (\mu+2)^{-2} \left[ (9/10)(\sigma'/c^2) + (\mu-1)^2 (\sigma/c^2) \right] a^5 \boldsymbol{\omega}. \quad (93)$$

### D. Comparison with Viscous Drag. Decay Time

The corresponding Stokes expressions for viscous drag are

$${}^s\mathbf{F} = 6\pi\eta a \mathbf{v} \quad (94)$$

and

$${}^s\mathbf{D} = 8\pi\eta a^3 \boldsymbol{\omega}, \quad (95)$$

where  $\eta$  is the coefficient of viscosity of the medium. A comparison of the two kinds of drags leads to the following:

(1) Both the viscous and induction drags are proportional to velocity.

(2) The expression  $(\sigma/c^2) H_0^2 a^2$  has the dimensions of the coefficient of viscosity and may be called the electromagnetic or inductive viscosity.

(3) The dependence of the numerical factors in the expressions for induction drags on the orientation of the dipole with respect to the direction of motion is sug-

gestive of the anisotropic nature of the electromagnetic viscosity. This anisotropy is brought about by the fact that the magnetic pressure is a tensor.

(4) The electromagnetic viscosity is dominant over the ordinary viscosity when

$$H_0^2 a^2 (\sigma/c^2 \eta) > 1. \quad (96)$$

(5) Under the action of induction drag alone, the kinetic energy of the sphere decays as  $\epsilon^{-t/\tau}$ , where

$${}^i\tau \sim (c^2/\sigma)(Ma^3/\nu^2) \sim N(c^2\rho/\sigma H_0^2) \quad (97)$$

with  $N$  as a constant factor of the order of  $16\pi/3$ , is the characteristic decay time.

These expressions for drag and the decay time are true only for small magnetic Reynolds numbers. In other words, these formulas apply to small bodies of a suitable size compatible with the velocity and electrical conductivity. They are certainly not applicable to bodies of cosmical dimensions. For example, consider a stellar body moving in interstellar space. On adopting the values

$$M \sim 10^{33} \text{ g}, \quad a \sim 10^{11} \text{ cm}, \quad \nu \sim 10^{33} \text{ emu}, \quad \sigma/c^2 \sim 10^{-10} \text{ cgs},$$

we have for the decay time  ${}^i\tau \sim 100$  years. This value of  ${}^i\tau$  is too small compared to the age of the universe. We could partly overcome this difficulty by assuming that there is no relative motion between the body and a part of the fluid surrounding it to the extent of a radius, say  $a'$ . The evidence for such a point of view is not entirely lacking in astrophysics; the outer solar corona has a radius  $a' \sim 10a$ . According to the foregoing calculations, if  ${}^i\tau$  is of the order of  $10^{10}$  years, then  $a'$  must be of the order of  $1000a$ .

### E. Sphere in a Viscous Fluid

The comparison of the viscous and the induction drags may not be carried too far. The two effects are not additive as might appear at first. In fact, according to Liepmann (18) the solution of the Stokes problem in a weak magnetic field cannot be obtained by a regular perturbation procedure starting from the known solution for the flow with  $\mathbf{B}=0$ . In support of this hypothesis, he gives two plausible reasons:

(1) If the electrical conductivity of the fluid is finite, Joule losses of the induced electric currents take place. The energy dissipated as heat is given by

$$Q = \frac{\sigma}{c^2} B^2 \int_0^\infty \int_0^\infty r v_r^2 dr dz \quad (98)$$

(in cylindrical coordinates). If the Stokes solution ( $\mathbf{B}=0$ ), viz.,  $v_r \sim 1/r^2$ , is inserted in this equation, the integral diverges at infinity, and therefore  $Q$  is indeterminate for a vanishing magnetic field and infinite for any finite value of  $\mathbf{B}$ , however small.

(2) Again, for a finite value of  $\mathbf{B}$ , however small, the character of flow at large distances departs from the

zero-field flow. This readily follows from the radial momentum equation (cylindrical coordinates)

$$\eta \nabla^2 v_r = [(\eta/r^2) + (\sigma B^2/c^2)] v_r + (\partial p/\partial r). \quad (99)$$

For every finite value of  $\mathbf{B}$ , there exists a distance  $r$  such that

$$\eta/r^2 \ll \sigma B^2/c^2. \quad (100)$$

Thus there exist two kinds of flow fields. If we define a distance  $L$  as

$$L \sim (c^2 \eta / \sigma B^2)^{1/2}, \quad (101)$$

then for  $r < L$ , the first term within the brackets on the right-hand side of Eq. (99) dominates the second and the flow velocity decreases as the inverse square of distance. For large distances,  $r > L$ , the second term is bigger than the first and we have an exponential decay of the velocity field with distance.

Chester (17) calculates the drag experienced by a sphere while an incompressible fluid of conductivity  $\sigma$ , and coefficient of viscosity  $\eta$  flows past it in the presence of a uniform magnetic field parallel to the flow velocity. The fluid as well as the sphere is assumed nonmagnetic so that the magnetic field is uniform throughout while the flow velocity is uniform at infinity and vanishes at the sphere. On assuming that the Reynolds number of the flow and the magnetic Reynolds number are small, and both the electrostatic and electromagnetic shielding effects are absent, he finds that the drag is given by

$${}^i\mathbf{F} = 6\pi\eta a \mathbf{v} [1 + \frac{2}{3}N_H + (7/960)N_H^2 + \dots], \quad (102)$$

where

$$N_H = Ba(\sigma/c^2 \eta)^{1/2} \ll 1 \quad (103)$$

is the Hartmann number. In the first instance, the linear term in  $\mathbf{B}$  in Eq. (102) is surprising. Following his ideas on the separation of flow characteristics at a distance  $L$ , Liepmann explains the phenomenon as due to the simulation of a cylindrical wall of radius  $L$  surrounding the fluid flow with the accompanying increase in drag of the flow by a factor of the order of

$$[1 + \text{constant}(a/L)].$$

### F. Sphere in a Strong Magnetic Field

Stewartson (15) has considered the motion of a perfectly conducting ( $\sigma' = \infty$ ) sphere of radius  $a$  in an inviscid and incompressible fluid of uniform conductivity  $\sigma$  and permeability  $\mu$  in the presence of a strong magnetic field  $\mathbf{H}_0$ . Displacement currents are neglected, and it is assumed that the electrostatic shielding is absent. Then the basic equations

$$\text{curl } \mathbf{H} = (4\pi/c)\mathbf{j}, \quad \text{curl } \mathbf{E} = -(\mu/c)(\partial \mathbf{H}/\partial t) \quad (104)$$

and

$$\mathbf{j} = \sigma[\mathbf{E} + (\mu/c)\mathbf{w} \times \mathbf{H}]$$

reduce to

$$\partial \mathbf{H}/\partial t = \text{curl}(\mathbf{w} \times \mathbf{H}) + (c^2/4\pi\mu\sigma)\nabla^2 \mathbf{H}, \quad (105)$$

where  $\mathbf{w}$  is the flow velocity in contrast to the velocity



$\mathbf{v}$  of the sphere. Again we may write

$$\mathbf{H} = \mathbf{H}_0 + \mathbf{h}, \quad (106)$$

where  $\mathbf{h}$  is the change caused in the magnetic field  $\mathbf{H}_0$  by the magnetohydrodynamic coupling. It is assumed that  $\mathbf{h}$  and  $\mathbf{w}$  are small and their products, squares and higher powers may be neglected. Subject to the condition

$$\text{div } \mathbf{w} = 0 = \text{div } \mathbf{h}, \quad (107)$$

the fields  $\mathbf{h}$  and  $\mathbf{w}$  are given by

$$(\partial \mathbf{h} / \partial t) - H_0 (\partial \mathbf{w} / \partial z) = (c^2 / 4\pi\mu\sigma) \nabla^2 \mathbf{h}$$

and

$$(\partial \mathbf{w} / \partial t) - (\mu H_0 / 4\pi\rho) (\partial \mathbf{h} / \partial z) = -\text{grad } \varphi, \quad (108)$$

where

$$\varphi = (p/\rho) + (\mu H_0 h_z / 4\pi\rho) \quad (109)$$

( $h_z$  being the  $z$  component of  $\mathbf{h}$ ) is the scalar potential.

The boundary conditions require that the normal component of  $\mathbf{h}$  and the tangential component of  $\mathbf{E}$  must be continuous at the surface of the sphere, and that the fluid and the electromagnetic fields remain undisturbed at infinity. The solutions are obtained for two cases according as the sphere moves in a direction parallel or perpendicular to the magnetic field;  $\mathbf{H}_0$  being directed along the  $z$  axis of a coordinate system with origin at the center of the sphere.

In the case when the sphere moves along the  $z$  axis (parallel to  $\mathbf{H}_0$ ), there is a cylindrical symmetry and all dependent variables are functions of  $r$  and  $z$ . For the ultimate solution ( $t \rightarrow \infty$ ), we have for  $r < a$

$$\omega_r \sim \left[ \frac{a}{t} \left\{ \frac{v^2}{(\mu H_0^2 / 4\pi\rho)^{1/2}} \right\} \right]^{1/2} \propto t^{-3/2},$$

$$\omega_z \rightarrow v$$

at  $r = a$

$$\omega_r \sim \left[ \left( \frac{\mu H_0^2}{4\pi\rho} \right)^{1/2} \frac{t}{a} \right]^{-1/2} \propto t^{-1/2},$$

$$\omega_z \sim \left[ \frac{\mu^2 H_0^2 a^2 t}{\rho c^2 z^2} \right]^{1/2} v \propto \frac{t^{1/2}}{z^{1/2}},$$

$$\rightarrow 0 \text{ as } z \rightarrow \infty$$

and for  $r > a$

$$\omega_r \sim \left[ \frac{a}{t} \frac{v^2}{(\mu H_0^2 / 4\pi\rho)^{1/2}} \right]^{1/2} \propto t^{-3/2},$$

$$\omega_z \sim \frac{av}{\pi r} \left[ \frac{3r^2}{a^2} \sin^{-1} \left( \frac{a}{r} \right) - \frac{3r^2 - a^2}{a(r^2 - a^2)^{1/2}} \right],$$

and  $E_\theta \propto t^{-3/2}$  and  $h \propto t^{-1/2}$  for all values of  $r$  and large  $t$ .

The ultimate flow and the electromagnetic fields are extremely simple. The resultant flow consists entirely of a velocity in the direction of motion of the sphere. A cylinder of fluid ( $r = a$ ) is pushed along in front of the sphere and behaves as if the fluid were solid. Outside

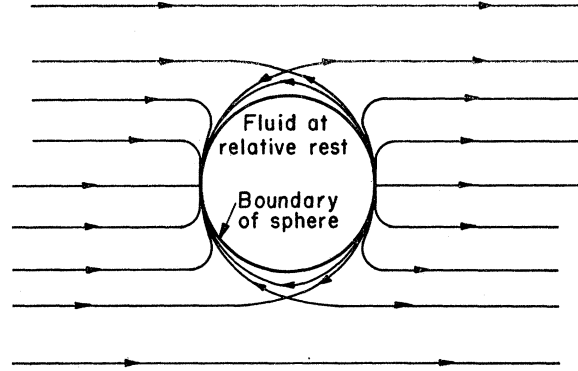


FIG. 1. Ultimate relative streamlines when the sphere moves in the  $X$  direction.

the cylinder ( $r > a$ ) the fluid moves parallel to the generators of the cylinder with a velocity which is singular at the cylinder ( $r = a$ ) and tends to zero as  $r \rightarrow \infty$ . The singularity at  $r = a$  can be removed by introducing nonlinear and viscous terms near  $r = a$ . The velocity inside the cylinder is independent of  $z$ , and there is ultimately no force on the sphere and the electromagnetic field is uniform and the same as before the motion began. (See Fig. 1.)

In the other case discussed by Stewartson, the sphere moves in a direction normal to the magnetic field  $\mathbf{H}_0$ . The cylindrical symmetry of the flow and the electromagnetic fields about the  $Z$  axis is destroyed, and hence the solutions are azimuth dependent. For the ultimate motion ( $t \rightarrow \infty$ ) we may expect that on a cylinder ( $r = a$ ) the several physical quantities will increase indefinitely just as in the preceding case of parallel motion. Excluding points on this cylinder, the velocity field has the following characteristics:

$$\omega_z \rightarrow 0 \text{ for all values of } r$$

$$\omega_r \propto (av/r) \cos\vartheta \text{ (for } r < a),$$

$$\propto \frac{av}{\pi r} \cos\vartheta \left[ \frac{3r^2}{a^2} \sin^{-1} \left( \frac{a}{r} \right) - \frac{3r^2 - a^2}{a(r^2 - a^2)^{1/2}} \right] \text{ (for } r > a)$$

$$\omega_\theta \propto (a/r) \tan\vartheta (\partial/\partial r)(r\omega_r). \quad (111)$$

Hence, the final velocity field is two dimensional and the streamlines lie in planes perpendicular to the magnetic field. Inside the cylinder ( $r < a$ ), the fluid is at rest relative to the sphere; at the cylinder ( $r = a$ ) it is singular; and outside the cylinder ( $r > a$ ), it dies away as  $r \rightarrow \infty$ . The field  $\mathbf{h}$  is ultimately zero.

These results imply that if a sphere is moving steadily through a conducting fluid in the presence of a strong magnetic field, the steady motion of the fluid which results is two dimensional, i.e., there is no variation in velocity components along the direction of the imposed field  $\mathbf{H}_0$ , and the magnetic field is not affected by the motion of the sphere provided that the ordinary Reynolds number of flow is large, the magnetic Reynolds

number is small, and the magnetic force dominates the inertial terms. In the specific case of liquid mercury with

$$\eta \sim 10^{-2} \text{ cgs}, \quad \rho \sim 13.6 \text{ g/cc}, \quad \sigma/c^2 \sim 10^{-5} \text{ cgs}$$

and

$$H \sim 10^4 \text{ gauss},$$

we must have  $v \ll 10^3$  cm/sec, and the size of the sphere must lie in the range  $10^{-6}$  cm  $< a < 10$  cm.

### G. Large Magnetic Reynolds Number

In contrast to the problems discussed in the preceding sections, Michael (65) considers a case which falls under the category of problems where a body moving through a conducting fluid medium encounters a distribution of magnetic field associated with the fluid in which case it is required to find the deformation of the field due to the passage of the body. He considers a two-dimensional problem of the flow of an incompressible fluid of uniform electrical conductivity  $\sigma$ , permeability  $\mu$ , and coefficient of viscosity  $\eta$ , past a cylinder with its axis oriented in a direction normal to the magnetic lines of force. It is assumed that there is no polarization of the fluid and therefore electrostatic shielding is absent. Displacement current is also neglected. The flow is supposed to take place at large magnetic Reynolds numbers. This implies that the convection and stretching of magnetic lines of force are more important than the diffusion of the magnetic field.

If the analogy between the equation of  $\mathbf{H}$  and vorticity is followed, then the solution may be obtained on the assumption that, except in a boundary layer around the surface, the fluid acts as a perfect conductor in which the lines of force follow the motion of the conductor. This means that the magnetic field is small enough for the effect of the electromagnetic stress in the fluid to be neglected. Consequently, the pure hydrodynamic motion of the fluid is not affected. In the boundary layer, however, diffusion of the magnetic field is important. If it is further assumed that

$$\eta \ll c^2 \rho / 4\pi\mu\sigma, \quad (112)$$

the magnetic boundary layer is expected to be much wider than the viscous boundary layer. Therefore, for the purposes of the study of the magnetic boundary layer, the flow may be treated as nonviscous.

The cylinder is assumed to be a perfect conductor. This simplifies the problem because the magnetic field cannot diffuse through it. A steady magnetic boundary layer is built up and maintained by a balance between the diffusive decay of the magnetic field and the conversion of mechanical energy into magnetic energy by a process of stretching of magnetic lines by the fluid. The total flux crossing the cylinder remains constant throughout the motion. Because of the large magnetic Reynolds number, all lines of force are carried by the fluid to within a boundary layer width of the surface of the cylinder. Let us take the axes  $XOY$  at this point

with  $OX$  being normal to the surface pointing upstream and  $OY$  being tangential, and assume that at  $t=0$ , a bandwidth  $X$  (from  $x=0$  to  $x=X$ ) contains a field of uniform strength  $\mathbf{H}_0$  in the direction of  $y$ . In a time  $t$  determined from

$$X \exp[-(\kappa^2 c^2 / 4\pi\mu\sigma)t] \sim 1/\kappa \quad (113)$$

(where  $\kappa$  is the dielectric constant) the bandwidth  $X$  is converted into the boundary layer width of the order of  $1/\kappa$ . In other words, the field distribution takes a time  $t$  given by Eq. (113) to settle to a steady state. The ultimate ( $t \rightarrow \infty$ ) magnetic field is given by

$$\mathbf{H}(x) = \mathbf{H}_0 X (2\kappa^2/\pi)^{1/2} \exp(-\frac{1}{2}\kappa^2 x^2) \quad (114)$$

which shows that the ultimate state depends only on the total flux  $\mathbf{H}_0 X$  and not on the particular initial distribution of  $\mathbf{H}_0$ .

Further, the boundary layer analysis shows that in a boundary layer region of thickness

$$\delta \sim a/(R_\lambda)^{1/2}, \quad (115)$$

where  $a$  is the radius of the circular cylinder, and  $R_\lambda$  is the magnetic Reynolds number, the radial and azimuthal components of the magnetic field are

$$H_r \sim H_0/(R_\lambda)^{1/2} \quad \text{and} \quad H_\theta \sim H_0(R_\lambda)^{1/2}, \quad (116)$$

respectively. Since the magnetic Reynolds number  $R_\lambda$  is considered large, the tangential component  $H_\theta$  of the magnetic field is the predominant component, and is a measure of the field concentration. As we go round the cylinder from the stagnation point, the concentration of the field is proportional to the product of the tangential velocity  $v_t$  and the difference between the value of the velocity potential  $\varphi$  at the point under consideration and the corresponding value  $\varphi_0$  at the stagnation point. Adopting polar coordinates  $(r, \vartheta)$  with  $\vartheta=0$  in the upstream direction, we have for a circular cylinder

$$v_t \propto \sin\vartheta, \quad \text{and} \quad (\varphi - \varphi_0) \propto (1 - \cos\vartheta)^{-1/2}.$$

Hence the field concentration is proportional to  $\cos(\vartheta/2)$ .

### H. Tumble of a Body in a Magnetic Field

A relatively less known but important work of Vinti (16) shows that the interaction between the induced electric currents and the pervading magnetic field may produce a torque tending to turn the axis of rotation of a body. He considers the spin of a hollow nonferromagnetic spherical shell of electrical conductivity  $\sigma'$ , and inner and outer radii  $b$  and  $a$  with angular velocity  $\omega$  about a fixed axis in a vacuum in the earth's magnetic field. Since the electromagnetic readjustments take place more rapidly than the mechanical ones, the problem can be separated into two parts: (i) electromagnetic problem in which a shell is considered to be rotating with constant angular velocity, and (ii) a mechanical problem in which the moment deduced from

the electromagnetic problem is applied to calculate the actual motion.

To a first approximation, the earth's magnetic field is considered uniform and constant, and eddy currents due to the orbital motion are neglected. The assumption that the ionosphere is to be treated like a vacuum is another serious limitation. The deduced electromagnetic torque refers to its instantaneous value equal to that which would arise from steady rotation in a constant magnetic field. The moment of the torque is given by

$${}^i\mathbf{D}_v = (I/4\rho_s)(\sigma'/c^2)(\boldsymbol{\omega} \times \mathbf{H}) \times \mathbf{H}, \quad (117)$$

where  $\rho_s$  is the density of the shell and  $I$  is the moment of inertia of the shell about any diameter. This moment has two components

$${}^iD_v(\text{decay}) = (I/4\rho_s)(\sigma'/c^2)\omega H_{\perp}^2, \quad (118)$$

tending to diminish the angular velocity, and

$${}^iD_v(\text{tumble}) = (I/4\rho_s)(\sigma'/c^2)\omega H_{\perp}H_{\parallel}, \quad (119)$$

tending to turn the axis of rotation. Here,  $H_{\perp}$  and  $H_{\parallel}$  are the components of  $\mathbf{H}$  perpendicular and parallel to  $\boldsymbol{\omega}$ , respectively.

The decay component of the moment vanishes only when  $H_{\perp}=0$ , i.e., when  $\mathbf{H}$  is parallel to  $\boldsymbol{\omega}$ . The component responsible for the tumble of the axis of rotation is zero if either (i)  $H_{\perp}=0$ , i.e.,  $\mathbf{H}$  is parallel to  $\boldsymbol{\omega}$  or (ii)  $H_{\parallel}=0$ , i.e.,  $\mathbf{H}$  is perpendicular to  $\boldsymbol{\omega}$ . For any other orientation of  $\mathbf{H}$  with respect to  $\boldsymbol{\omega}$ , the tumble component of the moment is nonzero.

In solving the mechanical problem he considers the satellite as composed of a conducting nonferromagnetic hollow sphere containing instrumentation of small moment of inertia near its center and having attached to it two similar line antennas along two perpendicular diameters. It is then a symmetrical top with axis of symmetry along a diameter perpendicular to the two antennas.

As the satellite moves through the magnetic field of the earth, its axis of rotation will continually change direction because of the turning torque. The satellite thus acquires a component of angular velocity perpendicular to its axis of symmetry, in addition to its angular velocity  $\boldsymbol{\omega}_s$  of spin along the latter. The dynamical equation for  $\boldsymbol{\omega}_s$  is a nonlinear differential equation which, in the event of the initial angular velocity being along the axis of symmetry, reduces to a simple form

$$I'(d\boldsymbol{\omega}_s/dt) = (I\sigma/4\rho_s c^2)\boldsymbol{\omega}_s \times \mathbf{H} \times \mathbf{H}, \quad (120)$$

where  $I'$  is the total moment of inertia of the satellite about its axis of symmetry. In this circumstance the perpendicular component of angular velocity remains negligible compared to  $\boldsymbol{\omega}_s$  for all times of interest in the motion of the satellite. A conservative estimate of the interval of interest for a satellite moving in a circular orbit at an altitude of 320 km is 25 days for  $I'=1.75I$ .

If the magnetic field remains constant along the orbit, the solution of Eq. (120) shows that the component of spin parallel to  $\mathbf{H}$  remains constant while the component perpendicular to  $\mathbf{H}$  diminishes exponentially with time. If  $\boldsymbol{\omega}_s$  initially has a component parallel or perpendicular to  $\mathbf{H}$ , the final orientation of  $\boldsymbol{\omega}_s$  is parallel or perpendicular to  $\mathbf{H}$ , respectively. The slightest departure of  $\boldsymbol{\omega}_s$  from initial perpendicularity to  $\mathbf{H}$  therefore starts  $\boldsymbol{\omega}_s$  turning towards one of the orientations of stable equilibrium which are parallel or perpendicular to  $\mathbf{H}$ .

The closest approximation to this situation is a circular equatorial orbit. Unless the initial spin is perpendicular or almost perpendicular to the equatorial plane (and thus to the plane of the orbit), the direction of the spin vector changes significantly in the course of the motion. This change is such as to make the spin vector ultimately point along or precess about the earth's axis of rotation. It is found that the component of spin in the equatorial plane diminishes as the exponential of  $[-(1+1.25\lambda^2)t/9.28]$ , while the component of spin perpendicular to this plane diminishes much more slowly as the exponential of  $[-2.5\lambda^2 t/9.28]$ , where  $t$  is the time measured (in sidereal days) from the instant of release of the satellite into its orbit, and  $\lambda=0.20345$  measures the inclination of the axis of the terrestrial magnetic dipole and the earth's axis of rotation. The corresponding decay times are 8.8 and 89.7 days, respectively.

## I. Conclusions and Discussion

The preceding sections have shown that the induced electric currents caused by the relative motion between a conductor and an external magnetic field lead to interesting phenomena depending on the physical properties of the conducting medium or of a body moving through it. These may be summarized as follows:

(1) A magnetic dipole moving in a conducting medium, or a conducting body moving in a conducting medium with a pervading magnetic field experiences an electromagnetic drag which is proportional to velocity. The term  $(\sigma/c^2)H_0^2 a^2$  has the dimensions of the coefficient of viscosity.

(2) The induction and viscous drags are not, however, additive. For example, the drag of a sphere moving in a viscous fluid across a transverse magnetic field contains a term which is linear in magnetic field. This is so because a simulated cylindrical wall of radius  $L \sim (c^2\eta/\sigma B^2)^{1/2}$  separates the flow characteristics. The flow velocity inside the cylinder decreases as the inverse square of distance while the decay outside the cylinder is exponential. This is the state of affairs for weak induced currents which neither alter the original magnetic field nor cause electrostatic charge separation, and the flow conditions correspond to low magnetic and viscous Reynolds numbers.

TABLE VII. Comparison of induction and neutral drag.  
 $a \sim 100$  cm,  $v_s \sim 8 \times 10^8$  cm/sec.

Altitude (km)	250	500	800
${}^iF/{}^nF$	0.04	65	$5 \times 10^8$
${}^i\tau$ (sec)	$1.3 \times 10^8$	$5 \times 10^7$	$2 \times 10^6$

(3) In the case of a strong magnetic field also, the flow characteristics are separated by a simulated cylinder but of radius equal to the radius of the cylinder. A cylinder of fluid of radius  $a$  is pushed along in front of the sphere and behaves as if the fluid were a solid. Outside the cylinder, the flow velocity decreases at infinity. There is ultimately no inductive force on the sphere. These results are expected for flow regimes characterized by low magnetic Reynolds numbers and high ordinary Reynolds numbers while the inertial forces are negligible compared to the magnetic force. Depending on the values of the physical parameters, these restrictions set limits on the velocity and size of the spherical body.

(4) When the magnetic Reynolds number is large, a magnetic boundary layer is formed which is wider than the viscous boundary layer if  $\eta < (c^2\rho/4\pi\mu\sigma)$ . The fluid may now be considered nonviscous. The steady state magnetic field distribution in the magnetic boundary layer has a predominant azimuthal component, which is inversely proportional to the square root of the magnetic Reynolds number and is azimuth dependent.

(5) The electric currents produced by the rotation of a conducting body in a magnetic field interact with the original magnetic field to produce a torque which has two components. One component tends to diminish the angular velocity and is absent only when the magnetic field is parallel to the angular velocity vector. The other tends to turn the axis of rotation and is nonzero unless the magnetic field is parallel or perpendicular to the angular velocity vector. Investigations on the spin of a spherical satellite in the equatorial plane indicate that the direction of the spin vector changes significantly, resulting in the spin vector ultimately pointing along or precessing about the earth's axis of rotation.

(6) Either one or both of the electromagnetic and electrostatic shielding phenomena, whichever present, results in the reduction of the induction drag with a corresponding increase in the decay time.

(7) The motion of the artificial earth satellites corresponds to a low magnetic Reynolds number. The linear or orbital induction drag of the satellite is due to (a) the decay of currents induced in the atmosphere, and (b) the tumbling caused by the electromagnetic torque produced by the currents induced inside the satellite. On ignoring the latter for the moment, the ratio of the induction to the neutral drag is given by

$${}^iF/{}^nF = (\sigma/\rho c^2)(H_0^2 a/v_s). \quad (121)$$

Some typical values of this ratio are given in Table VII.

Equation (121) shows that the relative importance of induction drag increases with the size of the body and the electrical conductivity of the medium. The toppling or tumbling of the satellite about a fixed axis may increase the neutral drag several times (Sec. II).

(8) Some critics raise an objection to the use of the macroscopic quantity electrical conductivity, when applied to the dynamics of bodies moving in the upper atmosphere of the earth, interplanetary or interstellar space. This objection is not as serious as it sounds. In terms of the effective collision frequency  $\nu_{ei}$ , the electrical conductivity may be written as

$$\sigma/c^2 \sim (e^2/m_e c^2) n_e \nu_{ei} \quad (122)$$

Expression (123) is independent of the charged particle density but shows a strong dependence on the temperature  $T$ . This is, however, approximate; and the conductivity has a logarithmic dependence on  $n_e$  [cf. expressions (24) and (25); also see Chap. V of (51)].

Jeffimenko (19) regards electrical conductivity as normally defined only for systems in which the mean-free-path of the charged particles is much smaller than the dimensions of the field inhomogeneities. The mean-free-path of ions and electrons is of the order of 25 cm and  $6.5 \times 10^8$  cm, respectively, corresponding to the charged particle density of  $2 \times 10^6$ /cc at 1500°K. In general, at least qualitatively, the mean-free-path of the charged particles is proportional to the charged particle density. Therefore, at very high altitudes, or in the interplanetary or interstellar space the mean-free-path is extremely large. If the linear dimension of the field inhomogeneity is characterized by the scale length of the body, then this criterion may justify the use of electrical conductivity for the motion of cosmical bodies in interstellar or interplanetary space. On the other hand, for bodies of the size of the artificial earth satellites at high altitudes in the upper atmosphere this criterion would make this concept of electrical conductivity invalid. Accordingly, the foregoing treatment must be regarded as a macroscopic approximation to the actual problem.

In order to find a meaning to the electrical conductivity one must then consider the interactions between the satellite and the surrounding particles. According to Jeffimenko, the satellite may be regarded as an electric dipole of moment  $4\pi a^3 v_s H/c$ , which constitutes a scattering center for the oncoming particles. The magnitude of the drag is then determined from the rate of momentum transfer to the satellite. Comparison with the induction drag, which is of the order of  $(\sigma/c^2) H_0^2 a^3 v_s$ , yields a value for the effective electrical conductivity. On neglecting the effect of the earth's magnetic field on the trajectories of the charged particles, the expression for the effective electrical conductivity approximates to

$$\sigma/c^2 \sim \Sigma(Z_i e)(n_i/cH), \quad (124)$$

where  $n_i$  is the number density of particles carrying a

charge  $Z_i e$ , and the symbol  $\Sigma$  takes account of different particles.

Expressions (122) and (123) for the electrical conductivity are, however, not comparable. They have strongly contrasting properties. While (122) demonstrates the dependence of  $\sigma/c^2$  on temperature, the relation (123) shows the dependence of  $\sigma/c^2$  on the magnetic field strength, charged particle density, and the amount of charge carried by each particle. For singly charged particles of density  $2 \times 10^6/\text{cc}$  in a magnetic field strength of 0.3 gauss, the effective electrical conductivity given by (123) is of the order of  $10^{-13}$  cgs units. On the other hand, expression (122) yields a value of  $10^{-10}$  cgs units corresponding to  $T \sim 1500^\circ\text{K}$ . These physical conditions correspond to an altitude of 300 km in the terrestrial atmosphere.

The ratio of the induction to neutral drag is given by

$${}^iF/{}^nF \sim (n_i/n)(Z_i e/m)(Ha/v_s c) \quad (125)$$

which for

$$Z_i \sim 1, \quad m \sim 10^{-23} \text{ g}, \quad H \sim 0.3 \text{ gauss}, \quad e \sim 4.8 \times 10^{-10} \text{ esu}, \\ c \sim 3 \times 10^{10} \text{ cm/sec}, \quad v_s \sim 8 \times 10^5 \text{ cm/sec}$$

reduces to

$${}^iF/{}^nF \sim 2 \times 10^{-4} a X, \quad (126)$$

where  $X = n_i/n$  is the charged to total particle density. Equations (124) and (125) indicate that the relative importance of the induction drag increases with the size of the body and the relative number of charged particles.

## VI. WAVE DRAG

### A. Introduction

The motion of a charged body in an ionized atmosphere with a pervading magnetic field may give rise to wave phenomena which may draw on the kinetic energy of the charged body. Studies in this connection were initiated by Chopra and Singer (27), Kraus and Watson (28), and Greifinger (33). Whereas the first theory deals with the excitation of extraordinary electromagnetic waves by the interaction between the charged body and the gyrating charged particles, the last two theories concern the generation of a collective disturbance of the charged particles. The works cited are of a very preliminary nature either lacking details and rigor or being unrealistic of the actual case, and hence are only suggestive of further investigation. In order to seek a better understanding of the wave phenomena associated with the motion of bodies in an ionized gas in the presence of an external magnetic field, it is essential first to take stock of the present knowledge of the excitation and properties of plasma waves.

### B. Waves in an Ionized Gas

A wide variety of oscillatory disturbances are possible in an ionized atmosphere with a pervading magnetic field. These disturbances are, in general, exceedingly

complex. Under ideal conditions, however, purely sinusoidal disturbances may be classified under three categories: (a) electromagnetic waves, (b) magneto-hydrodynamic waves, and (c) electrostatic waves. We first describe the properties of these waves.

#### (a) Electromagnetic Waves

The electromagnetic waves are essentially high-frequency transverse waves characterized by having the electric field vector  $\mathbf{E}$  of the wave transverse to the direction of propagation. For a two-dimensional case, the velocity of propagation in an ionized gas, in the absence of an external magnetic field, is given by

$$V_w^2 = c^2/[1 - (\omega_{pe}/\omega)^2] \quad (127)$$

where  $\omega_{pe} = (ne^2/\pi m_e)^{1/2} = 8.97 \times 10^3 n_e^{1/2}$  cps. The waves of a frequency less than the critical frequency  $\omega_{pe}$  are very highly damped; their amplitude falling to  $1/\epsilon$  times its initial value in a distance less than the wavelength in vacuum,  $d < c/\omega$ . This critical frequency is identified with the electron plasma frequency and is proportional to the square root of the electron density. Conversely, a wave of a given frequency does not propagate in a medium with electron density exceeding a certain value. The reason for the breakdown of the wave propagation is inherent in the interference of electrons with the high-frequency wave propagation. Here the time derivative of the electric field vector  $\mathbf{E}$  and the material current density  $\mathbf{j}$  have a phase difference of  $\pi$ , and hence the material current opposes the displacement current.

An external longitudinal magnetic field  $\mathbf{B}$  introduces an interaction term  $\mathbf{j} \times \mathbf{B}$  in a direction normal to both  $\mathbf{E}$  and  $\mathbf{V}_w$ . This term produces components of  $\mathbf{j}$  and  $\mathbf{E}$  transverse to their initial directions. Thus the magnetic field rotates the plane of polarization of the initially plane-polarized wave. In the case of a uniform magnetic field, the phase velocity is given by

$$V_w^2 = \frac{\omega(\omega \mp \omega_{ce})}{\omega^2 - \omega\omega_{ce} - \omega_{pe}^2}, \quad (128)$$

where  $\omega_{ce} = eB/2\pi m_e c$  is the electron cyclotron frequency. The minus and plus signs are to be adopted according as  $\mathbf{E}$  rotates in the same or opposite sense as the electrons gyrate, and the corresponding waves are called extraordinary and ordinary, respectively. The presence of a longitudinal magnetic field makes it possible for the waves of a frequency less than the critical frequency to propagate as long as the wave frequency is less than the electron cyclotron frequency.

Twiss and Roberts (66) point out that a fast electron rotating with velocity  $v_e \ll c$  in a plasma permeated by a uniform field radiates energy in both the ordinary and extraordinary modes but predominantly in the latter, because (i) the polarization of the extraordinary mode rotates in the same sense as does the radiating electron, (ii) the propagation constant of the extraordinary mode

near the gyro-frequency is very much greater than the propagation constant for the ordinary mode, and (iii) the ordinary mode can be excited appreciably over only a limited range of values of the direction angle.

Bleviss (67) has considered a problem of some practical interest. A body moving at a hypersonic speed causes ionization of the gas in its neighborhood. An electromagnetic wave passing through this region may suffer attenuation due to collisions or reflection thereby affecting its effective transmission. He finds that, for bodies moving at speeds up to about  $7.5 \times 10^5$  cm/sec and at altitudes up to 750 km, vacuum wavelengths of 1 mm and 1 m are necessary for transmission through the blunt-nose region and the high-speed boundary layer, respectively, provided the gas is in thermodynamic equilibrium.

### (b) Magnetohydrodynamic Waves

The magnetohydrodynamic waves are waves of low frequency—lower than the ion cyclotron frequency—produced by the term  $\mathbf{j} \times \mathbf{B}$  representing the interaction between the induced electric current density and the magnetic field, while the ions supply the inertia of oscillations. In the presence of a magnetic field, the medium behaves as if it possesses increased dielectric constant

$$\kappa = 1 + (4\pi\rho c^2/B^2), \quad (129)$$

where  $\rho/B^2$  is called the polarizability. The magnetohydrodynamic waves then resemble the electromagnetic waves with a phase velocity

$$V_w = c/\kappa^{\frac{1}{2}} = c/(1 + 4\pi\rho c^2/B^2)^{\frac{1}{2}}. \quad (130)$$

For large  $\rho/B^2$ , the phase velocity  $V_w$ , Eq. (130), reduces to the well-known Alfvén speed (68),  $\mathbf{B}/(4\pi\rho)^{\frac{1}{2}}$  along the magnetic field. If the wave propagation is along a direction inclined to the magnetic field, the component of  $\mathbf{B}$  along the direction of propagation determines the phase velocity. These waves are excited by an initial displacement of the material in a direction perpendicular to  $\mathbf{B}$ . For any significant propagation of these waves, the medium must be a good electrical conductor.

In a rare ionized gas, the mean free path of ions and electrons may be much greater than their radii of gyration, and the assumption regarding perfect electrical conductivity may then require reexamination. Ferraro (69) has investigated this problem. For an ionized gas with equal electron and ion density  $n$ , he finds a dispersion relation

$$(\omega - \omega_{ce})(\omega + \omega_{ci})(\omega^2 - k^2 c^2) = (ne^2/\pi)(1/m_e + 1/m_i)\omega^2, \quad (131)$$

where  $k = 1/\lambda$  is the wave number. This relation shows that magnetohydrodynamic waves with phase velocity

$$V_A = \mathbf{B}/[4\pi n(m_e + m_i)]^{\frac{1}{2}} \quad (132)$$

are possible in a rare ionized gas provided that the wave

frequency is less than the electron cyclotron frequency and is such that  $\omega^2 \ll \omega_{ce}\omega_{ci} \ll \omega_p^2$ , and the phase velocity is less than the speed of light. In other words, we must have  $B^2 \ll 4\pi n(m_e + m_i)c^2$  showing thereby that the waves can be excited only if the magnetic field is small compared to the critical field  $B_c = [4\pi n(m_e + m_i)c^2]^{\frac{1}{2}}$ . Here the plasma frequency  $\omega_p$  is defined as  $[(ne^2/\pi) \times (1/m_e + 1/m_i)]^{\frac{1}{2}}$ . Further, for  $\omega \ll \omega_{ce}$  the medium behaves as if it were a perfect conductor. For a vanishing magnetic field, however, Eq. (131) reduces to  $k^2 c^2 = \omega^2 - \omega_p^2$  indicating that only wave frequencies exceeding the plasma frequency can propagate.

### (c) Electrostatic Waves

The electrostatic waves are essentially longitudinal waves characterized by having the electric vector  $\mathbf{E}$  oriented parallel to the direction of propagation. The introduction of electric fields by an external disturbance or by incomplete space-charge neutralization excites these waves, which may be separated into two classes according as the electrons or ions take part in oscillations. Here, the electrostatic fields provide the restoring forces while the charged particles provide the inertia.

The ion oscillations are essentially of low frequency, whereas the electron oscillations are characterized by high frequencies. In the absence of random thermal motions, the characteristic frequencies are given (70) by

$$\omega_{pi} = (ne^2/\pi m_i)^{\frac{1}{2}} \quad \text{and} \quad \omega_{pe} = (ne^2/\pi m_e)^{\frac{1}{2}},$$

respectively. These oscillations are localized and their wavelength must exceed the Debye length  $\lambda_D$ . If random thermal motions are taken into account, the respective dispersion relations (70–74) become

$$\omega^2 = \omega_{pi}^2 / (1 + \lambda^2 / 4\pi^2 \lambda_D^2) \quad (134)$$

and

$$\omega^2 = \omega_{pe}^2 + \alpha(kT_e m_e)k^2, \quad (135)$$

where  $\alpha = 3$  and  $5/3$  in one- and three-dimensional cases, respectively. Equations (134) and (135) demonstrate the dependence of  $\omega$  on  $k$ , and hence these waves are of the traveling type. It is only at extremely low temperatures that approximately localized waves prevail. Further, for  $\lambda \ll 2\pi\lambda_D$ , the ion-plasma waves cease to resemble electron-plasma waves, and behave like sound waves; their group and phase velocities approaching a constant limit  $3.9 \times 10^5 (T_e m_e / m_i)^{\frac{1}{2}}$ .

The most acceptable theory at the moment is due to Bohm and Gross (76) in which each electron moves in the smoothed-out field of all the other particles. This assumption requires that the wavelength must exceed the interparticle distance. In a coordinate system moving with the wave, the wave potential

$$\varphi = \varphi_0 \exp i(\mathbf{k} \cdot \mathbf{x})$$

is static. The response of each electron to the potential  $\varphi$  depends on its being fast or slow. Fast electrons with

sufficient energy are carried over the crests of the potential waves and are free, whereas the slow electrons get trapped in between the crests of the wave. The former contribute to the space charge which produces the potential but do no net work. The latter, on the other hand, are reflected back and forth from each potential crest and exert a pressure so that in the laboratory system the wave does work on the slow electrons. Each particle suffers a wavelike perturbation in its velocity which is larger for particles moving in the direction of the wave than for those moving in the opposite direction. This results in the damping of the wave. The effect of the increase in the number of trapped particles is to reduce the wave velocity. In the special case of no thermal motion, we obtain

$$V_w^2 = (\omega/k)^2 = \omega_p^2 / \{1 + [4\pi en_1/k^2(\varphi_1 - \varphi_2)]\}, \quad (136)$$

where  $n_1$  is the trapped electron density; and  $\varphi_1$  and  $\varphi_2$  are the potentials at the top and the bottom of the trough.

In general, it is possible to excite an oscillation with arbitrary  $\omega$ , for a given  $\mathbf{k}$ , as long as  $\omega/k$  is less than the maximum electron velocity. But those waves, not given by the steady-state dispersion relation, get out of phase with each other in a time of the order of  $\lambda/\pi r$ , where  $r$  is the range of electron velocities. A beam of fast particles near the wave velocity may excite plasma oscillations while a slow beam causes damping. In the presence of a beam of velocity  $v_b$  and plasma frequency  $\omega_b$ , corresponding to the beam-electron density  $n_b$ , dispersion relation (74, 75) is

$$[\omega_p^2/(\omega^2 - k^2v^2)] + [\omega_b^2/(\omega - kv_b)^2] = 1. \quad (137)$$

Lampert (75) finds that the stationary plasma waves grow for beam velocities less than a critical value  $v_b^c = [1 + 0.5(n_b/n)^{1/2}]^{1/2}(\omega_p/k)$  with a maximum growth occurring at a velocity equal to  $[1 - 0.4(n_b/n)^{1/2}]^{1/2}(\omega_p/k)$ . Similarly, traveling waves of lengths shorter than a critical length  $\lambda^c = \lambda_b(v/v_b)^{1/2}(n/n_b)^{1/2}$  grow, the maximum amplification occurring at  $\lambda = 1.7\lambda_b(v/v_b)^{1/2}(n/n_b)^{1/6}$ . Coulomb collisions leave the ordered wave motion unaltered, whereas the close collisions dampen the waves in a time of the order of mean collision time exceeding the period of plasma oscillations. For most problems of interest, collision damping is not very serious. A more serious problem is the scattering of electrons out of the primary beam, resulting in inefficiency of the growth, the growth factor varying as  $s = s_0(n_b/n_{b,0})$ . Similarly, a wave propagating in a medium with decreasing density has a tendency to grow and the one in a medium with increasing density has a tendency to decay. Imperfect reflection at a sheath of finite thickness also contributes to damping.

Plasma oscillations exhibit a complicated behavior (76-79, 83) in the presence of a magnetic field. A new feature is the existence of the gaps (76, 79) in the frequency spectrum at multiples of electron-cyclotron frequency; the gap width being proportional to tempera-

ture (79) and not to its square root (76). The appearance of gaps has been interpreted in terms of selective reflection of waves incident on a plasma with a frequency in the forbidden range. Subject to the condition  $k\epsilon \ll \omega_{ce} \ll \omega_{pe}$ ,

$$\omega^2 = \omega_{pe}^2 + c^2k^2 + (\omega_{pe}^2\omega_{ce}^2/c^2k^2) \quad (138)$$

and longitudinal plasma oscillations

$$\omega^2 = \omega_{pe}^2 + \omega_{ce}^2 + \beta(kT/m\omega_{ce}^2) \quad (139)$$

with  $\beta$  as a function of  $\omega_{pe}$  and  $\omega_{ce}$  (at low temperatures or strong magnetic field), and

$$\omega^2 = \omega_{pe}^2 + \omega_{ce}^2 + 3kT(k^2/m) + 9(\omega_{ce}^2/\omega_{pe}^2)(kT/m)k^2 \quad (140)$$

(at high temperatures or weak magnetic field) are possible. The effects of random thermal motions and magnetic field are coupled in the second-order term in Eq. (140). Stix (80) considered cylindrical symmetric waves of frequency  $\omega \ll (\omega_{pi}^2 + \omega_{ci}^2)^{1/2}$  and found that the waves of lengths shorter than the vacuum wavelength  $\lambda_0$  are the extraordinary and ordinary magneto-hydrodynamic waves of Alfvén (81) and Åström (52). For  $\lambda > \lambda_0$ , the extraordinary wave has a natural frequency close to  $\omega_{ci}$ . More recently, Chang (82) obtained a complicated dispersion relation which assumes simplified forms at low and high frequencies. The low-frequency waves are of the Alfvén and magnetoacoustic types (long wavelength) and gyromagnetic ion waves (short wavelength). At high frequencies subject to the condition  $\omega \ll (\omega_{pi}^2 + \omega_{ci}^2)^{1/2}$ , both the long and short waves contain the plasma and transverse ordinary and extraordinary electromagnetic modes.

Next we consider the (d) space-charge waves produced by interpenetrating ionized streams, and (e) collective motions induced by the long-range Coulomb fields.

#### (d) Space-Charge Waves

The interpenetration of two ionized streams moving with velocities  $\pm v$  causes an instability of the resulting plasma. As a result, the counterstreaming is arrested (83) in a distance of the order of  $\lambda_{\min} \sim (\pi m_0 v^2 / 2ne^2)^{1/2}$  compared to  $2m_0^2 v^4 / \pi ne^4$  due to collisions. The steady-state analysis (74, 83) reveals the possibility of the amplification of plasma oscillations if initially present. According to Piddington (84) this instability results in the growth, both in density and time, of a space-charge cloud. The dispersion relation

$$[\omega_p^2/(\omega - vk)^2] + [\omega_p^2/(\omega + vk)^2] = 1 \quad (141)$$

yields, for real  $\omega$  and complex  $k$ , an attenuated wave with amplitude varying exponentially in space and sinusoidally in time. Buneman (85) finds that a current carrying plasma becomes unstable; the instability growing exponentially with very little oscillation coupled to it. The ions and electrons get accelerated in

bunches emitting radiation stronger than bremsstrahlung. Interaction of a single electron beam with magneto-ionic modes of propagation in an electron atmosphere capable of slow-wave propagation supplies a mechanism (86) for conversion of the kinetic energy of the beam into space charge energy to be released as electromagnetic energy.

#### (e) Collective Motion

Bohm and Pines (61) have analyzed the behavior of electrons in an ionized gas in terms of its density fluctuations which may be split into short range and long range components. The long range part is associated with the organized oscillations of the system as a whole and corresponds to distances greater than  $\lambda_D$ . The short-range part is associated with the random thermal motion and has a tendency to disrupt organized motion. It merely represents a collection of individual electrons surrounded by co-moving clouds of charge which screen the electron's field within a distance of the order of  $\lambda_D$ . Screening and organized oscillations are manifestations of the response of the collective behavior of the plasma to the field of a specified particle. For the particle speed less than the mean thermal speed, the particle is screened by an elliptical space charge. On the other hand, for particle speed exceeding the mean thermal speed, the screening is imperfect, but a wake resembling Čerenkov radiation (62) is excited behind the particle. The energy loss to the collective oscillation is of the same order as that caused by the short-range collisions.

Properties of waves in ionized gases have been reviewed by Gabor (87), Bernstein (79), Spitzer (88), Van Kampen (89), and Allis (90).

#### C. Chopra-Singer Hypothesis

Among other mechanisms contributing to the drag of a spherical body moving in an ionized atmosphere pervaded by a steady magnetic field, Chopra and Singer (27) consider the possibility of a mechanism depending on the excitation of plasma waves by the motion of the charged body. These waves propagate with a frequency below a critical frequency and with a phase velocity less than the material velocity of the body. As a consequence, the body loses energy to the waves and therefore experiences a drag force. The phenomenon bears a certain resemblance to Čerenkov radiation and to the operation of traveling wave tubes.

The ionosphere, pervaded by the terrestrial magnetic field, is capable of slow-wave electromagnetic propagation characteristics for  $\omega < \omega_{ce}$ . These slow waves correspond to the extraordinary electromagnetic mode given by

$$(V_{ph}/c)^2 = \omega(\omega - \omega_{ce}) / (\omega^2 - \omega\omega_{ce} - \omega_p^2). \quad (142)$$

This mode may be excited by the motion of a highly charged body along the lines of magnetic field provided

TABLE VIII. Wave drag.

Altitude (km)	Satellite potential $V_{eq}$ (v)	Wave drag ${}^\omega F$ (d)	Decay time ${}^\omega \tau$ (sec)
250	-2.0	0.04	2.0
800	-6.4	0.41	0.2

that the velocity of the body exceeds the phase velocity  $V_{ph}$  of the slow wave. It follows from Eq. (142) that the presence of a magnetic field is essential for this kind of wave propagation. The charged body supplies energy for the propagation of the waves, and is consequently slowed down. The resistance experienced by the body is given by

$${}^\omega F \sim (\omega Q/v_s)^2 \quad (143)$$

and is called the wave drag. Subject to the wave drag alone, the kinetic energy of the body decays in a time

$${}^\omega \tau \sim mv_s^2 / (\omega Q)^2. \quad (144)$$

The same mechanism may be responsible for the whistling atmospherics—low-frequency radiation emanating from fast charged particles moving along the terrestrial magnetic field lines. A body of macroscopic size, e.g., an earth satellite, may also emit a similar kind of radiation, but in this case the frequency of the emitted wave is closer to the electron-cyclotron frequency  $\omega_{ce}$ .

We consider an interstellar dust particle and an artificial earth satellite moving in the terrestrial atmosphere as illustrations.

A dust particle of mass  $m \sim 4 \times 10^{-13}$  g, carrying a charge  $Q \sim 8 \times 10^4$  e, and moving with velocity  $v_s \sim 3 \times 10^6$  cm/sec, and exciting waves of frequency  $\omega \sim 10^6$  cps experiences a drag force  ${}^\omega F \sim 10^{-9}$  d with a corresponding decay time  ${}^\omega \tau \sim 10^3$  sec. On the other hand, a spherical satellite of radius  $a \sim 25$  cm,  $m \sim 10$  kg, satellite potential  $V_{eq}$  (volts) and moving at a speed  $v_s \sim 8 \times 10^3$  cm/sec, and exciting waves of frequency  $\omega \sim 10^6$  cps experiences a drag force

$${}^\omega F \sim 10^{-2} V_{eq}^2 \text{ d,}$$

with the corresponding decay time

$${}^\omega \tau \sim 8 \times 10^{11} V_{eq}^{-2} \text{ sec.}$$

The values of  ${}^\omega F$  and  ${}^\omega \tau$  corresponding to the observed satellite potentials at altitudes of 250 and 800 km respectively, are given in Table VIII.

#### D. Greifinger's Theory

Bohm and Pines (61) demonstrated that a charged particle moving with velocity  $v_s$ , exceeding the mean thermal electron speed, is capable of exciting collective motion of the plasma in the form of an ionized wake trailing behind the particle. Kraus and Watson (28) considered the excitation of a plasma wake for the particle speed less than the mean thermal electron



speed but exceeding a critical speed  $v_c = v_i(T_e/T_i)^{1/2}$ , where  $T_e/T_i$  is the ratio of the electron-to-ion temperature, and  $v_i$  is the mean thermal ion speed. Contrary to the findings of Bohm and Pines, they find that a wake of ionized plasma is excited behind the charged particle even if the particle speed is less than the mean thermal electron speed provided that it exceeds the critical value. This work has been discussed in Sec. IV.D. Both treatments assume that there is no external magnetic field pervading the plasma, and that the size of the particle must be smaller than the Debye shielding length  $\lambda_D$ . Greifinger (33) has considered the Kraus-Watson problem in the presence of a magnetic field.

A steady-state solution for the electric field vector  $\mathbf{E}$  is obtained, and a general expression for the energy loss per unit path length, for arbitrary values of  $\mathbf{B}_0$ , is derived from the force on the particle and may be expressed as  $Q(\mathbf{v}_s/v_s) \cdot \mathbf{E}$ . It is assumed that the plasma is of low density and the particles have a Maxwellian velocity distribution, that the electromagnetic perturbations are small, the external magnetic field is constant, and the zero-order electric field is zero. The cases of weak and strong magnetic fields are analyzed for longitudinal  $\mathbf{E}$ .

In the limit of a weak magnetic field, the dispersion relation yields longitudinal electron oscillations for  $3k^2\lambda_D^2 < 1$  and  $\omega_{ce}^2 < \omega_{pe}^2$ ; and longitudinal ion oscillations for  $3(T_e/T_i)(1+k^2\lambda_D^2) < 1$  and  $k^2\lambda_D^2/(1+k^2\lambda_D^2) > (\omega_{ci}^2/\omega_{pi}^2) \ll 1$ . The corresponding dispersion relations are independent of magnetic field for propagation parallel to  $\mathbf{B}_0$ . The energy loss is increased, over the zero magnetic field value, by a factor of the order of  $(\omega_{ce}^2/2\omega_{pe}^2)(1+\cos^2\psi)$  for particle speed exceeding the mean thermal electron speed, and by a factor of the order of  $(\omega_{ci}^2/2\omega_{pi}^2)(1+\cos^2\psi)$ , for  $(T_e/T_i)v_i^2 < v_s^2 < v_e^2$ , provided the particle is considered a point charge. Here  $\cos\psi = (\mathbf{v}_0 \cdot \mathbf{B}_0)/v_0B_0$ . The results are slightly modified for particles of finite dimensions but smaller than the Debye length.

In the limiting case of extremely large magnetic field plasma behaves as if the charged particles were free to move only along the magnetic lines of force; the group velocity vanishing for the transverse propagation constant. The energy loss varies from zero for  $\mathbf{v}_s$  parallel to  $\mathbf{B}_0$  to a value roughly one-half the energy loss for vanishing magnetic field when  $\mathbf{v}_s$  is perpendicular to  $\mathbf{B}_0$ . Electrons and ions are excited in oscillations in the limiting situations of (i)  $v_s > v_e$ , and (ii)  $(T_e/T_i)^{1/2}v_i < v_s < v_e$ , respectively.

## E. Conclusions

The two theories, just discussed, of the excitation of plasma waves by the motion of charged bodies in an ionized atmosphere pervaded by a magnetic field, refer to the two different wave mechanisms. Chopra-Singer theory predicts excitation of extraordinary electromagnetic waves propagating along the magnetic lines of

force. This theory, however, lacks rigor and exactness. All the same it indicates that the phenomenon may be quite significant. On the other hand, the mechanism discussed by Kraus-Watson and Greifinger deals with the organized oscillations by a particle of linear dimension smaller than the Debye length, and hence does not apply to the real problem. It may be of interest for interstellar dust particles or small satellites in the interplanetary space where the Debye length is large because of the high temperatures and low electron density. Greifinger's work demonstrates that the importance of electrostatic organized oscillations is enhanced in the presence of a magnetic field by a factor of the order of  $(\omega_{ce}/\omega_{pe})^2$  and  $(\omega_{ci}/\omega_{pi})^2$  for electron and ion oscillations, respectively. The two theories have one common feature that the wave mechanisms form the wake of the charged body.

Another phenomenon which may be of importance is the following: During the course of its motion, a satellite sweeps ions along its path and hence an ion cloud is formed in front of it. The motion of this ion cloud induces motion in the ionized atmosphere such that a cylinder of plasma, of radius equal to the radius of the satellite, moves ahead of the satellite with the satellite speed. The motion of this cylindrical plasma in the terrestrial magnetic field sets up magnetohydrodynamic waves propagating along the terrestrial magnetic lines of force. The condition necessary for excitation of these waves is that  $B^2 < 4\pi n_e(m_e + m_i)c^2$  which for  $m_i \sim 12 \times 1840 m_e$  reduces to  $B < 10^{-2} n_e^{1/2}$ . The electron density in the earth's upper atmosphere varies from  $10^3$  to  $10^6$  per cc. Evidently this inequality is favorably satisfied. Furthermore, the arresting of the relative motion of the plasma ahead of the satellite body causes instability of the medium which in the terrestrial magnetic field may generate long-wavelength radio noise.

## VII. UPPER ATMOSPHERE

### A. Introduction

In the preceding sections we have considered several physical phenomena which a body may encounter during its flight in an ionized atmosphere with a pervading magnetic field. First we summarize the results and then apply them to help gain a better understanding of the upper atmosphere, and allied problems:

(1) Coulomb collision cross section is many orders of magnitude larger than the neutral particle collision cross section. But the effect of large Coulomb cross section is usually offset by the comparatively large neutral particle density. For Coulomb collisions to be more important than the close neutral collisions, the charged particle density must at least be greater than  $10^{-5}$  times the neutral particle density. Except at low altitudes in the upper atmosphere, this condition is satisfied, and the respective Coulomb mean free paths are shorter than the corresponding neutral mean free paths. For

example, at an altitude of 300, km  $\lambda_n \sim 10^5$  cm,  $\lambda_e \sim 6.5 \times 10^3$  cm, and  $\lambda_s \sim 25$  cm. The Coulomb collision frequency is very sensitive to temperature ( $\propto T^{-3/2}$ ) and is proportional to the charged particle density.

(2) In a magnetic field, the charged particles gyrate around the magnetic lines of force with the cyclotron frequency, proportional to the magnetic field strength and inversely proportional to the mass of the particle. For free gyration of the charged particles the cyclotron frequency must exceed the collision frequency. This leads to the criterion that the charged particle density must be less than a critical value  $n_c = (H/A)T^3$ , where  $A$  is the atomic weight of the charged particle. At altitudes of interest in the upper atmosphere of the earth, the electrons are free to spiral while the ions do not. At an altitude of 300 km the typical radii of gyration of electrons and singly charged ions are 5 cm and 5 m, respectively.

(3) A body moving at a speed of  $v_s \sim 8 \times 10^6$  cm/sec in the terrestrial atmosphere acquires a charge through collisions with charged particles. The ions hit it from the front while the electrons are incident along the magnetic lines of force. The surface-particle interactions are not very important except in that 20% of the electrons are reflected back with the incident speeds. The photoelectric effect of the solar radiation, on the dayside, tends to charge the satellite positively. The Sputnik data reveal that the satellite charge at altitudes of 250 and 800 km is predominantly negative, the satellite potential being higher than that predicted on the basis of the temperature equilibrium for ions and electrons and neglecting the photoelectric effect.

(4) A charged body is generally surrounded by a space charge cloud which shields the body's charge within a distance of the order of the Debye shielding length. The shielding is brought about by the Coulomb repulsion between similar charges and is determined by balance of thermal and electrostatic energies of the interacting particles. This shielding distance is large for high temperatures and low electron densities, and varies from a few millimeters to several centimeters at various altitudes in the upper atmosphere. This space charge is spherical for bodies at rest and becomes an ellipsoid for body speed less than the mean thermal speed of electrons and a paraboloid for body speed exceeding the

mean thermal speed of electrons. For a negatively charged satellite in the earth's atmosphere, there is therefore a concentration of positive ions in front of it and trails of positive ions along the equipotential lines and extending to large distances behind it. The shielding is imperfect here.

(5) A highly charged body interacts with the charged particles in the atmosphere. Owing to these Coulomb forces, these particles describe hyperbolic orbits around the body. Consequently, the body experiences a drag force. On Chopra-Singer theory, the Coulomb drag contributes significantly to the total drag at altitudes of 350 km, becomes comparable to the neutral drag at an altitude of 500 km, and is predominant above 650 km.

(6) The motion of a satellite in an ionized atmosphere with a prevailing magnetic field may excite electromagnetic waves in a manner which resembles that of Čerenkov radiation and that of the operation of traveling wave tubes. The waves are of frequencies lower than a critical frequency and propagate along the magnetic lines of force at a speed slightly less than the speed of the satellite. The contribution to the total drag due to this cause is negligible at an altitude of 250 km, but is comparable to the Coulomb drag at an altitude of 800 km.

(7) Following the work of Bohm and Pines, Kraus and Watson have suggested that the motion of an artificial earth satellite may excite an ionized wake behind it. This wake is characterized by electrostatic plasma oscillations. These oscillations derive energy from the kinetic energy of the satellite. The presence of the terrestrial magnetic field enhances this effect. But their work is valid only for bodies of size smaller than the Debye length. Even if it were assumed to apply to the satellite motions, this mechanism would not make a substantial contribution to the total drag.

(8) Another phenomenon of some significance is the onset of instability caused by the arresting of motion of the ion-cloud ahead of the satellite in the terrestrial atmosphere. The conditions are favorable for the generation of magnetohydrodynamic waves. The significance and analysis of this work are yet unexplored.

(9) Another phenomenon is due to electromagnetic induction. The motion of the satellite in the terrestrial atmosphere generates induced electric currents in the body of the satellite as well as in the atmosphere. These currents have a tendency to decelerate both the translational and rotational motions of the satellite. Induction drag is negligible compared to the neutral drag at an altitude of 250 km and becomes extremely large at an altitude of 500 km. A novel feature of the induction drag is to cause the tumbling of the satellite. This tumbling of the satellite has a tendency to increase the neutral drag by a factor of 1 to 15. Since the electrical conductivity is sensitive only to temperature and has only a logarithmic dependence on the electron density, the macroscopic concept of electrical conductivity is valid at altitudes of interest.

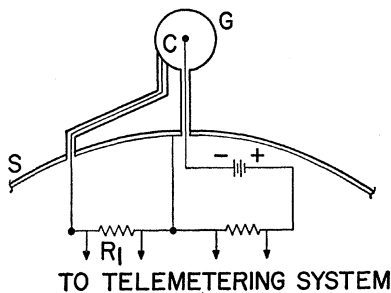


FIG. 2. Measurement of the charge on Sputnik III. C, collector of the ion trap; G, grid of the ion trap; S, satellite surface.

### B. Satellite Potential

An artificial earth satellite is expected to acquire an electric charge due to several causes as discussed in Sec. III. The Russian scientists (91–93) were also aware of this expected effect. Therefore they equipped (94) the third Soviet Sputnik with an instrument capable of measuring directly the electrostatic potential of the Sputnik. This instrument consists of two spherical grid ion-traps attached to thin bars and mounted on diametrically opposite sides of the Sputnik. Each of the ion traps (Fig. 2) represents a spherical grid  $G$ , in the center of which there is a spherical collector  $C$ . A negative voltage ( $\sim -150$  v) is applied to the collector with respect to the grid. This enables the collector to attract all the ions inside the trap and remove all the negatively charged particles out of the trap. The current of the positive ions gathered on the collector flows to the Sputnik's surface by the surrounding medium. Saw-tooth impulses are applied between the covering grid and the Sputnik's surface. The ion current is plotted against the potential difference between the Sputnik surface and the trap grid. Increasing the potential of the grid decreases the current, until at the grid potential, with respect to the surrounding medium, equal to the ion-retardation potential, any further increase in the grid potential does not bring about a further decrease in the current. At this moment the potential difference (observed) between the trap grid and the Sputnik surface is equal to the algebraic sum of the ion-retardation potential and the potential of the Sputnik with respect to the surrounding medium. The retardation potential corresponding to the satellite speed  $v_s \sim 8 \times 10^5$  cm/sec, and for ions of atomic mass 16 is given by

$$V_{\text{ret}} \sim mv_s^2/2e \sim 5.1 \text{ v.} \quad (145)$$

Subtracting this value from the grid-Sputnik potential difference, corresponding to no further decrease in current, yields the Sputnik's potential. At altitudes of 242 and 795 km, respectively, the Sputnik's potential is observed to have values of  $-2.0$  and  $-6.4$  v, respectively.

### C. Ion-Concentration

The third Sputnik was also equipped with a Bennett-type mass spectrometer for determining the nature of atmospheric ions with mass number of 6 to 50 units. It is found that the ions of atomic oxygen and nitrogen are the principal constituents above 250 km, the ions of atomic oxygen being predominant. The predominance of oxygen ions over nitrogen ions indicates that the oxygen atom is easily ionized. The results indicate in general that the upper atmosphere at 250 km and higher is mainly of atomic composition.

The ion density in the atmosphere in the neighborhood of the Sputnik is also determined from the measurements of the collector ion current. Corresponding to the zero-grid potential with respect to the surrounding

medium, the value of the collector current yields the value of the undisturbed ion concentration in the neighborhood of the Sputnik. At this moment the trap grid is at a positive potential with respect to the Sputnik, and the Sputnik-grid potential difference is equal numerically to the potential of the Sputnik with respect to the surrounding medium. The ion density is calculated by using the relation

$$n_i = \frac{1}{\pi a^2 e v_s \alpha} \frac{I_0}{V_{s,0}} = \frac{1}{\pi a^2 e v_s \alpha} \frac{\Delta I}{\Delta V_s}, \quad (146)$$

where  $I_0$  is the collector current,  $V_{s,0}$  is the satellite potential and  $\alpha$  is a transparency coefficient of the order of unity. In the alternative expression  $\Delta I$  is the difference in current corresponding to two values of the Sputnik-grid potential difference around the zero-grid potential with respect to the surrounding medium. The ion density has values of  $5.2 \times 10^5$  and  $1.8 \times 10^5$  per cc at altitudes of 242 and 795 km, respectively.

### D. Electron Concentration

The electron density was determined by the use of an ultra-short wave dispersion interferometer. The electron density increases with altitude, attains a maximum value of  $1.8 \times 10^6$  per cc at an altitude of 290 km and then falls. At an altitude of 475 km it has a value of  $1.0 \times 10^6$  per cc. This information suggests that the scale height for electrons in the upper atmosphere is very large above the level of maximum electron concentration.

United States scientists<sup>7</sup> have estimated the electron density of the ionosphere from observations of 20 Mc transmissions from Sputniks. The method involves observing the change in lag of the radio waves due to the ionosphere as the satellite passes from horizon to horizon. The results applied to the determination of electron distribution above the  $F$  region maximum appear to be erratic. The theoretical and experimental bases of various experiments for exploring the ionosphere with artificial earth satellites are outlined and discussed, with emphasis on limitations, by Berning (95).

### E. Electron Temperature

A comparison of the observed potentials of the Sputnik III with the corresponding values calculated in Sec. III on the basis of thermodynamic equilibrium between ions and electrons indicates that the assumption of such a thermodynamic equilibrium in the upper atmosphere is nonexistent. In other words, the electron temperature is much higher than the ion or the gas temperature. The observed Sputnik potentials at altitudes of 242 and 795 km correspond to effective electron temperatures of  $7500^\circ$  and  $15\,000^\circ\text{K}$ , respectively.

Such a departure from thermodynamic equilibrium is

<sup>7</sup> See W. W. Kellogg, *Planetary Space Science* 1, 71 (1959).

possible and can be explained in terms of collision processes. Starting with an arbitrary velocity distribution, the electron-ion collisions deflect the electrons and tend to organize an isotropic velocity distribution, while the electron-electron and ion-ion collisions tend to establish Maxwellian velocity distributions for electrons and ions, respectively, which correspond, in general, to different electron and ion temperatures. The electron-electron and ion-ion collision frequencies being of the same order, the electrons, possessing higher speeds than the ions, come to a Maxwellian distribution more rapidly than the ions do. Collisions with neutral particles result in a general heating of the gas. In the absence of other phenomena ions, being heavier, lose energy to electrons in Coulomb encounters. This explains the slight difference between the electron- and ion-temperatures of an ionized gas.

In the terrestrial atmosphere, the electrons may acquire relatively higher temperature due to other causes. According to Chapman (96) solar corona extends to the earth's orbit. At distances where the earth's atmosphere vanishes into the interplanetary medium, the temperature is postulated at  $10^5$  °K. The temperature falls at a gradient of  $5^\circ$  K/km as we proceed inwards in the terrestrial atmosphere. Krasovskiy (96, 97) believes that the high temperature of the electrons is due to accelerations which they receive in short-period geomagnetic fields.

Another approach to explain the observed negative values of the Sputnik's potential postulates the existence of a tail of high-energy electrons in the terrestrial atmosphere. According to Lehnert (24) photoionization of air releases electrons of 15-ev energy and mean life of  $10^5$  secs. Jastrow and Pearse (26) have suggested the existence of a very high (up to 60 ev) energy electron tail which originates in the solar corpuscular radiation. These high-energy electrons form 1/1000th part of the total electron density in the upper atmosphere and have a degradation time of the order of 10 sec.

#### F. Satellite Potential as a Diagnostic Tool

Measurement of satellite potential—or the potential of any body in an ionized medium—may be used for the purposes of diagnostics of an ionized medium. Consider the case where the photoelectric effect is negligible or completely absent. For equal ion and electron temperatures, as in a dense ionized gas the observed potential of the test body must be given by the relation

$$eV_{\text{eq}} = -\frac{1}{2}T_e \log_n(m_i/m_e), \quad (147)$$

where  $V_{\text{eq}}$  is in volts and  $T_e$  is expressed in electron volts. When  $T_e$  and  $T_i$  are different, the relation

$$(m_e/m_i)(T_i/T_e)\epsilon^{-2eV_{\text{eq}}/T_e} = 1 \quad (148)$$

must be used in place of Eq. (147). For slight departures from thermodynamic equilibrium between electrons and ions, the potential of the body is not

altered appreciably. On the other hand, if the photoelectric effect is more important than the ion accretion, we can still determine the electron temperature by using the relation

$$(3m_e n_e/n_{\text{ph}})(1/T_e)\epsilon^{-2eV_{\text{eq}}/T_e} = 1. \quad (149)$$

If the electron-temperature is already determined from Eq. (148) when the photoelectric effect was absent, or by other methods, the relation (149) yields a value of the electron density or vice versa. If a beam of high-energy electrons is present in the ionized medium, the electron flux due to the beam incident on the test body may exceed that corresponding to the equilibrium electron temperature. The observed potential of the test body is then higher than that predicted by Eq. (147). The magnitude of the potential on the test body yields information about the density or the energy of electrons in the beam.

#### G. Satellite Wake

Kraus and Watson (28) postulate that the motion of a charged satellite in an ionized atmosphere excites an ionized wake behind it. This wake is brought about by the long-range collective Coulomb interaction between the charged satellite and the charged particles. The wake has the shape of a small-angle cone of half-angle of the order of  $10^\circ$ . Inside the wake the electron density increases by an approximate factor of 10 and falls off inversely as the distance. The collision frequency (of the order of  $10^3$ /sec) determines the length of the trail and it comes out to be of the order of 0.1 km. The effect of the magnetic field is expected to enhance cooperative motion.

Jastrow and co-workers (98) postulate, on the other hand, that the satellite sweeps out a region free of atoms or ions. In the case of a satellite moving at 10 times the ion speed, the length of the ion-free trail behind the satellite is expected to be about 10 times the linear dimension of the satellite. The wake disappears by diffusion of ions into it.

Meteors have been observed to produce ionized wakes behind them. The typical length of such trails is 30 km. It is not possible, however, to detect similar ionization produced by satellites, because (i) the ionization depends on the satellite speed—the lower the satellite speed, the less the ionization, and (ii) the echo from the wake is considerably attenuated due to diffusion of the ion trail. The use of a 20-Mc frequency would require a line density of  $10^{16}$  electrons/cc.

#### H. Satellite Spin

The rate of spin of an artificial earth satellite is obtained by counting the maxima or minima in the radio signals from the satellite. In general, this signal fading is a complicated phenomenon and may be attributed to several causes. The spin fading is produced by lobes or zeros in the pattern of the transmitting

antennas of the satellite. Multiple fading is caused by receipt of signals from two directions simultaneously along different paths. Also the Faraday fading results from different paths followed by the ordinary and extraordinary ionic modes between the satellite and the receiving antennas, and is characterized by lines of constant or relative phase between ordinary and extraordinary waves at the surface of the earth.

At about 200 km, the expected Faraday fading is about a quarter of a turn, so that the observed fading at this altitude is due to the rotation of the satellite. The rotational fading of Sputnik I was observed (99) at 13 and 6.5 fades/min, concluding thereby that the satellite was rotating at 6.5 rpm. The fading rate decreased from 14 to 13 fades/min in the first few days and then remained constant until transmission ceased. Much of the observed fading during transits when the satellite was in the  $F_2$  layer was caused by Faraday effect in the ionosphere. At about 500 km the Faraday fading is expected at 10 times that due to rotation. The fading caused by rotation then appeared as an envelope to the Faraday fading. The records show alternating maxima, and also a distinctive effect in which the secondary maxima increase in amplitude as one might expect for a precessing and spinning satellite. The analysis of these records may yield information about the total ionization up to the satellite and about the orientation of the rotation axis of the satellite. A discontinuous change in the fading rate at 40 Mc is observed to take place at about the time of closest approach. This change is believed to be an effect of the aspect of the satellite relative to the observer. The fact that the change of aspect occurred at almost the same position relative to Cambridge on each of the five successive days, each with 15 orbits between, suggests that the rotation of the axis of the satellite was in a constant direction.

Assuming that the secular decrease in the spinning rate is due to aerodynamic drag between the rotating antenna system and the residual atmosphere near perigee in the orbit, and that the dissipation torque on the spherical satellite is negligible compared to the torque on the antennas. Warwick (10) estimates the density of the atmosphere using the relation

$$\Delta\omega = -3.8 \times 10^8 C_D \rho, \quad (150)$$

where  $\Delta\omega$  is the measured deceleration for one perigee passage, and  $C_D=2$  is the aerodynamic drag coefficient. Corresponding to the measured value of  $2.9 \times 10^{-4}$  rad/sec per passage for the deceleration of spin at an altitude of 220 km, the atmospheric density is then  $3.8 \times 10^{-13}$  g/cc. This value is about 10 times higher than that given by the ARDC model.

The fluctuations in spin fading suggest that the spinning may even increase in frequency over short intervals of time. Possibly the simplest explanation of such effects is that the orientation of the satellite about the constant direction of spin angular momentum

changes slightly from time to time. Such an internal dynamical mechanism would allow any shift from the direction of the greatest moment of inertia to some faster spinning rate, to be canceled by a shift back to the stable condition. Warwick (10) seeks a mechanism of this kind in the interactions between the satellite and the surrounding charged particles. According to him, positive ions are attracted by a negatively charged satellite. An ion may acquire an electron before impact and get reflected at energy including the relative kinetic energy and also the potential energy of the negative charge on the satellite. This additional energy may conceivably result in the acceleration of the satellite at the ultimate expense of the energy of the ionospheric electrons. This interpretation requires a satellite potential of at least  $10^4$  v.

Arendt (100) has reported the spin behavior of satellite Vanguard I. The spin of this satellite indicates a nearly exponential decay during the first eight months of its life time, a very low rate of spin decay during December, 1958 and January, 1959 and an exponential decay in February, 1959 again. In order to explain it we may have to look into the theories of induction drag (Sec. V). It is found that the spin decay is exponential for a circular equatorial orbit. In the case of a non-equatorial noncircular orbit large changes of the spin direction occur due to the turning or tumble component of the torque. In this most general case, the spin movement is described by a "smooth" decay function of the spin rate and by the turning of the spin axis until this axis is parallel to the axis of the earth. In other words, the spin is changing until the spin axis revolves once per day around an axis parallel to the rotational axis of the earth. This quasi-stabilized condition may be achieved only in orbits which are symmetrical with respect to the shape of the magnetic field of the earth. According to Vinti (16) this smooth decay function may be disturbed by four periodic perturbations, three of which are related to the orbital data and one to the rotation of the earth. Arendt has invoked another perturbation related to the precessional period of the plane of the orbit. This precessional movement of the orbital plane of the earth results in a very remarkable change of the magnetic forces which apply during each successive orbit. This period is a very low-frequency term as compared with the period of one orbit or compared with the daily rotation of the earth and would need an exceedingly long interval of observations to be detected. It is interesting to note that the duration of the anomaly in December coincides with half of the period of the precession of the orbital plane. This indicates that there is a fair probability that the observed perturbations are related to the precession of the orbital plane. This statement does not, however, explain the long duration of the anomaly. Such a long deviation could result from a coincidence of perturbations if the difference of the two perturbing periods is nearly equal to the duration of the anomaly.

Now the precession of the equator crossing is the only other perturbation period of considerable duration. The difference between the orbital precessional period 876 orbits and the equatorial-crossing-precessional period of 1286 orbits comes quite close to the observed duration of 436 orbits of the anomaly.

### I. Atmospheric Density, Pressure, and Temperature

Before the launching of the first Russian satellite, the structure of the upper atmosphere was repeatedly measured by rockets. Summaries of these measurements, often quoted in the United States are "The rocket panel atmosphere" and "The ARDC model atmosphere." These two model atmospheres agree within a few percent up to about 220 km. There were no rocket data above 220 km, but the ARDC model extends to 500 km by a theoretical extrapolation. Recent rocket data obtained by LaGow and collaborators [for source see reference (6)] reveals interesting seasonal and latitude dependence of the atmospheric density. It indicates that at 200 km the summer day time density at Arctic latitude is six times greater than the corresponding density at temperate latitudes. Also the northern atmosphere is two times heavier in summer than in winter. The temperature is determined indirectly from the logarithmic plot of density against altitude. It is given by the formula  $\rho = \rho_0 \exp[-(h-h_0)/\bar{H}]$ , where  $\rho$ ,  $h$ , and  $\bar{H}$  are the density, altitude, and scale height, respectively. The scale height is obtained from the relationship  $\bar{H} = kT/\bar{M}g$  between the Boltzmann constant  $k$ , temperature  $T$ , acceleration due to gravity  $g$ , and molecular weight of the atmosphere  $\bar{M}$ . This formula for the density is valid if the collision mean free path in the atmosphere is less than the scale height and the fractional change in temperature is small over a distance equal to the scale height. Data obtained by LaGow and co-workers indicate that during a summer day the temperature of air in the auroral zone is approximately 200°K as compared with 1100°K over New Mexico.

Russian scientists obtained data on atmospheric density and pressure by rockets and Sputniks equipped with magnetic and ionization manometers. The pressure observed by a magnetic manometer in the Sputnik decreased over the first few days. This was interpreted, in contradiction to Mirtov's theoretical analysis, as due to the gas leaving the Sputnik. The results from a magnetic manometer in a Sputnik gave values of  $10^{-3}$  g/cc at 260 km and  $8.8 \times 10^{-15}$  g/cc at 355 km. The added advantage of the ionization manometers is that they provide determination of scale heights at different layers of the upper atmosphere. It is established that the scale height increases with altitude.

Spin and orbital data of the artificial earth satellites have also been used to estimate the atmospheric density. Warwick obtained a value of  $3.8 \times 10^{-13}$  g/cc for the atmospheric density at an altitude of 220 km from the satellite spin observations. The calculations

TABLE IX. Upper atmosphere.

Altitude (km)	Electron density (per cc)	Neutral particle density (per cc)	Density (g/cc)	Temperature (°K)	Pressure (d/cm <sup>2</sup> )
200	$4 \times 10^5$	$2.5 \times 10^{10}$	$6 \times 10^{-13}$	900	$2.0 \times 10^{-8}$
225	$7.5 \times 10^5$	$1.2 \times 10^{10}$	$3 \times 10^{-13}$	1000	$1.0 \times 10^{-8}$
300	$1.8 \times 10^6$	$2 \times 10^9$	$5 \times 10^{-14}$	1500	$2.5 \times 10^{-4}$
350	$1.6 \times 10^6$	$10^9$	$2 \times 10^{-14}$	1800	$1.0 \times 10^{-4}$
500	$10^6$	$10^8$	$2 \times 10^{-15}$	2500	$1.6 \times 10^{-5}$
800	$4 \times 10^5$	$2.5 \times 10^7$	$6 \times 10^{-17}$	4000	$8.3 \times 10^{-7}$
20 000	$10^3$	?	$5 \times 10^{-20}$	100 000	$1.5 \times 10^{-7}$ (?)
100 000	$10^2$	?	$10^{-21}$	200 000	$3.0 \times 10^{-8}$ (?)

based on the orbital data of the satellites have been made by several groups of workers. These calculations are based on relations between the orbital elements of the earth satellites and the atmospheric density. For example, Jastrow and co-workers (3, 4, 6) used the relations

$$dP/dt = 3\pi(GM_\odot)^{4/3}(P/2\pi)^{5/3}\langle\rho v^3/B\rangle_{av} \quad (151)$$

and

$$[e/(1-e^2)](de/dt) = \frac{1}{2}\langle\rho v/B\rangle_{av} - (R/GM_\odot)\langle\rho v^3/B\rangle_{av}. \quad (152)$$

Here  $e$  and  $R$  are the eccentricity and semimajor axis of the satellite orbit (assumed quasi-elliptic),  $P$  is the orbital period,  $B$  is the conventional ballistic drag parameter,  $M_\odot$  is the mass of the earth, and  $G$  is the universal gravitational constant. The ballistic parameter  $B$  is defined as the ratio of the satellite's weight and the aerodynamic force per unit gas-dynamic pressure  $\frac{1}{2}\rho v^2$ . Averages are over the entire orbit. Since density falls rapidly with altitude, the value of  $dP/dt$  determines, to the first approximation, the atmospheric density at the perigee. This result, however, depends on the scale height at perigee. Other workers (2, 5, 7-10) have used minor variations of the foregoing expressions to estimate the atmospheric density. King-Hele (10) has incorporated the effect of the rotation of the terrestrial atmosphere to account for the diurnal, seasonal, and latitude-dependent fluctuations in density. Table IX gives average estimates at various altitudes.

All these estimates lead to higher values of density than anticipated. The reason for this general agreement is that the basic method of calculation is the same. All the calculations are based on the aerodynamic drag theory which in itself is in a very unsatisfactory state. The electrical nature of the atmosphere has been completely ignored. The other drag mechanisms discussed in the preceding sections play an important role, and their neglect in calculations is likely to subject the results to inaccuracies which may become serious. Other factors affecting the accuracy of these estimates are the uncertainties involved in (i) the measurement of the rate of change of the orbital period, (ii) knowledge of the scale height and its distribution in the atmosphere, and (iii) the effective cross-sectional area, and

hence the ballistic drag parameter. Therefore, it appears that the attempts made thus far to construct models of the terrestrial atmosphere have been mere exercises in curve-fitting.

VIII. EXPERIMENTAL STUDIES

Simulated Studies in the Laboratory

The electric charge of an artificial earth satellite is an important physical parameter because its precise knowledge may lead to important information about the physical properties of the upper atmosphere:

(1) If the satellite is charged, there is a contribution to its drag force due to the interaction between the charged particles and the satellite. Accordingly, the orbital motion of the satellite is modified. In order to evaluate the upper-atmosphere densities we need to have information on orbital motions and the drag force. Therefore, we must know precisely the value of the satellite charge and its contribution to the drag force.

(2) A charged satellite may excite an ionized wake behind it and excite plasma oscillations. The knowledge of the length of the wake, the degree of ionization in the wake and the nature of plasma oscillations depends on the precise knowledge of the charge on the satellite.

(3) A knowledge of the satellite charge would lead to some information about the electron-temperature and electron-density in the vicinity of the satellite.

(4) The satellite charge exerts an influence on the ion trajectories. Therefore, in order to appreciate the reliability of the ion concentration and composition of the upper atmosphere, we must know the nature and magnitude of the satellite charge and potential.

(5) Observations on the fluctuations in satellite charge may be related to changes in the solar radiation.

(6) Measurements of the charge of the satellite lead to information which may prove useful in the dynamics of the interplanetary or interstellar dust particles.

In order to obtain first-hand information about these mechanisms, it is essential to perform laboratory experiments under controlled conditions. It is important to simulate conditions in the laboratory which, in some measure, should correspond to temperature  $T \sim 10^3$  to  $4 \times 10^3$  °K, pressure  $p \sim 10^{-6}$  to  $10^{-8}$  mm Hg, and degree of ionization in the range  $10^{-4}$  to  $10^{-1}$ . These physical conditions would roughly represent the upper atmosphere between the altitudes of 250 to 800 km.

Experiment I

One simple experiment proposed by Singer (101) is sketched in Fig. 3. The test chamber, Fig. 3(a), consists of a large bell jar which is evacuated through the outlet  $O$  in its base by means of a fast oil diffusion pump to achieve pressures of the order of  $10^{-6}$  mm Hg. An electron source  $F_1$ , placed at the bottom of the bell jar,

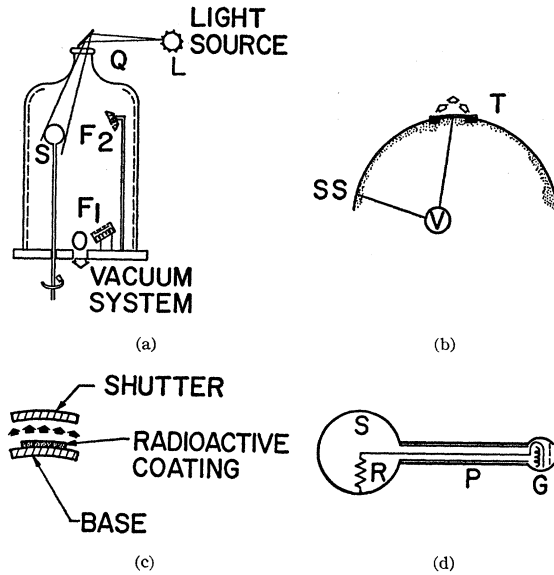


FIG. 3. Laboratory studies of the charge on a satellite. (a) Bell jar arrangement.  $S$ , model satellite surface;  $L$ , light source;  $F_1$ , electron source;  $F_2$ , positive ion source;  $Q$ , quartz window;  $O$ , outlet leading to vacuum system. (b) Schematic description of the test section.  $T$ , test section;  $SS$ , satellite surface;  $V$ , voltmeter. (c) Schematic description of the test section. (d) Electron gun arrangement.  $R$ , resistance;  $P$ , probe;  $G$ , electron gun;  $S$ , satellite surface.

consists essentially of a sheet of pure tungsten metal which is evenly heated indirectly by a Chromel A wire. The whole arrangement is imbedded in a metal cover to assure that the satellite is within the preferred direction of the emitted electrons. The ion source  $F_2$  is a Kunsman electrode or a hollow cathode and is built similarly. The ion and electron sources are directional and produce wide beams which are directed on the model satellite  $S$ . This directional arrangement of ion and electron beams is meant to represent the directional incidence of ions and electrons in the actual motion of the satellite in the atmosphere where the electrons are incident only along the magnetic lines of force, and ions hit the satellite only from the front. It is more effective to use two symmetrically situated electron sources instead of one.

In order to simulate the photoelectric effect of the sun, let us assume that the satellite has a metal surface with a threshold corresponding to a wavelength somewhere between 3000–5000 Å. For example, aluminum with a threshold of 2.81 eV is 4400 Å. Only the part of the spectrum with wavelengths shorter than these is of interest. Unfortunately there is a lack of data for the spectral distribution of the solar radiation especially in the region between 100 and 1000 Å; the best available values appear to be the data given by Friedman.<sup>8</sup> The photoyields for various metals in the whole wavelength range between 0 and 3000 Å show a

<sup>8</sup> H. Friedman, in *The Sun's Ionizing Radiation in Physics of the Upper Atmosphere*, edited by J. A. Ratcliffe (Academic Press Inc., New York, 1960).



similar dependence on the wavelength and all metals give photoyields in the same order of magnitude.

For a negatively charged satellite only the long-wavelength part of the spectrum is important and gives almost all photoelectrons. The sun emits long-wavelength radiation like a blackbody of about 4500 °K. The photoelectric effect of the sun for long-wavelength part of the radiation can be easily simulated in the laboratory. The light source *L* in Fig. 3(a) is a carbon arc with carbons in the rectangular position. The crater of the positive carbon radiates like a gray body of temperature of 4000 °K with an emission coefficient of the order of 0.7. In order to get the ultraviolet radiation into the bell jar, a quartz window made of ultrasil quartz is placed at the top of the bell jar. This type of quartz has a high and almost constant transmission down to 2000 Å, where the absorption of air begins.

If the satellite is positively charged, however, then the only high-energy electrons produced by the short-wavelength photons (from 1000 Å down) can escape from the satellite. Then the sun works as a blackbody of about a million-degree temperature. It is extremely difficult, at the moment, to simulate this part of the solar radiation in the laboratory. A soft x-ray source (1000 v) placed inside the bell jar is sufficient for preliminary studies.

Two techniques for the measurement of the satellite charge are proposed. The first method involves the measurement of difference in potential of the satellite which is assumed constant, and that of an insulated test section which is varied by artificial means. This arrangement is illustrated schematically in Figs. 3(b) and 3(c). The base of the test section is coated with a radioactive source which emits positive or negative  $\beta$  rays of energy large compared to the potential of the satellite. The shutter and the base are connected electrically and remain at the same potential. When the shutter is closed, it absorbs  $\beta$  rays but the potential does not change. When the shutter is open, the  $\beta$  rays escape from the test section unaffected by the potential of the satellite or the test section resulting in the test section acquiring a high potential. If the source is turned off by closing the shutter, the potential of the test section returns to its equilibrium value. The satellite potential is then estimated from the observed rate of variation at which the section returns to its equilibrium potential. The test section has a very small electrical capacity compared to the capacity of the satellite, and hence its variation in potential does not affect the satellite potential. The shutter may be opened or closed electrically or mechanically. An electrical shutter is constructed by placing the source at a very high potential with respect to the perforated test section so that the  $\beta$  rays do not escape. In order to obtain a desired variation in potential, it is necessary that the  $\beta$  source be strong. A better idea is to simulate the  $\beta$  source with a hot filament source and a low voltage (100 v) accelerating grid assembly.

Another method of measuring charge, illustrated in Fig. 3(d), consists of having a small electron gun *G* at the end of a probe *P* which ejects electrons into space until the outer shell of the electron gun has reached a positive potential, equal in magnitude to the accelerating potential of the gun, with respect to the undisturbed plasma surrounding the satellite. At this moment electrons begin to return to the shell of the gun. The electrostatic potential of the gun is the same as that of the undisturbed plasma and serves as a potential reference. If the probe is sufficiently long, the satellite potential is not appreciably disturbed. The satellite potential with reference to the undisturbed plasma can then be obtained by measuring the potential across the large resistance *R*.

### Experiment II. Low-Density Wind Tunnel (31)

The low-density wind tunnel (102) is the one of the free jet-type constructed at the University of Southern California Engineering Center. The entire system is inside a steel tank of 10.1 m length and 5.4 m in diameter. The test chamber into which the free jet exhausts measures 4.5 m in the horizontal cross-stream direction, 2.75 m in the vertical direction and 3.06 m parallel to the gas stream. The chamber static pressure during operation can be maintained from 0.1 to  $10^{-5}$  mm Hg, corresponding to altitudes from 60 to 90 km in the terrestrial atmosphere by the combined use of a forepump and a cryopump. The forepump shown in Fig. 3(a) has a working capacity of 140 ft<sup>3</sup>/min. The cryopumping (103) utilizes the principle of reduction in pressure by low-temperature condensation. Here a helium refrigerated condenser at 20 °K maintains the necessary vacuum and high volume flow. Nozzles up to 1 m in exit diameter can be installed in the test chamber.

The working medium in the wind tunnel can be nitrogen or any mixture of nitrogen and oxygen. In general any gas or a gas mixture with vapor pressure less than  $10^{-5}$  mm Hg at 28 °K may be used. The supply gas is first heated up to about 2000 °K before entering the nozzle. It is further energized (104) in the supersonic part of the nozzle by the decay of the partial ionization of the flow created by a radio frequency discharge. A low-density high-temperature hypersonic flow with Mach numbers up to 11, stagnation pressure up to 10 atm, stagnation temperature up to 800 °K and altitude simulation up to 90 km is produced by the combination of cryopumping and plasma heating. A continuous flow can be maintained for about 10 hr. With improved refrigeration and plasma heating techniques, it should be possible to extend the flow regime up to Mach number 20, stagnation temperature up to 8000 °K and altitude simulation up to 150 km. Also the operating time of the flow can be increased. A test model or a diagnostic probe is placed on the base which is capable of motion in all the three directions: vertical, sideways, and forwards (or backwards).



The exact reproduction of full scale conditions in the laboratory brings in several practical difficulties. Reduced scale model experiments are, however, within the limitation of present day technology. In order to obtain meaningful results we must scale the various physical parameters in such a way that the model test and full-scale situations have complete correspondence in every respect; geometrically, aerodynamically, and electromagnetically. The following considerations show that such a scaling is possible.

Suppose, for example, that the characteristic length  $l$  (e.g., the radius of a nose cone) is reduced in the test model by a scaling factor which is less than unity. If the temperature in the laboratory is maintained equal to that in the full scale situation, then the application of the principle of dimensional similitude to the relaxation processes in the gas requires that the mass density  $\rho$  and hence the electron density  $n_e$  be increased by a factor of  $\alpha^{-1}$ . This statement involves the assumption that the ratio of charged to neutral particle densities is kept the same in the two cases. The plasma frequency  $\omega_p \propto n_e^{1/2}$  is increased by a factor of  $\alpha^{-1/2}$ . The corresponding plasma wavelength  $\lambda_p$  is reduced by a factor of  $\alpha^{1/2}$ . Similarly, the sheath thickness characterized by the Debye shielding length  $\lambda_D \propto (T/n_e)^{1/2}$  is reduced by a factor of  $\alpha^{1/2}$ . The mean free paths  $\lambda_n, \lambda_e, \lambda_i$  being inversely proportioned to the density, are also reduced by a factor of  $\alpha$ . But the velocity of sound  $c_s \propto T^{1/2}$  remains the same in the two situations.

In order to simulate the effect of the terrestrial magnetic field in the model test, we must keep the ratio  $H/\rho$  similar in the laboratory and actual cases. The similarity in this respect requires that the magnetic field in the model test be increased by a factor of  $\alpha^{-1}$  over the actual full scale value. In other words, the radii of gyration  $r_c$  are reduced in the test model experiment by a factor of  $\alpha$ . Similarly, the cyclotron frequency  $\omega_c$  of the charged particles in the model experiment is  $\alpha^{-1}$  times the actual full scale value.

These conditions secure the physical and electromagnetic simulation of the specific atmospheric conditions in the laboratory corresponding to the specific linear-dimensional scaling factor. The various scaling relationships, in this example, may be summarized as follows:

$$\frac{l_m}{l_0} = \frac{\rho_0}{\rho_m} = \frac{n_{e,0}}{n_{e,m}} = \frac{\lambda_m}{\lambda_0} = \left( \frac{\lambda_{D,m}}{\lambda_{D,0}} \right)^2 = \left( \frac{\lambda_{p,m}}{\lambda_{p,0}} \right)^2$$

$$= \left( \frac{\omega_{p,0}}{\omega_{p,m}} \right)^2 = \frac{H_0}{H_m} = \frac{r_{c,m}}{r_{c,0}} = \frac{\omega_{c,0}}{\omega_{c,m}} = \alpha \quad (153)$$

and

$$T_m/T_0 = c_{s,m}/c_{s,0} = 1.$$

We next consider the aerodynamic similitude. The aerodynamic behavior of the flow may be determined by the Mach number  $M = v/c_s$ , the Reynolds number  $R = \rho l v / \eta$ , and the Knudsen number  $K = \lambda / l$ . The

Mach number determines the sonic behavior of the flow. The Reynolds number determines the relative significance of the nonviscous and viscous effects. In flows with predominant viscous effects, the Knudsen number describes the flow better than the Reynolds number. On using the scaling relations (151) it is easy to see that

$$M_m/M_0 = R_m/R_0 = K_m/K_0 = 1. \quad (154)$$

In the actual experiment the scaling factor  $\alpha = \frac{1}{10}$  may be quite suitable. Then the physical conditions in the laboratory model experiment correspond to the altitude simulation corresponding to local density equal to  $\frac{1}{10}$  times that in the laboratory. The model satellite may be mounted on the base or suspended from one arm of a sensitive balance by means of a suspension wire shielded by an insulating cylindrical tube. The photoelectric effect is produced as in experiment I. In order suitably to scale down the spiral path of the charged particle, it is necessary to increase the magnetic field of the earth by means of Helmholtz coils. The measuring instrumentation includes (i) conventional pressure and vacuum gauges, (ii) specially designed McLeod gauge and a high-frequency breakdown gauge, (iii) free molecule pressure and temperature probes, (iv) electron density probe, and (v) X- and K-band microwave interferometers. The satellite potential may be measured by any of the methods discussed earlier.

*Note added in proof.* Further developments have been reported since this paper was written. The serial numbers of equations and references in this note form a continuous sequence with those in the main paper.

*I. Properties of the upper atmosphere.* Estimates of density of the upper atmosphere of the earth, based on measurements of the first three Soviet Sputniks, are given by Lidov (105), Elíasberg (106), and Sedov (107). They take particular note of diurnal variation of density. Their respective estimates at a given altitude vary by an order of magnitude. Sedov has also reviewed several causes of perturbations in the orbital and rotary motions of the Sputniks.

The data (108) transmitted by Sputnik III reveal that atomic oxygen is the main ionized constituent between altitudes of 230 and 885 km. Atomic nitrogen is in amounts of 3 to 8% of atomic oxygen, the proportion of nitrogen ions increasing with altitude.

A detailed comparison of the manometric and the satellite data on the structure of the upper atmosphere between altitudes of 225 and 500 km is made by Mihknevich and co-workers (109).

The University of Michigan Space Physics Research Laboratory has gathered evidence (private communication) of high electron temperatures in the  $F_2$  layer. The measurements of electron temperatures were made in rocket flights carrying Langmuir probes to altitudes ranging from 300 to 420 km.

Singer (110) predicts the existence of a dust belt in the upper atmosphere of the earth. He applies the considerations of Coulomb drag (25,27) to the dynamics

of the interplanetary dust particles in the cislunar space. The expression for the electrostatic potential  $V$  of a dust particle in the cislunar space takes a convenient form

$$V = 7.5r - 15, \quad (155)$$

where  $V$  is expressed in volts, and  $r$  is the distance from the center of the earth, expressed in earth radii. At a distance of two earth radii (or at an altitude of about 6000 km), the dust particle is electrically neutral, and it carries a positive or a negative charge according as  $r$  is greater or less than two earth radii. The dynamics of a dust particle in the interplanetary space is strongly influenced by the Coulomb drag (25). Therefore, a dust particle can have its orbit perturbed by Coulomb drag to find itself in a circular orbit in a region where its electric charge, and hence the Coulomb drag, vanishes. This happens at an altitude of about 6000 km, and here the particle can survive for a long period of time thereby contributing appreciably to the density of the dust. This results in the formation of a dust belt. The density of dust at an altitude of 6000 km is greater than the corresponding atmospheric density, and the density peak of the dust belt is estimated to occur at an altitude of about 1000 km.

*II. Electrodynamic drag.* Beard has brought the author's attention to the revised version (111) of his earlier paper (29) in which he attempts to correct an oversight in his earlier paper. This revised version suggests that the voltage induced in the satellite may affect the interpretation of measurements of satellite potential and that the magnetic drag resulting from induced currents may exceed the mass drag for satellites larger than 50 m in diameter at altitudes above 1200 km. Unfortunately, I find it difficult to reconcile myself with the work of Beard and Johnson, and maintain that the electric polarization, induced electric field and the phenomenon of electromagnetic shielding adjust each other to produce closed electric currents in the satellite. For satellites bigger than 50 m in diameter, the electromagnetic shielding nullifies the induction effect. Furthermore, the electric charge on the satellite is shielded by a mechanism different from that suggested by Jastrow and Pearse and endorsed by Beard and Johnson. This point is taken up in Sec. IV.

After giving a brief critical review of the Jastrow-Pearse and Kraus-Watson theories of Coulomb drag, Wyatt (112) proceeds to tackle the problem by separating the aerodynamic and electrodynamic effects and by assuming the spherical satellite to be completely permeable to both ions and electrons. Wyatt's theory subjects itself to the condition that the Debye shielding length is smaller than the size of the satellite, and yields a result which is three orders of magnitude smaller than that obtained by Jastrow and Pearse. Whereas Wyatt attributes this disagreement to spherical symmetry of electron distribution in the Jastrow-Pearse theory, Licht (113) explains the difference in results as due to the

assumption of complete permeability of the satellite to electrons and ions in Wyatt's theory.

*III. Electrohydrodynamic phenomena.* In the first of his three papers, Rand (114) applied the microscopic approach to determine the distortion of the Debye shielding field when the test particle—a very heavy ion—moves with velocity small compared to the mean thermal speed of the gas. The result is an asymmetric correction proportional to the ratio of the test particle velocity to the mean thermal velocity of the gas. In the second paper, he extends the method to the case of a supersonic flow about a thin disk of radius greater than the Debye length. The particles incident near the edge of the disk produce a wake behind it in a process akin to diffraction of light at an edge. The wake contains two conical regions with surface charge densities higher than their respective ambient velocities. The various assumptions made in the analysis are its chief limitations. For example, one may raise a question as to the validity of the use of Debye length as a characteristic length for diffraction in preference to any other length, say de Broglie wavelength of the incident particles. The electrodynamic drag is found to increase with decreasing density. Rand explains this result as due to insufficient shielding of the disk and the consequent large angle scattering. But, presumably, he had neglected the large angle scattering in his analysis. In the third paper, he estimates the damping of a wake behind a line charge which begins a Mach number of Debye lengths behind it. The damping becomes unimportant for  $T_e/T_i > 10$ , and the decrease in the wake is quadratic with distance behind the charge.

Pappert (115) has considered the excitation of plasma oscillations in the wake of a massive point ion moving at a speed less than the root mean square speed of the electrons in a gas containing ions of vanishing kinetic temperature and pervaded by a constant longitudinal magnetic field. He finds that in the weak field limit, the wake angle is not changed appreciably from the field free case. Over some regions of space, the frequency of these oscillations is approximately equal to the ion cyclotron frequency.

Yoshihara (116) has applied the self-consistent field approach to the motion of a thin charged body moving at a speed in the range of electron- and ion-thermal speeds in a plasma with electron and ion distributions of the Maxwellian and collision-free-Boltzmannian types, respectively, and assuming the surface-particle interactions to be specular, he finds that the resultant motion is composed of a free molecule flow component superimposed by a collective component; the latter affecting the entire wake in the high-rarefied limit.

*IV. Nature of ionized cloud around the body.* In almost all problems involving interactions of plasma with a rapidly moving body, the least understood and the most important factor is the nature and shape of the space charge in the vicinity of the body. Debye shielding length loses meaning when the speed of the body ex-

ceeds the mean thermal speed of the charged particles. The author (117) has developed a physical picture of the situation in which a concentric spherical belt (of a suitable radius) of positive ions is formed around a negatively charged spherical body. The radius of the belt depends on the charge to mass ratio of the ions, and the speed and charge of the body. The positive ions in the belt describe circular (or nearly circular) orbits around the body at a speed equal to the speed of the body. The charged particles outside the belt are not affected by the electric charge of the body whereas those able to penetrate the space enclosed by the belt are subject to Coulomb interaction with the charged body. The ions falling in the second category spiral around the body and finally hit it, while the electrons are scattered out of the region. Those charged particles scattered in the forward direction are responsible for the formation of longitudinal column of ionized gas ahead of the body.

The spherical belt is not affected by the presence of a magnetic field if its radius is less than a critical value which depends on the strength of the magnetic field, speed of the body, and the charge, mass, and mean thermal speed of ions. The longitudinal column of ionized gas experiences an effect which may be called the magnetic wind effect.

This spherical ion belt and the longitudinal ionized column present an unusual radar cross section and therefore may explain the sometimes extraordinarily large response to radar detection of satellites and other bodies moving through the  $F_2$  layer (118).

The Coulomb drag is enhanced by an increase in the effective collision diameter of the body, conversion of translational energy of the belt ions into their orbital energy and the loss of momentum in successive (multiple) Coulomb encounters of each charged particle with the body as a result of the magnetic wind effect. The unexpected and considerable slowing down of the recent Russian space shot towards the planet Venus can be attributed to the enhanced Coulomb drag.

*V. Excitation of plasma waves.* In a recent paper (119), the author elaborated on the phenomena of excitation of plasma waves by rapidly moving bodies. It was found that the dispersion relation for extraordinary (slow) electromagnetic waves yields a set of two values for the frequency. The higher value of the frequency corresponds to the cyclotron frequency of the charged particles and the lower frequency is indeed very very low and depends on the Alfvén speed, speed of the body, and the ratio of the electron mass to ion mass. The frequency of the electrostatic waves is limited by the plasma frequency. Both the electrostatic and electromagnetic waves propagate at speeds of the order of the speed of the body. The magnetohydrodynamic waves of suitably low frequencies can also be excited. These waves propagate at the Alfvén speed. In the application of these considerations to the flight of missiles and artificial earth satellites, we find that the Alfvén speed

is of the order of a few hundred km/sec compared to the few (1 to 8) km/sec speed of the space vehicles.

In contrast, Lighthill (120) concludes from his investigations that the magnetohydrodynamic waves cannot be excited by missiles and artificial earth satellites because the Alfvén speed exceeds the speed of the space vehicles. This criterion does not apply to the wave phenomena in general. The wave propagation is usually a characteristic property of the medium, and the excitation of waves depends on the specific phenomenon. In the process discussed in (119), the excitation is caused by the propagation of the longitudinal ionized column ahead of the body. Each oppositely charged oncoming particle in the ionized cloud is scattered with its longitudinal momentum reversed in the forward direction, the momentum transfer corresponding to twice the speed of the moving body. This causes a jump of its guiding center which is analogous to the plucking of a string.

*VI. Magnetohydrodynamic (or induction) phenomena.* A number of papers (121–126) have recently appeared which describe flow characteristics past solid bodies. The wakes form a special feature of some of these. Sears (121) reviews the cases of steady flow past a solid body in the presence of an external magnetic field in the distinguishing cases of low and high magnetic Reynolds numbers. The low magnetic Reynolds number flows are characterized by large wakes of vorticity and electric current in the downstream and upstream directions as demonstrated by Hosimoto (122). Gotoh (123) has considered flow of an incompressible, viscous, and electrically conducting fluid past a sphere in the presence of a uniform magnetic field parallel to the undisturbed flow. He finds that the flow character depends on the Reynolds number, the magnetic Reynolds number, and the Hartmann number. The neutrality of the electric charge density appears to have been violated with the vorticity, electric current density, and the electric charge density confined in a paraboloidal region. Ludford (124) has also considered the flow characteristics of an electrically conducting compressible fluid past an obstacle. An essential point is the demonstration of the equivalence of the method of Joule dissipation (13) of electric currents for the calculation of drag force and that of perturbed pressure distribution. It is shown that the drag force can then be calculated from the unperturbed potential flow and the magnetic field, and is proportional to the product of the magnetic Reynolds number and the ratio of magnetic pressure to inertial pressure. In the case of slow viscous flow, he predicts two paraboloidal wakes due to magnetic intensity and vorticity. Imai (125) applies the perturbation theory to the three-dimensional flow of a compressible, inviscid and perfectly conducting fluid in the presence of a uniform magnetic field, and finds that the flow is essentially similar to the ordinary flow of a hypothetical nonconducting gas with an appropriate pressure density relation. Stewartson (126) demonstrates that the flow field

at infinity is affected by the body because small perturbations propagate, without diffusion along lines of force, at Alfvén speed which is augmented downstream by the stream velocity. As an example he considers the case of the force and moment experienced by a sphere.

Zonov (127) has investigated the currents induced in an artificial earth satellite, and their contribution to its drag and other perturbation effects. In the case of a rotating satellite, he finds a negligible translational drag and considerable rotational drag. He predicts that a nonrotating satellite, under the effect of electromagnetic perturbation effects, will be set into rotation.

*VII. Surface-particle interactions.* With reduced pressure, as in free molecule flow situations, evaporation from the surface takes place, the vapor density depending on the surface temperature of the body. Therefore, a correction due to the interaction between the vapor and the oncoming beam needs to be calculated. Secondly, the incident particles are reflected (or reemitted) diffusely or reflected specularly depending on the de Broglie wavelength of the incident particles and the structure of the surface lattice. Accordingly, the accommodation coefficient depends on these two parameters.

#### ACKNOWLEDGMENTS

It gives me great pleasure to express my gratitude to Professor D. S. Kothari, who, in 1955, introduced me to the drag problems. The close association and friendship of Professor S. Fred Singer has been a constant source of inspiration all along this study. I wish to thank Professor Singer and Dr. Raymond L. Chuan for several useful discussions. Last, but not least, I am pleased to record my deep sense of appreciation to Mrs. F. Maurine Martin and Mrs. Ann R. Heymann for their help in the preparation of the manuscript.

#### BIBLIOGRAPHY

1. T. E. Sterne, B. M. Folkart, and G. F. Schilling, *Smithsonian Contr. Astrophys.* **2**, 207 (1958).
2. R. A. Mizner and W. S. Ripley, ASTIA Document No. 110-223 (1956).
3. I. Harris and R. Jastrow, *Astronautics* **3**, 72 (1958).
4. I. Harris and R. Jastrow, *Science* **127**, 471 (1958).
5. (a) G. F. Schilling and T. E. Sterne, *J. Geophys. Research* **64**, 1 (1959); (b) G. F. Schilling and C. A. Whitney, *Planetary Space Sci.* **1**, 136 (1959); (c) T. E. Sterne, *Science* **127**, 1245 (1958); **128**, 420 (1958); *Astron. J.* **63**, 81 (1958); *Phys. Fluids* **1**, 165 (1958).
6. I. Harris and R. Jastrow, *Planetary Space Sci.* **1**, 20 (1959); *Astronautics* **4**, 24 (1959).
7. H. K. Kallmann, *J. Geophys. Research* **64**, 615 (1959).
8. J. W. Siry, *Planetary Space Sci.* **1**, 184 (1959).
9. H. K. Paetzold, *Planetary Space Sci.* **1**, 115 (1959).
10. J. W. Warwick, *Planetary Space Sci.* **1**, 43 (1959).
11. King-Hele, *Nature* **184**, 1267 (1959).
12. T. G. Cowling, "Solar electrodynamics," in *The Sun*, edited by G. P. Kuiper (University of Chicago Press, Chicago, Illinois, 1953).
13. K. P. Chopra, *Indian J. Phys.* **30**, 605 (1956); *J. Geophys. Research*, **62**, 143 (1957); also see University of Southern California Engineering Center Rept. No. 56-205, Chap. II (January, 1959).
14. E. J. Öpik, *Irish Astron. J.* **4**, 214 (1957).
15. K. Stewartson, *Proc. Cambridge Phil. Soc.* **52**, 301 (1956).
16. J. P. Vinti, *Ballistic Research Lab. Rept.* 1020 (1957).
17. W. Chester, *J. Fluid Mech.* **3**, 304 (1957).
18. H. W. Liepmann, "Hydromagnetic effects in Couette and Stokes flow," in *Plasma in a Magnetic Field*, edited by R. K. M. Landshoff (Stanford University Press, Stanford, California, 1959).
19. O. Jeffimenko, *Am. J. Phys.* **27**, 344 (1959).
20. Y. Krumin, *Latvijas PSR Zinātņu Akad. Vēstis.* **1958**, 97.
21. W. F. G. Swann, *Phys. Rev.* **15**, 365 (1920); **19**, 38 (1922).
22. L. Davis, Jr., *Phys. Rev.* **72**, 632 (1947).
23. A. Baños, Jr., *J. Appl. Phys.* **23**, 1294 (1952).
24. B. Lehnert, *Tellus* **8**, 408 (1956).
25. S. F. Singer, "Measurement of interplanetary dust," in *Scientific Uses of Earth Satellites*, edited by J. A. Van Allen (University of Michigan Press, Ann Arbor, Michigan, 1956).
26. R. Jastrow and C. A. Pearce, *J. Geophys. Research* **62**, 413 (1957).
27. K. P. Chopra and S. F. Singer, University of Maryland, Physics Department, Tech. Rept. 97 (1958); also reprinted in *Heat Transfer and Fluid Mechanics Institute* (Stanford University Press, Stanford, California, 1958), p. 166.
28. L. Kraus and K. M. Watson, *Phys. Fluids* **1**, 480 (1958).
29. D. B. Beard, "Interactions of satellites with a conducting fluid in the presence of a magnetic field," in *Aerodynamics of the Upper Atmosphere*, compiled by D. J. Masson (Rand Corporation, Santa Monica, California, 1959).
30. S. F. Singer and K. P. Chopra, *Bull. Am. Phys. Soc. Ser. II*, **4**, 360 (1959).
31. R. L. Chuan and K. P. Chopra, *Bull. Am. Phys. Soc. Ser. II*, **4**, 360 (1959).
32. H. H. C. Chang and M. C. Smith, *J. Brit. Interplanetary Soc.* **17**, 199 (1959-60).
33. P. S. Greifinger, "Induced oscillations in a rarefield plasma in a magnetic field," in *Aerodynamics of the Upper Atmosphere*, compiled by D. J. Masson (Rand Corporation, Santa Monica, California, 1959); also see *Phys. Fluids* **4**, 104 (1961).
34. R. N. Thomas, *Astrophys. J.* **116**, 203 (1952); also see **113**, 475 (1951); **114**, 448 (1951); **118**, 555 (1953).
35. B. J. Levin, *The Physical Theory of Meteors and Meteoric Matter in the Solar System* (Academy of Sciences of U.S.S.R., Moscow, 1956); AFOSR translation by J. Miller and D. Kraus, ASTIA Document No. 110-091.
36. E. J. Öpik, *Physics of the Meteor Flight in the Atmosphere* (Interscience Publishers, Inc., New York, 1958).
37. J. C. Maxwell, *The Scientific Papers of James Clark Maxwell* (Cambridge University Press, New York, 1890), Vol. 2, p. 681.
38. M. V. Smoluchowski, *Wied. Ann.* **64**, 101 (1898).
39. S. A. Schaaf and P. L. Chambré, "Flow of rarefied gases," in *Fundamentals of Gas Dynamics*, edited by H. W. Emmons (Princeton University Press, Princeton, New Jersey, 1958).
40. S. A. Schaaf, "Aerodynamics of satellites," in *Aerodynamics of the Upper Atmosphere*, compiled by D. J. Masson (Rand Corporation, Santa Monica, California, 1959).
41. F. C. Hurlbut and R. P. Stein, "Progress in studies of sputtering by beam techniques," in *Aerodynamics of the Upper Atmosphere*, compiled by D. J. Masson (Rand Corporation, Santa Monica, California, 1959).
42. R. Schamberger, "Analytic representation of surface interaction for free molecule flow with application to drag of various bodies," *Aerodynamics of the Upper Atmosphere*, compiled by D. J. Masson (Rand Corporation, Santa Monica, California, 1959); also see M. Schamberger, RM-2313; ASTIA Document No. AD-215-301 (1959).
43. R. M. L. Baker, Jr., and A. F. Charwat, *Phys. Fluids* **1**, 73 (1958).
44. M. C. Adams and R. F. Probst, *Jet Propulsion* **28**, 86 (1958).
45. G. P. Kuiper, *The Earth as a Planet* (University of Chicago Press, Chicago, Illinois, 1954); C. W. Allen, *Astrophysical Quantities* (University of London, The Athlone Press, London, 1955).
46. M. Nicolet, *J. Atmospheric and Terrest. Phys.* **3**, 200 (1953).
47. A. von Engel, *Ionized Gases* (Clarendon Press, Oxford, England, 1955), p. 60-65.
48. S. Chapman and T. G. Cowling, *The Mathematical Theory of Non-Uniform Gases* (Cambridge University Press, New York, 1939), p. 346.
49. N. Bohr, *Phil. Mag.* **25**, 10 (1913); **30**, 581 (1915).

50. E. Fermi, *Nuclear Physics* (University of Chicago Press, Chicago, Illinois, 1951), p. 27.
51. L. Spitzer, Jr., *Physics of Fully Ionized Gases* (Interscience Publications, Inc., New York, 1956).
52. E. Åström, *Arkiv Fysik* **2**, 443 (1950).
53. S. Chapman, "Kinetic theory of gases," in *Fundamental Formulas of Physics*, edited by D. H. Menzel (Prentice-Hall, Inc., Englewood Cliffs, New Jersey, 1955).
54. R. C. Mazumdar, *Z. Physik* **107**, 599 (1937).
55. T. G. Cowling, *Proc. Roy. Soc. (London)* **A183**, 453 (1945).
56. H. Grad, Institute of Mathematical Sciences, New York University Rept. No. NYO-2543 (June, 1959).
57. J. M. Burgers, "Some aspects of particle interaction in gases," Institute of Fluid Dynamics and Applied Mathematics, University of Maryland Tech. Note BN-176 (June, 1959).
58. H. S. W. Massey, and E. H. Burhop, *Electronic and Ionic Impact Phenomena* (Clarendon Press, Oxford, England, 1956), Chaps. V and IX.
59. G. Wehner, "Studies of the interaction of high velocity atoms with solid surfaces by means of gas discharge devices," in *Aerodynamics of the Upper Atmosphere*, compiled by D. J. Masson (Rand Corporation, Santa Monica, California, 1959).
60. S. F. Singer, *Trans. Am. Geophys. Union* **38**, 175 (1957).
61. D. Bohm and D. Pines, *Phys. Rev.* **82**, 625 (1951); **85**, 338 (1952).
62. P. A. Čerenkov, *Phys. Rev.* **52**, 378 (1937).
63. S. Chandrasekhar, *Astrophys. J.* **97**, 255 (1943); also see *Principles of Stellar Dynamics* (University of Chicago Press, Chicago, 1942).
64. L. Spitzer, Jr., *Monthly Notices Roy. Astron. Soc.* **100**, 396 (1940); also see reference 51, Chap. V.
65. D. H. Michael, *Mathematika* **1**, 131 (1954).
66. R. Q. Twiss and J. A. Roberts, *Australian J. Phys.* **11**, 424 (1958).
67. Z. O. Bleviss, Douglas Rept. No. SM-22-965 (1957).
68. H. Alfvén, *Cosmical Electrodynamics* (Clarendon Press, England, 1953), Chap. IV.
69. V. C. A. Ferraro, *Proc. Roy. Soc. (London)* **A233**, 1310 (1955).
70. L. Tonks and I. Langmuir, *Phys. Rev.* **33**, 195 (1929).
71. J. J. Thomson and J. P. Thomson, *Conduction of Electricity through Gases* (Cambridge University Press, New York, 1933), Vol. 2, p. 353.
72. V. A. Bailey, *Phys. Rev.* **78**, 428 (1950).
73. A. A. Vlasov, *J. Exptl. Theoret. Phys. U.S.S.R.* **8**, 291 (1938).
74. D. Bohm and E. P. Gross, *Phys. Rev.* **75**, 1851, 1864 (1949); **79**, 992 (1950).
75. M. A. Lampert, *J. Appl. Phys.* **27**, 5 (1956).
76. E. P. Gross, *Phys. Rev.* **82**, 232 (1951).
77. G. V. Gordeyev, *J. Exptl. Theoret. Phys. U.S.S.R.* **6**, 660 (1952).
78. H. K. Sen, *Phys. Rev.* **88**, 816 (1952).
79. I. B. Bernstein, *Phys. Rev.* **109**, 10 (1958).
80. T. H. Stix, *Phys. Rev.* **106**, 1146 (1957).
81. H. Alfvén, *Arkiv Mat. Astron. Fysik* **29B**, No. 2 (1942).
82. H. H. C. Chang, *Bull. Am. Phys. Soc. Ser. II*, **4**, 352 (1959).
83. F. D. Kahn, *J. Fluid Mech.* **2**, 601 (1957).
84. J. H. Piddington, *Phil. Mag.* **3**, 1241 (1958).
85. O. Buneman, *Phys. Rev. Letters* **1**, 8 (1958).
86. J. Feinstein, "Conversion of space-charge-wave energy into electromagnetic radiation," in *Proceedings of the Symposium on Electronic Wave Guides* (Polytechnic Press, New York, 1958).
87. D. Gabor, *Brit. J. Appl. Phys.* **2**, 209 (1951).
88. L. Spitzer, Jr., see reference 51, Chap. IV.
89. N. G. Van Kampen, *Physica* **23**, 641 (1957).
90. W. P. Allis, "Electron plasma oscillations," in *Proceedings of the Symposium on Electronic Wave Guides* (Polytechnic Press, New York, 1958).
91. I. M. Imyanitov, *Uspekhi Fiz. Nauk* **63** (1957).
92. K. I. Gringauz and M. Kh. Zelikman, *Uspekhi Fiz. Nauk* **63** (1957).
93. B. S. Danilin, V. V. Michnevich, A. I. Repnev, and Ye. S. Shvidkovskiy, *Uspekhi Fiz. Nauk* **63** (1957).
94. V. I. Krassovsky, *Proc. I. R. E.* **47**, 289 (1959).
95. W. W. Berning, *Proc. I. R. E.* **47**, 280 (1959).
96. S. Chapman, *Smithsonian Contr. Astroph.* **2**, 1 (1957).
97. V. I. Krassovsky, *Planetary Space Sci.* **1**, 14 (1959).
98. R. Jastrow, C. A. Pearce, I. Harris, and A. Davis, "Mechanism for the formation of satellite trails," *Proceedings of the Conference on Interaction of Satellites with the Ionosphere* (U. S. Naval Research Laboratories, Washington, D. C., 1958).
99. J. H. Thomson, "Rotation of the first Russian earth satellite," Jodrell Bank Expt. Station, University of Manchester, England (1958).
100. P. R. Arendt, U. S. Army Research and Development Lab. Tech. Rept. No. 2025 (1959).
101. S. F. Singer (private discussion, 1957); also see reference 30.
102. R. L. Chuan and K. Krishnamurthy, *USEC Rept.* 42-201 (1956).
103. R. L. Chuan and B. M. Bailey, "Cryo-pumping for high vacuum by low power," presented at the 5th Natl. Vacuum Symposium, San Francisco (1959).
104. F. O. Smetana, *USCEC Rept.* 56-207 (1959).
105. M. L. Lidov, *Artificial Earth Satellites U.S.S.R.* No. 1, 9 (1958).
106. P. E. Elfasberg, *Artificial Earth Satellites U.S.S.R.* No. 1, 21 (1958).
107. L. I. Sedov, *Artificial Earth Satellites U.S.S.R.* No. 2, 3 (1958).
108. V. G. Istomin, *Artificial Earth Satellites U.S.S.R.* No. 2, 32 (1958).
109. V. V. Mihnevich, B. S. Danilin, A. I. Repnev, and V. A. Sokolov, *Artificial Earth Satellites U.S.S.R.* No. 3, 84 (1958).
110. S. F. Singer, "Distribution of dust in cislunar space—Possible existence of a terrestrial dust belt," presented at the meeting of the American Astronautical Society held on December 27, 1960, New York.
111. D. B. Beard and F. S. Johnson, *J. Geophys. Research* **65**, 1 (1960).
112. P. J. Wyatt, *J. Geophys. Research* **65**, 1673 (1960).
113. A. L. Licht, *J. Geophys. Research* **65**, 3493 (1960).
114. S. Rand, *Phys. Fluids* **2**, 649 (1959); **3**, 265, 588 (1960).
115. R. A. Pappert, *Phys. Fluids* **3**, 966 (1960).
116. H. Yoshihara, *Phys. Fluids* **4**, 100 (1961).
117. K. P. Chopra, "On the nature of ionized clouds around a space vehicle," to appear in *Proceedings of the American Astronautical Society Symposium on Interactions of Space Vehicles with Ionized Atmospheres* (The Macmillan Company, New York, 1961).
118. J. D. Kraus, R. C. Higgy, D. J. Schees, and E. R. Crone, *Nature* **185**, 520 (1960).
119. K. P. Chopra, "Plasma-wave-excitation by rapidly moving bodies in ionized atmospheres," presented at the American Physical Society Meeting held on November 2-4, 1960, Gatlinburg, Tennessee, and *Planetary Space Sci.* (to be published).
120. M. J. Lighthill, *J. Fluid Mech.* **9**, 465 (1960).
121. H. R. Sears, *Revs. Modern Phys.* **32**, 701 (1960).
122. H. Hosimoto, *Revs. Modern Phys.* **32**, 860 (1960).
123. K. Gotoh, *J. Phys. Soc. Japan* **15**, 189, 696 (1960).
124. G. S. S. Ludford, *Revs. Modern Phys.* **32**, 1000 (1960).
125. I. Imai, *Revs. Modern Phys.* **32**, 992 (1960).
126. K. Stewarton, *Revs. Modern Phys.* **32**, 855 (1960).
127. Iu. V. Zonov, *Artificial Earth Satellite U.S.S.R.* No. 3, 118 (1958).